NACA

RESEARCH MEMORANDUM

AIR-FLOW SURVEYS IN THE VICINITY OF REPRESENTATIVE NACA 1-SERIES COWLINGS

By

Robert W. Boswinkle, Jr.

Langley Memorial Aeronautical Laboratory
Langley Field, Va.

NATIONAL ADVISORY COMMITTEE
FOR AERONAUTICS

WASHINGTON

May 7, 1948

NATIONAL ADVISORY COMMITTEE FOR AERONAUTICS

RESEARCH MEMORANDUM

AIR-FLOW SURVEYS IN THE VICINITY OF REPRESENTATIVE NACA 1-SERIES COWLINGS

By Robert W. Boswinkle, Jr.

SUMMARY

Air-flow surveys in the vertical plane of symmetry of six NACA 1-series cowling-spinner combinations and one NACA 1-series nose inlet have been conducted in the Langley propeller-research tunnel to obtain quantitative propeller-removed flow-field information useful for the design of propeller shanks and cuffs. The results of the investigation show that in the case of the cowling-spinner combinations the speeds and directions of the flow had appreciable gradients in the region in which the propeller shanks would normally operate; flow conditions in this region were also changed appreciably by changes in the angle of attack, inlet-velocity ratio, spinner proportions, and cowling proportions. Flow conditions for the rotating cowling were much more uniform in the propeller-shank region (located downstream of the inlet) than was the case for the cowling-spinner combinations. Data are presented from which the flow-speed ratios and flow angles may be estimated for similar configurations at angles of attack and inlet-velocity ratios of the order of those investigated. A calculation of the effects of compressibility indicates that the results obtained are directly applicable for propeller design for low and moderate subsonic Mach numbers; corrections to the data are necessary for high subsonic Mach numbers.

INTRODUCTION

A requisite for the design of propeller shanks and cuffs is a knowledge of the flow field in the vicinity of the body to which the propeller is attached. The flow velocities in the vicinity of the nose of a streamlined body of revolution can be calculated easily and with good accuracy. The speeds and directions of the flow near an irregularly shaped body or one with an air inlet near the nose, however, have proved difficult to calculate; little information of this type is available for the design of propellers. Experimental investigations, therefore, have been undertaken in the Langley propeller-research tunnel to supply these urgently needed propeller-design data. A study of the flow conditions in the vicinity of the inlet of an NACA D_S-type cowling was reported in reference 1. The present paper extends this work by reporting the results of air-flow surveys in the vicinity of six representative

NACA 1-series cowling-spinner combinations and one NACA 1-series nose inlet (references 2 and 3) suitable for use as a rotating cowling (the type of cowling in which the forward part rotates with the propeller such as the NACA E cowling described in reference 4).

The speeds and directions of flow in the vertical plane of symmetry of the model were measured (without the propeller) by means of flush surface orifices and tufts installed on a bisecting center plate alined with the flow. The test conditions investigated included the values of inlet-velocity ratio and angle of attack considered most likely to be encountered in both high-speed and climbing flight.

SYMBOLS

d	cowling-inlet diameter
D	maximum cowling diameter, 27.25 inches
D_S	maximum spinner diameter
M	free-stream Mach number
M_{cr}	design critical Mach number of cowling
M_t	test Mach number
X	cowling length, measured from inlet to maximum diameter station
X_s	spinner length, measured from spinner nose to maximum diameter station of spinner (which is located at the inlet)
y'	ordinate of point in vertical plane of symmetry of cowling-spinner combination, measured from model center line (positive upward)
V_i/V_o	inlet-velocity ratio, ratio of average velocity of air in inlet to free-stream velocity
V_l/V_o	local flow-speed ratio, ratio of local flow speed to free-stream velocity
α	angle of attack of model, degrees
ϕ	flow-divergence angle referred to model center line (positive upward), degrees

MODEL AND METHODS

The NACA 1-series nose-inlet ordinates (reference 3) and the method of their application to the design of the cowlings and spinners used in the present investigation are given in table I. The number system used for cowlings and spinners conforming to these ordinates is the same as the one used in references 2 and 3. An NACA 1-series cowling-spinner combination having $d/D = 0.70$, $X/D = 1.00$, $D_s/D = 0.40$, and $X_s/D = 0.80$ is referred to as the NACA 1-70-100 cowling with the NACA 1-40-080 spinner. Thus the first terms in the designations refer to the series, the second terms refer to the cowling-inlet diameter or maximum spinner diameter in percentages of the maximum cowling diameter (cowling-inlet-diameter ratio and spinner-diameter ratio, respectively), and the third terms refer to the cowling length or spinner length in percentages of the maximum cowling diameter (cowling-length ratio and spinner-length ratio, respectively).

The seven cowling configurations investigated in these tests are shown in figure 1 along with the configuration previously investigated in the tests of reference 1. The NACA 1-70-100 cowling was tested with short spinners of three different diameters suitable for single-rotating propellers and one long spinner suitable for a dual-rotating propeller. Design conditions for these configurations fall in the range of internal-flow quantity suitable for current gas-turbine and reciprocating-engine installations. The NACA 1-70-050 cowling (design $M_{cr} \approx 0.71$) and the NACA 1-55-100 cowling (design $M_{cr} \approx 0.81$) were tested in conjunction with the short spinner of intermediate diameter to show the effects of the inlet-diameter ratio and length ratio of the cowling on the speeds and directions of the flow in the region of the propeller. The NACA 1-55-100 cowling also was tested without a spinner to obtain information applicable to the design of a propeller for a rotating cowling.

The center plates used in determining the local speeds and directions of the flow in the vertical plane of symmetry of the model are shown in figures 2 and 3. Each of the plates was 0.5 inch thick and had a sharp-nosed ogival leading edge 1.25 inches long. Removable sections were provided in the two longer center plates to permit the use of these plates with different spinners.

Local flow speeds along the center plates were determined from static pressures obtained from the flush surface orifices installed in the left sides of these plates. With the center plates removed, the flow speeds on top of the spinners and the cowlings were obtained by means of pressures measured on the surfaces. The flow-speed ratios near the surfaces of the spinners and the cowlings obtained with the center plates removed agreed well with those obtained with the center plates in place; this corroborates the validity of the method used.

The flow directions along the center plates were determined from photographs of tufts fastened to the right sides of the plates. Check runs with tufts on wires showed that there were no measurable differences in the flow angles inside and outside the boundary layers of the center plates except within about 1/4 inch of the spinner surfaces. Total-pressure surveys showed that the boundary layers in the intersection of the center plates with the spinners were somewhat thicker than the corresponding boundary layers on the isolated spinners. However, the differences in boundary-layer thickness were not excessive and separation did not occur for any of the conditions investigated.

The internal-flow system of the model, figure 2, included a 25-horsepower axial-flow fan which was necessary to obtain the inlet-velocity ratios for the climb conditions. Control of the flow quantity was obtained by varying the rotational speed of the fan and the position of the butterfly-type shutters. Internal-flow quantities were measured by means of the total-pressure and static-pressure tubes at the throat of the venturi and were checked by a rake of tubes at the exit. A thermocouple attached to the exit rake was used to obtain the temperature rise through the fan.

Prior to the tunnel tests, the venturi in the tail of the model was carefully calibrated to assure the accuracy of the internal-flow quantity measurements. It was found that accurate measurements could be obtained if the fan did not introduce appreciable rotation in the flow through the throat of the venturi. It was also determined that such rotation could be avoided for any desired flow quantity by simultaneous adjustment of the fan rotational speed and the position of the flow-control shutters. During the tunnel tests, the existence of a uniform static-pressure distribution in the venturi throat which was indicative of the absence of flow rotation was established for each test condition by visual observation of a multitube manometer.

The test conditions investigated are listed in table II. The inlet-velocity ratios used for the high-speed conditions correspond approximately for the NACA 1-70-100 cowling to the minimum value for which an essentially flat surface-pressure distribution (reference 2) was obtained on the cowling; for the NACA 1-55-100 cowling and the NACA 1-70-050 cowling these inlet-velocity ratios were somewhat above the minimum values. The climb inlet-velocity ratios were set arbitrarily at from 150 to 200 percent of these values. Since the tufts and orifices were installed only on the upper halves of the center plates, data applicable to the flow in the region of the bottom of the model at positive angles of attack were obtained by testing at the numerically equal negative angles of attack.

Tests on the NACA 1-55-100 cowling with the NACA 1-40-040 spinner were conducted at a tunnel speed of about 100 miles per hour. All other tests were conducted at a tunnel speed of about 80 miles per hour which corresponds to a Mach number of 0.10 and a Reynolds number of about 1.6×10^6 based on the maximum cowling diameter.

RESULTS AND DISCUSSION

Basic data.- The tuft photographs used to determine the directions of the flow along the center plates are presented in figures 4 to 10. Speed-ratio contours and lines of constant flow angle in the vertical plane of symmetry of the seven cowling configurations are presented in figures 11 to 17 for the test conditions tabulated in table II. In the case of the cowling-spinner combinations the local speeds and directions of the flow have appreciable gradients in the region in which the propeller shanks normally operate. Flow conditions in the propeller-shank region of the rotating cowling are much more uniform for all the operating conditions investigated than is the case with the cowling-spinner combinations.

It should be noted that V_l/V_o is a scalar quantity. The inlet-velocity ratio V_1/V_o is the integrated average of the local values of $(V_l/V_o)\cos\phi$. The high values of ϕ at the inlet, together with the boundary layer on the spinner, account for the differences between V_l/V_o and V_1/V_o near the inlet. It also should be noted that the lines of constant-speed ratio are true contours and form closed curves in the plane of the center plates whereas the lines of constant flow angle do not necessarily close in this plane and may end at the surface of the model or at a point in space.

The speed-ratio contours are estimated to be accurate within 1 percent. It was not necessary in any instance to refair the contours to make them consistent when compared on the basis of the various test variables. The values of ϕ are believed to be accurate within 2° throughout the flow region investigated, except in the immediate vicinity of the cowling nose where it was more difficult with the tufts to get accurate measurements of the high flow angles. Some of the flow-angle curves were refaired to make them more consistent.

Effects of inlet-velocity ratio and angle of attack.- The data obtained in the present investigation do not permit exact determination of the variation of the flow characteristics in the vicinity of the several cowlings with V_1/V_o and α. However, the trends of the flow characteristics of the cowling of reference 1 (in which a more complete range of these variables was covered) may be used as a guide in the interpolation and extrapolation of the present data.

The flow characteristics in the propeller-shank region of the configuration of reference 1 are plotted in figure 18. It should be noted that a first approximation to these curves can be made by replacing each set of curves with straight, parallel lines, equally spaced. This approximation is closer for the local flow-speed-ratio curves than for the flow-angle curves; however, propeller design is relatively insensitive to moderate variations in the flow-divergence angles.

Effects of changes in the inlet-velocity ratio and angle of attack on the flow characteristics in the propeller-shank region of each configuration of the present investigation are shown in figure 19. As listed in table II, the local flow speeds and flow angles were obtained

for inlet-velocity ratios ranging from 0.51 to 0.68 for the high-speed conditions and from 0.91 to 1.03 for the climb conditions. The flow characteristics for figure 19 and for some of the following figures were adjusted to values corresponding to inlet-velocity ratios of 0.60 for the high-speed conditions and 1.00 for the climb conditions by assuming the linear variation shown to be valid for the first approximation of the data from reference 1. This was done to get better comparisons of the effects of the different variables on the several cowlings. These adjustments should cause small error in the data.

The variations of flow characteristics with inlet-velocity ratio for $\alpha = 2.5^\circ$ (fig. 19) are plotted from two points, $V_i/V_o = 0.60$ and 1.00. The variations of V_l/V_o and ϕ with α were obtained at two different inlet-velocity ratios. For $V_i/V_o = 0.60$ the flow characteristics are plotted for two points, $\alpha = 0^\circ$ and 2.5°. For $V_i/V_o = 1.00$ the flow characteristics are plotted for three points, $\alpha = 2.5^\circ$, 5°, and 10°. The small curvature in the three-point curves, together with the trends observed in figure 18, indicate that connecting the two-point curves in this figure with straight lines leads to small error.

The local flow-speed ratios (fig. 19) near the surfaces of the spinners of the several cowling-spinner combinations increase considerably with increases in inlet-velocity ratio. At points farther than the cowling-inlet radius from the model center line the effects of inlet-velocity ratio on the local flow-speed ratios are very small. The divergence of the flow at both the top and the bottom of the cowlings decreases with increases in inlet-velocity ratio. Near the surfaces of the spinners these variations of the flow angles with inlet-velocity ratio are large and differ widely for the different cowling-spinner combinations; at points of greater radii than the cowling inlet, however, the flow angles vary only a small amount with inlet-velocity ratio.

The local flow-speed ratios and flow angles in the propeller-shank region of the rotating cowling are almost constant and independent of inlet-velocity ratio (fig. 19 (f)).

Increase in the angle of attack (at a constant inlet-velocity ratio) causes the local flow-speed ratios in the propeller-shank region at the top of the model generally to increase and those at the bottom to decrease. The flow angles generally become more positive at both the top and bottom of the model with increases in the angle of attack. These effects are larger for the cowling-spinner combinations than for the rotating cowling.

The flow characteristics in the propeller-shank region of the cowling configurations investigated are readily obtained for $V_i/V_o \approx 0.60$ and $0^\circ < \alpha < 2.5^\circ$ and for $V_i/V_o \approx 1.00$ and $2.5^\circ < \alpha < 10^\circ$ by the use of figure 19. Values of V_l/V_o and ϕ are read at the desired angle of attack from the curves plotted for the inlet-velocity ratio closest to the desired one. These values are then corrected for V_i/V_o differences in the V_i/V_o plot. For

example, the flow characteristics for the NACA 1-70-100 cowling with the NACA 1-40-040 spinner for $\alpha = 1^\circ$ and $V_i/V_o = 0.70$ will be found. In figure 19(b) from the α curves for $V_i/V_o = 0.60$ the following values of V_l/V_o and ϕ are found at $\alpha = 1^\circ$:

y'/D	$V_i/V_o = 0.60$, $\alpha = 1^\circ$	
	V_l/V_o	ϕ (deg)
0.25	0.82	18
.35	.82	26
.50	.93	15
.825	.99	3

These values are plotted on the V_i/V_o plot at $V_i/V_o = 0.60$ and curves parallel to the corresponding y'/D curves are constructed through these points. At $V_i/V_o = 0.70$ the following desired values of V_l/V_o and ϕ are read:

y'/D	$V_i/V_o = 0.70$, $\alpha = 1^\circ$	
	V_l/V_o	ϕ (deg)
0.25	0.86	15
.35	.84	21
.50	.93	13
.825	.99	3

For angles of attack and inlet-velocity ratios outside the range of the variables plotted in figure 19, the data may be extrapolated in the same manner, but, of course, with less assurance of accuracy.

Effects of spinner proportions.- The effects of changes in the spinner-diameter ratio and spinner-length ratio on the local flow-speed ratios and flow angles in the propeller-shank region of the NACA 1-70-100 cowling are shown in figure 20.

For the same spinner-length ratio, the local flow-speed ratios show increases with an increase in the spinner-diameter ratio; this would be expected from a consideration of the increased deviation of the stream-lines adjacent to the spinners and, in the case of the high-speed conditions

(low V_1/V_o), the reduction in area of the low velocity field in the region of inlet. Increasing the spinner-length ratio for $\alpha = 0^\circ$ causes the flow to be initially deviated farther upstream so that the flow speeds are closer to the free-stream value for the longer spinner at 0.1D ahead of the inlet. At a positive angle of attack the direction of the flow on the under side of the spinners tends to prevent the formation of thick boundary layers so that an increase in the spinner-length ratio has little effect on the flow-speed ratios in this region. However, on the top of the spinners (at a positive angle of attack), the boundary layers tend to thicken with increases in the spinner-length ratio so that the local flow speeds near the spinner are lower in the case of the longer spinner.

The divergence of the flow does not vary in a uniform manner with changes in either spinner-diameter ratio or length ratio, and it appears that for each inlet-velocity ratio there is a spinner for each cowling for which the flow deviation in the region of the propeller shanks is a minimum. In the case of the spinners of equal length it is believed that this phenomenon results from the decreases in internal-flow quantity (for a constant inlet-velocity ratio) associated with the increases in spinner-diameter ratio. The data obtained do not permit determination of this characteristic quantitatively.

Local flow-speed ratios and flow angles downstream from the inlet of the NACA 1-55-100 cowling with the NACA 1-40-040 spinner and with no spinner are shown in figure 21. It should be noted that the flow characteristics of the two configurations are very nearly the same in the region in which a propeller would be installed in a spinner-cowling (0.2D to 0.6D downstream from the inlet). Data for the NACA 1-70-100 cowling with different spinners (fig. 22) also show that spinner proportions do not have large effects on the flow characteristics in this region. Flow characteristics downstream of the inlet obtained for cowling-spinner combinations may therefore be used for rotating cowlings with small error.

Effects of cowling proportions.- The effects of changes in the cowling-inlet-diameter ratio and the cowling-length ratio on the speeds and directions of the flow in the propeller-shank region are indicated in figure 23. The NACA 1-40-040 spinner was used with the three cowlings investigated.

A comparison of the flow characteristics in the propeller-shank region of the NACA 1-70-100 cowling and the cowling with the smaller inlet-diameter ratio, the NACA 1-55-100 cowling, shows that reducing the inlet-diameter ratio causes the point of minimum flow speed and the point of maximum flow deviation to shift nearer to the surface of the spinner. In the high-speed conditions ($V_1/V_o = 0.60$; $\alpha = 0^\circ$, 2.5°) the flow-speed ratios in general are closer to the free-stream value for the cowling with the smaller inlet-diameter ratio and in the climb conditions ($V_1/V_o = 1.00$; $\alpha = 2.5^\circ$, 5°, 10°) are closer in general to the free-stream value for the cowling with the larger inlet-diameter ratio. This phenomenon results

from the smaller area of reduced velocities in the region of the inlet for the cowling with the smaller inlet-diameter ratio in the high-speed conditions ($V_1/V_o = 0.60$). The higher inlet-velocity ratios required for the climb conditions cause the flow speeds in the region of the inlet to approach free-stream values. The blunter nose of the cowling with the smaller inlet-diameter ratio therefore becomes the factor which reduces the flow-speed ratios in front of the nose to values below those for the cowling with the larger inlet-diameter ratio. The blunter nose of the smaller inlet-diameter-ratio cowling also generally causes the flow-divergence angles to be greater.

A comparison of the flow characteristics for the NACA 1-70-100 cowling and the cowling with the shorter length ratio, the NACA 1-70-050 cowling, shows that a reduction in the cowling-length ratio has little effect on the location of the points of minimum flow speed and the points of maximum flow deviation. A reduction in the cowling-length ratio (which also makes the cowling nose more blunt) generally makes the flow speeds more substream and increases the divergence of the flow.

As previously noted, increasing the angle of attack increases the flow-speed ratios above the spinner and decreases those below. Also the angle of divergence of the flow becomes more positive both above and below the spinner with increases in the angle of attack.

The approximate effects of changes in the cowling proportions on the flow characteristics downstream of the inlet (in the region of the propeller) for rotating cowlings are shown in figure 24. Data for cowling-spinner combinations were used in accordance with the observation noted in the preceding section that the presence of a spinner affects the flow characteristics downstream of the inlet by only small amounts. Decreases in cowling-length ratio cause the flow-speed ratios to increase while changes in inlet-diameter ratio for cowlings of equal length have only a small effect on the flow speeds (especially at distances greater than 0.2D downstream from the inlet). These effects result from the fact that the magnitude of the flow-speed ratios is a function of the bluntness of cowling-lip shape. (See discussion in reference 2). Decreases in cowling-inlet-diameter ratio cause the flow-divergence angles to become larger because of the increased slope of the cowling surface; no such increase in magnitude of the flow angles occurs with a decrease in cowling length because the characteristics of the cowling with the smaller length ratio are shown for a location much closer to the maximum diameter station than for the longer cowlings, and consequently the magnitude of the flow-divergence angles is less than it would be at a corresponding location.

Effects of compressibility.- The Prandtl-Glauert method (one development of which is given in reference 5) was used to estimate the effects of compressibility on the speeds and directions of the flow in the region in which a propeller would normally operate (0.1D upstream from the inlet). The theory was developed for a slender body of revolution for which the departures of the local velocities from the free-stream velocity are small.

Obviously the method is not generally applicable to a cowling. When the inlet-velocity ratio is approximately unity, however, the results obtained by the Prandtl-Glauert method should give a first-order indication of the compressibility effects, except in the immediate vicinity of a stagnation point. The calculations were confined, therefore, to the NACA 1-70-050 cowling with the NACA 1-40-040 spinner for the conditions of $\alpha = 2.5°$ and $V_i/V_o = 1.0$.

The details of the calculations were as follows:

(1) The coordinates of the cowling and spinner were stretched in the stream direction by the factor $\sqrt{\frac{1 - M_t^2}{1 - M^2}}$ where M was taken as 0.736, the critical Mach number of the installation. (This stretched body would correspond to an NACA 1-70-074 cowling with an NACA 1-40-059 spinner).

(2) The incremental velocities u' and v' in the x and y directions, respectively, were obtained for the stretched body for $M_t = 0.1$ (essentially incompressible flow). These perturbation velocities could be calculated for incompressible flow from potential flow considerations by the aid of reference 6. In the present instance, however, they were obtained from linear interpolation of the data for the NACA 1-70-050 cowling with the NACA 1-40-040 spinner (at the station 0.1D ahead of the inlet) and the data for the NACA 1-70-100 cowling with the NACA 1-40-080 spinner (at the station 0.2D ahead of the inlet).

(3) The incremental velocities in the propeller region of the unstretched body in compressible flow were calculated from the corresponding incremental velocities obtained in step (2) by the relations

$$u = u' \left(\frac{1 - M_t^2}{1 - M^2}\right) \text{ and } v = v' \sqrt{\frac{1 - M_t^2}{1 - M^2}}.$$

The speeds and directions of the flow in the propeller-shank region of the NACA 1-70-050 cowling with the NACA 1-40-040 spinner, calculated for $M = 0.736$, are compared with the experimental values measured at $M = 0.1$ in figure 25. For the case investigated, these results indicate that within this region the large assumed increase in flight Mach number would have little effect on the flow angles and would decrease the local flow-speed ratios by less than 0.1. The effect of Mach number on the change of flow-speed ratio due to compressibility at the points above and below the spinner where this change is the greatest is shown in figure 26. It should be noted that these maximum changes in flow-speed ratio are quite small, less than 0.03 up to $M = 0.5$. Somewhat greater changes would be expected for the lower inlet-velocity ratios which correspond to the high-speed conditions and for the higher angles of attack which correspond to the climb conditions. The reasonably small variation of the flow-speed ratios with Mach number for the case investigated, however, indicates that, with respect to compressibility effects, the data presented can be

used directly for propeller design at low and moderate subsonic Mach numbers. Corrections, which can be roughly estimated by reference to figures 25 and 26, are necessary for application of the data for propeller design for high subsonic Mach numbers.

CONCLUDING REMARKS

The present study of flow conditions in the vertical plane of symmetry of representative NACA 1-series cowlings indicates that the gradients in the speeds and directions of the flow are sufficient to warrant consideration in the design of propeller shanks or cuffs for cowling-spinner combinations. The gradients are much less severe over the cowling where the propeller is located in the case of the rotating cowling. The basic flow-field contours (which were obtained over a wide area in the vicinity of the cowlings and spinners) are presented. Variations of the flow characteristics with the several variables are shown only for typical propeller locations, but the variations may be obtained for other locations from the basic data. The results appear to be directly applicable for propeller design for low and moderate Mach numbers; corrections for the effect of Mach number are necessary for high subsonic Mach numbers. The flow conditions may be estimated for similar configurations at angles of attack and inlet-velocity ratios of the order of those tested through application of the data presented.

Langley Memorial Aeronautical Laboratory
National Advisory Committee for Aeronautics
Langley Field, Va.

REFERENCES

1. Boswinkle, Robert W., Jr., and Bryant, Rosemary P.: An Experimental Investigation of Flow Conditions in the Vicinity of an NACA D_S-Type Cowling. NACA MR No. L6H14, 1946.

2. Nichols, Mark R., and Keith, Arvid L., Jr.: Investigation of a Systematic Group of NACA 1-Series Cowlings with and without Spinners. NACA RM No. L8A15, 1948.

3. Baals, Donald D., Smith, Norman F., and Wright, John B.: The Development and Application of High-Critical-Speed Nose Inlets. NACA ACR No. L5F30a, 1945.

4. Becker, John V., and Mattson, Axel T.: The Effect of Spinner-Body Gap on the Pressures Available for Cooling in the NACA E-Type Cowling. NACA CB, March 1943.

5. Göthert, B.: Plane and Three-Dimensional Flow at High Subsonic Speeds. NACA TM No. 1105, 1946.

6. Küchemann, D.: Tables for the Stream Function and the Velocity Components of a Source-Ring and a Vortex-Ring. Reps. and Translations No. 308, British M.A.P. Völkenrode, Nov. 15, 1946.

TABLE I

NACA 1-SERIES ORDINATES AS APPLIED TO COWLING AND SPINNER

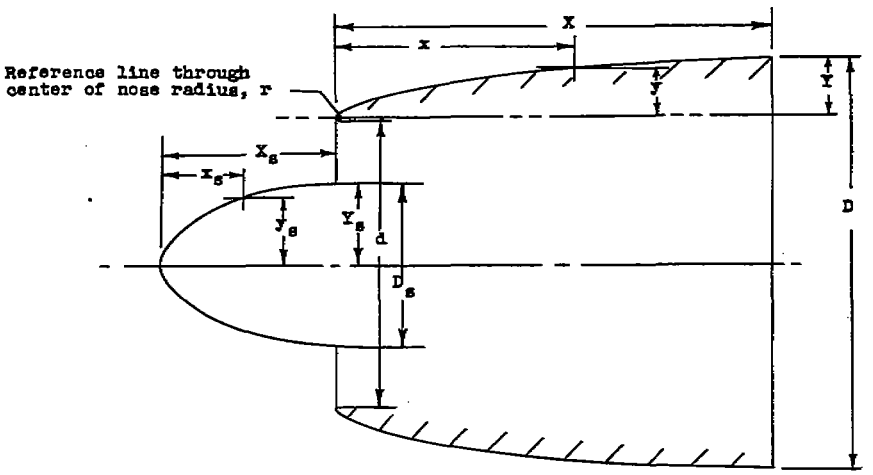

$$X = \left(\frac{X}{D}\right) D \qquad X_s = \left(\frac{X_s}{D}\right) D$$

$$Y = \frac{D - d}{2} - r \qquad Y_s = \frac{D_s}{2} = \frac{\left(\frac{D_s}{D}\right) D}{2}$$

For $r = 0.025Y$:

$$Y = \frac{D - d}{2.05} = \frac{D\left(1 - \frac{d}{D}\right)}{2.05}$$

[Ordinates in percent; taken from reference 3]

x/X or x_s/X_s	y/Y or y_s/Y_s	x/X or x_s/X_s	y/Y or y_s/Y_s	x/X or x_s/X_s	y/Y or y_s/Y_s	x/X or x_s/X_s	y/Y or y_s/Y_s
0	0	13.0	41.94	34.0	69.08	60.0	89.11
.2	4.80	14.0	43.66	35.0	70.08	62.0	90.20
.4	6.63	15.0	45.30	36.0	71.05	64.0	91.23
.6	8.12	16.0	46.88	37.0	72.00	66.0	92.20
.8	9.33	17.0	48.40	38.0	72.94	68.0	93.11
1.0	10.38	18.0	49.88	39.0	73.85	70.0	93.95
1.5	12.72	19.0	51.31	40.0	74.75	72.0	94.75
2.0	14.72	20.0	52.70	41.0	75.63	74.0	95.48
2.5	16.57	21.0	54.05	42.0	76.48	76.0	96.16
3.0	18.31	22.0	55.37	43.0	77.32	78.0	96.79
3.5	19.94	23.0	56.66	44.0	78.15	80.0	97.35
4.0	21.48	24.0	57.92	45.0	78.95	82.0	97.87
4.5	22.96	25.0	59.15	46.0	79.74	84.0	98.33
5.0	24.36	26.0	60.35	47.0	80.50	86.0	98.74
6.0	27.01	27.0	61.52	48.0	81.25	88.0	99.09
7.0	29.47	28.0	62.67	49.0	81.99	90.0	99.40
8.0	31.81	29.0	63.79	50.0	82.69	92.0	99.65
9.0	34.03	30.0	64.89	52.0	84.10	94.0	99.85
10.0	36.13	31.0	65.97	54.0	85.45	96.0	99.93
11.0	38.15	32.0	67.03	56.0	86.73	98.0	99.98
12.0	40.09	33.0	68.07	58.0	87.95	100.0	100.00

Cowling nose radius: 0.025Y

TABLE II.- KEY TO BASIC DATA

Reference figures	Cowling configurations		Inlet-velocity ratio				
			High-speed		Climb		
	NACA cowlings	NACA spinners	$\alpha = 0^\circ$	$\alpha = 2.5^\circ$	$\alpha = 2.5^\circ$	$\alpha = 5^\circ$	$\alpha = 10^\circ$
4, 11(a)	1-70-100	1-30-040	0.58	-------	-------	------	-------
4, 11(b)	1-70-100	1-30-040	------	0.60	-------	------	-------
4, 11(c)	1-70-100	1-30-040	------	-------	0.91	------	-------
4, 11(d)	1-70-100	1-30-040	------	-------	-------	0.91	-------
4, 11(e)	1-70-100	1-30-040	------	-------	-------	------	0.91
5, 12(a)	1-70-100	1-40-040	0.63	-------	-------	------	-------
5, 12(b)	1-70-100	1-40-040	------	0.66	-------	------	-------
5, 12(c)	1-70-100	1-40-040	------	-------	0.99	------	-------
5, 12(d)	1-70-100	1-40-040	------	-------	-------	0.99	-------
5, 12(e)	1-70-100	1-40-040	------	-------	-------	------	0.99
6, 13(a)	1-70-100	1-50-040	0.62	-------	-------	------	-------
6, 13(b)	1-70-100	1-50-040	------	0.68	-------	------	-------
6, 13(c)	1-70-100	1-50-040	------	-------	1.03	------	-------
6, 13(d)	1-70-100	1-50-040	------	-------	-------	1.03	-------
6, 13(e)	1-70-100	1-50-040	------	-------	-------	------	1.03
7, 14(a)	1-70-100	1-40-080	0.61	-------	-------	------	-------
7, 14(b)	1-70-100	1-40-080	------	0.65	-------	------	-------
7, 14(c)	1-70-100	1-40-080	------	-------	1.00	------	-------
7, 14(d)	1-70-100	1-40-080	------	-------	-------	1.00	-------
7, 14(e)	1-70-100	1-40-080	------	-------	-------	------	1.00
8, 15(a)	1-55-100	1-40-040	0.53	-------	-------	------	-------
8, 15(b)	1-55-100	1-40-040	------	0.53	-------	------	-------
8, 15(c)	1-55-100	1-40-040	------	-------	0.93	------	-------
8, 15(d)	1-55-100	1-40-040	------	-------	-------	0.93	-------
8, 15(e)	1-55-100	1-40-040	------	-------	-------	------	0.93
9, 16(a)	1-55-100	No spinner	0.52	-------	-------	------	-------
9, 16(b)	1-55-100	No spinner	------	0.52	-------	------	-------
9, 16(c)	1-55-100	No spinner	------	-------	1.02	------	-------
9, 16(d)	1-55-100	No spinner	------	-------	-------	1.02	-------
9, 16(e)	1-55-100	No spinner	------	-------	-------	------	1.02
10, 17(a)	1-70-050	1-40-040	0.51	-------	-------	------	-------
10, 17(b)	1-70-050	1-40-040	------	0.51	-------	------	-------
10, 17(c)	1-70-050	1-40-040	------	-------	1.00	------	-------
10, 17(d)	1-70-050	1-40-040	------	-------	-------	1.00	-------
10, 17(e)	1-70-050	1-40-040	------	-------	-------	------	1.00

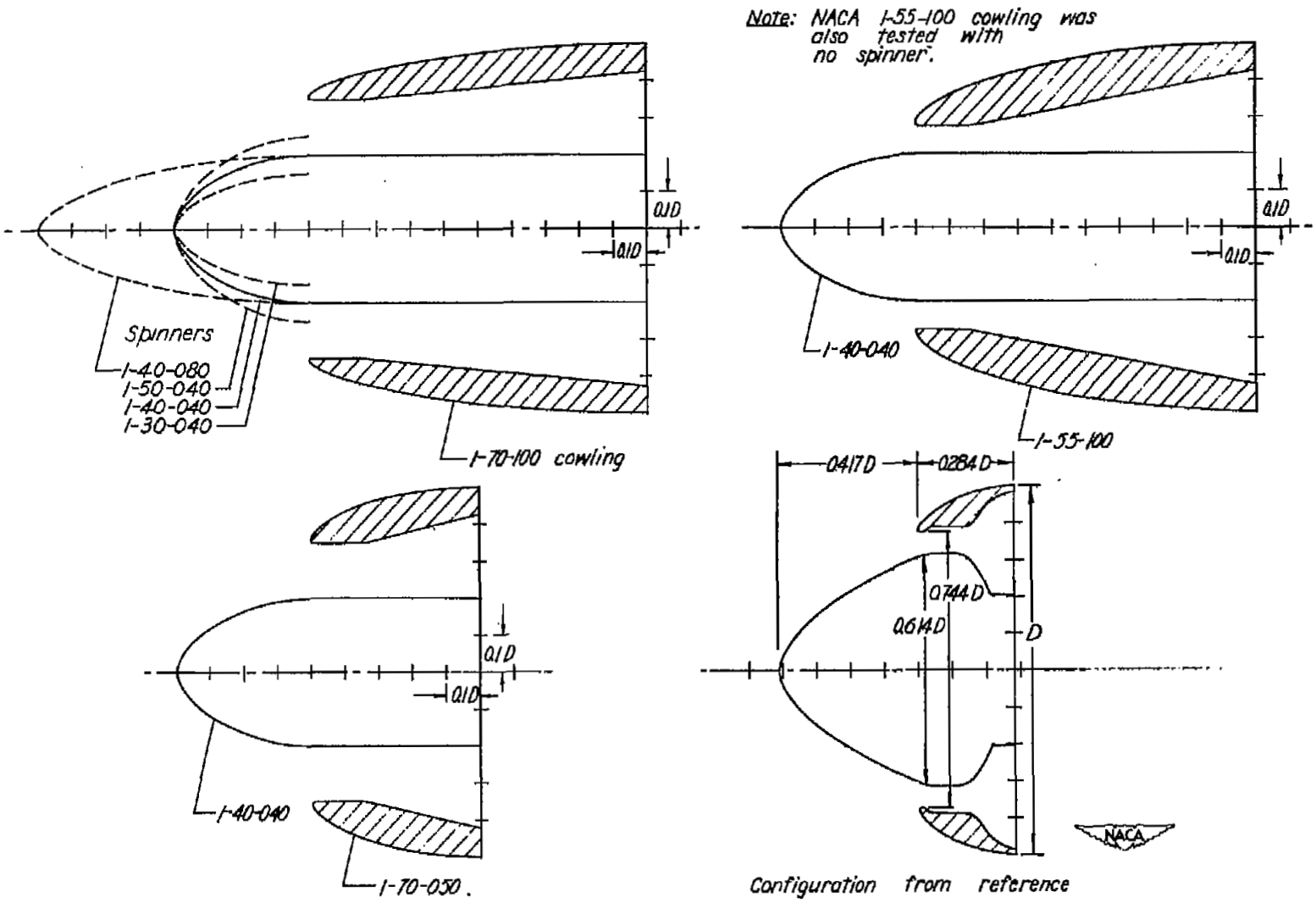

Figure 1.- NACA 1-series configurations investigated and configuration from reference 1.

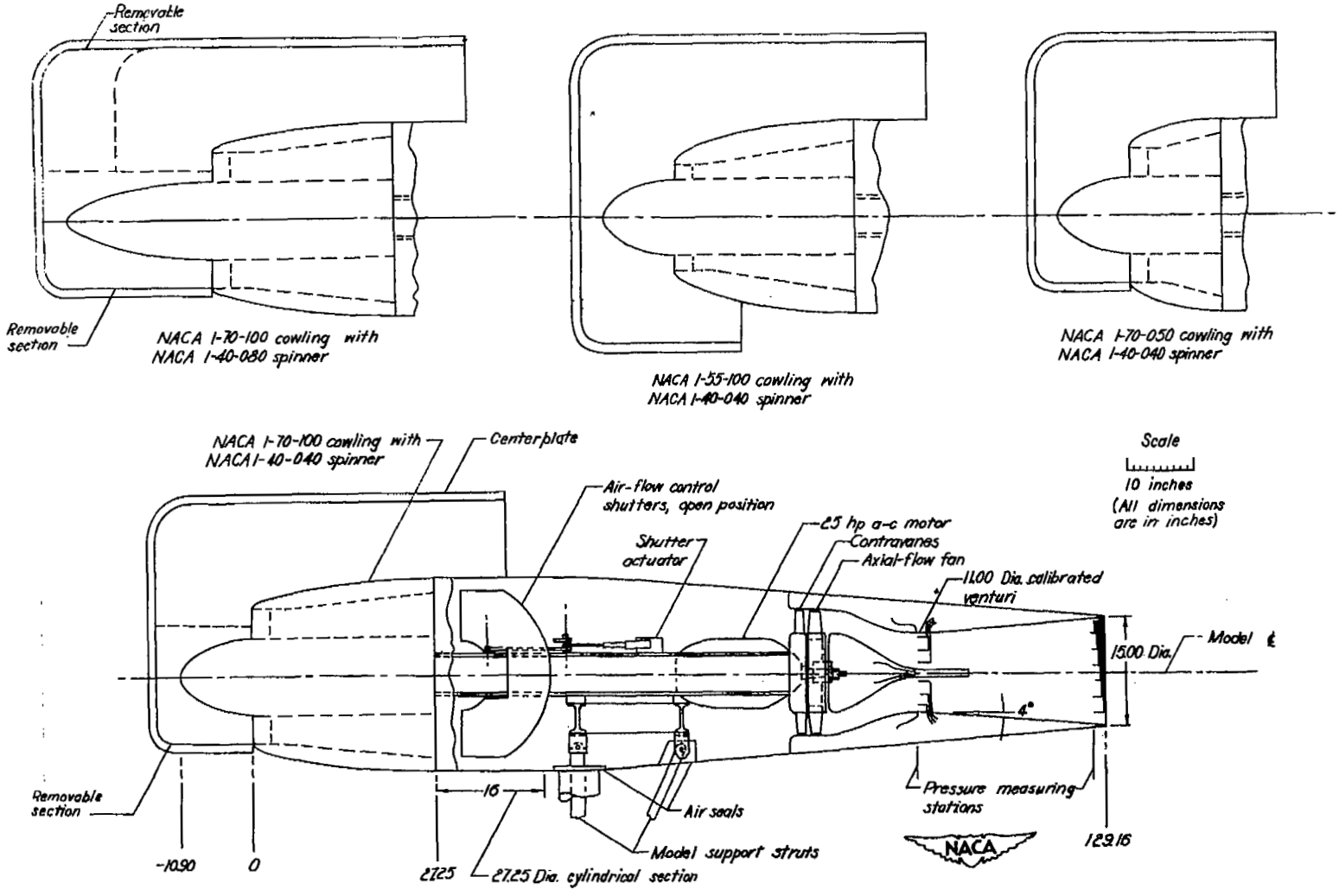

Figure 2.-Arrangement and overall dimensions of model.

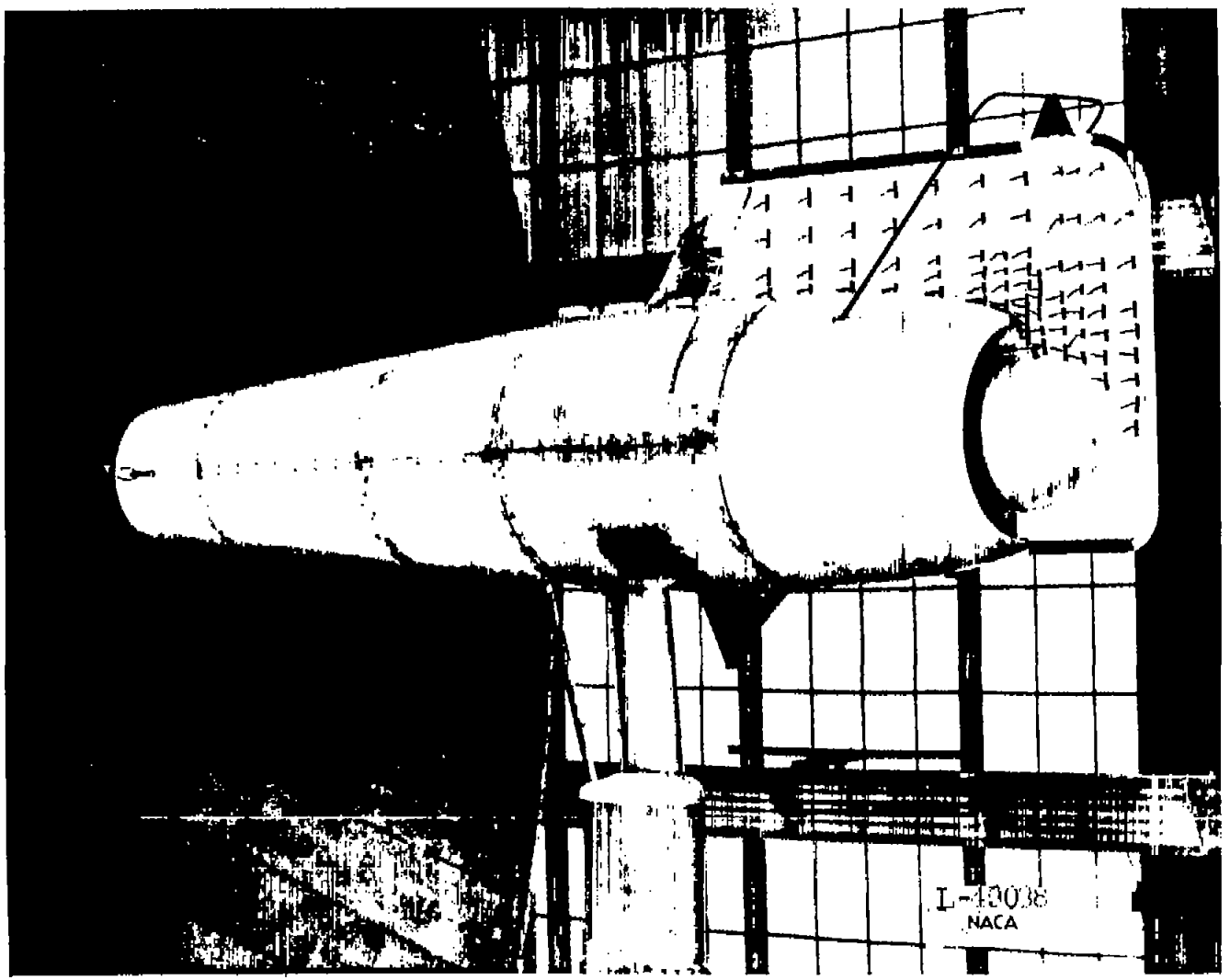

Figure 3.- General view of model with tunnel not running. NACA 1-70-100 cowling with NACA 1-40-040 spinner.

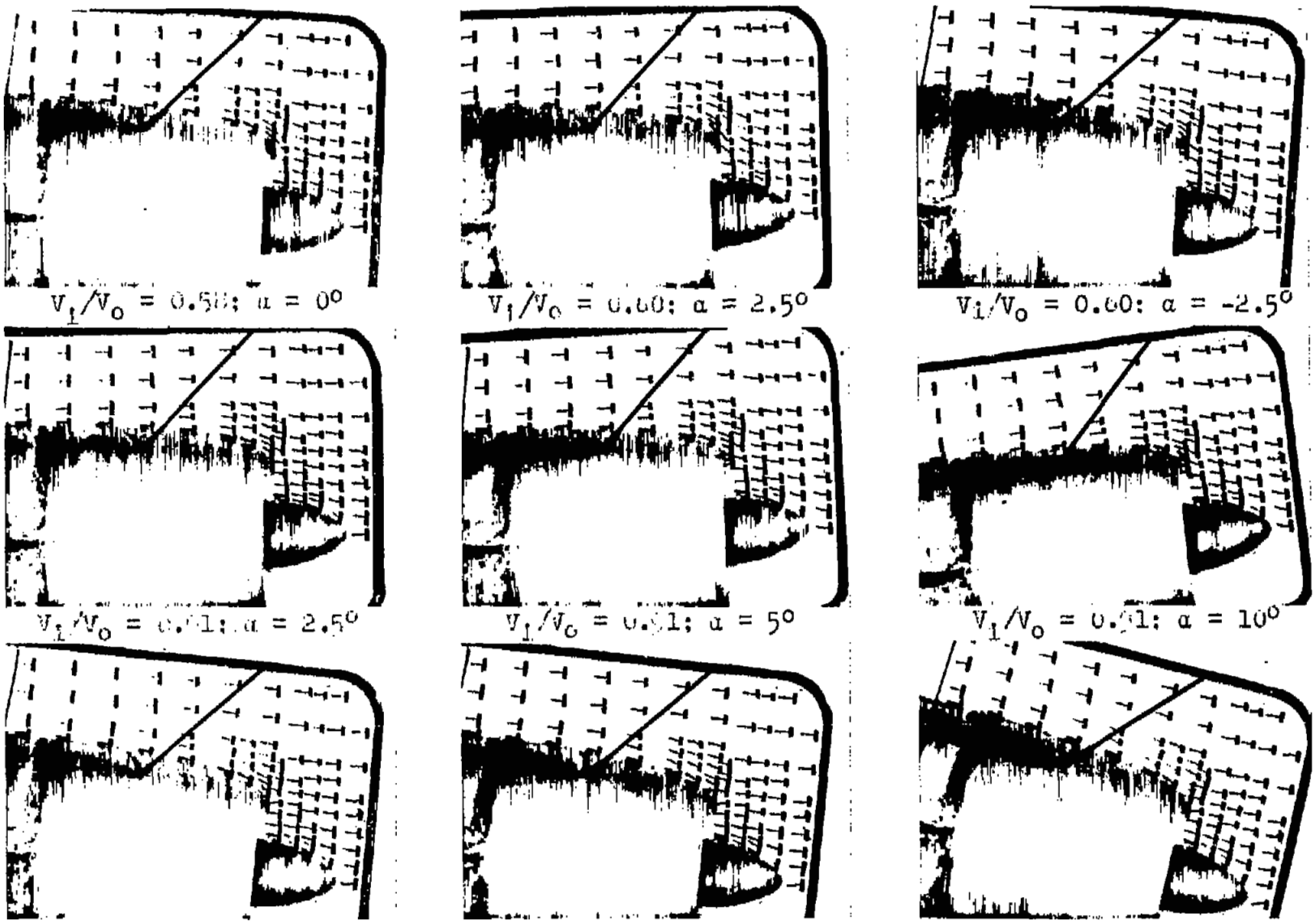

Figure 4.- Tuft photographs of NACA 1-70-100 cowling with NACA 1-30-040 spinner.

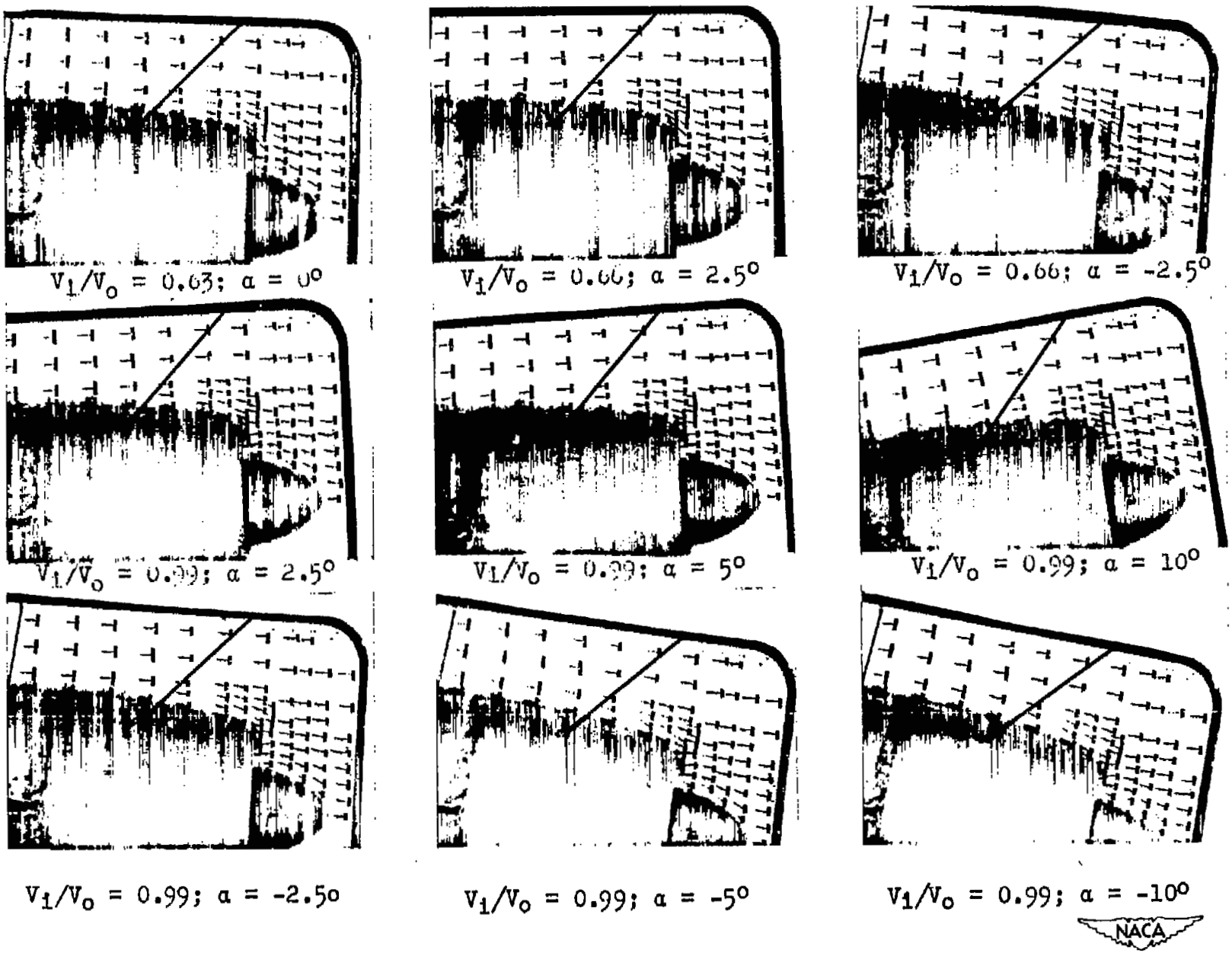

Figure 5.- Tuft photographs of NACA 1-70-100 cowling with NACA 1-40-040 spinner.

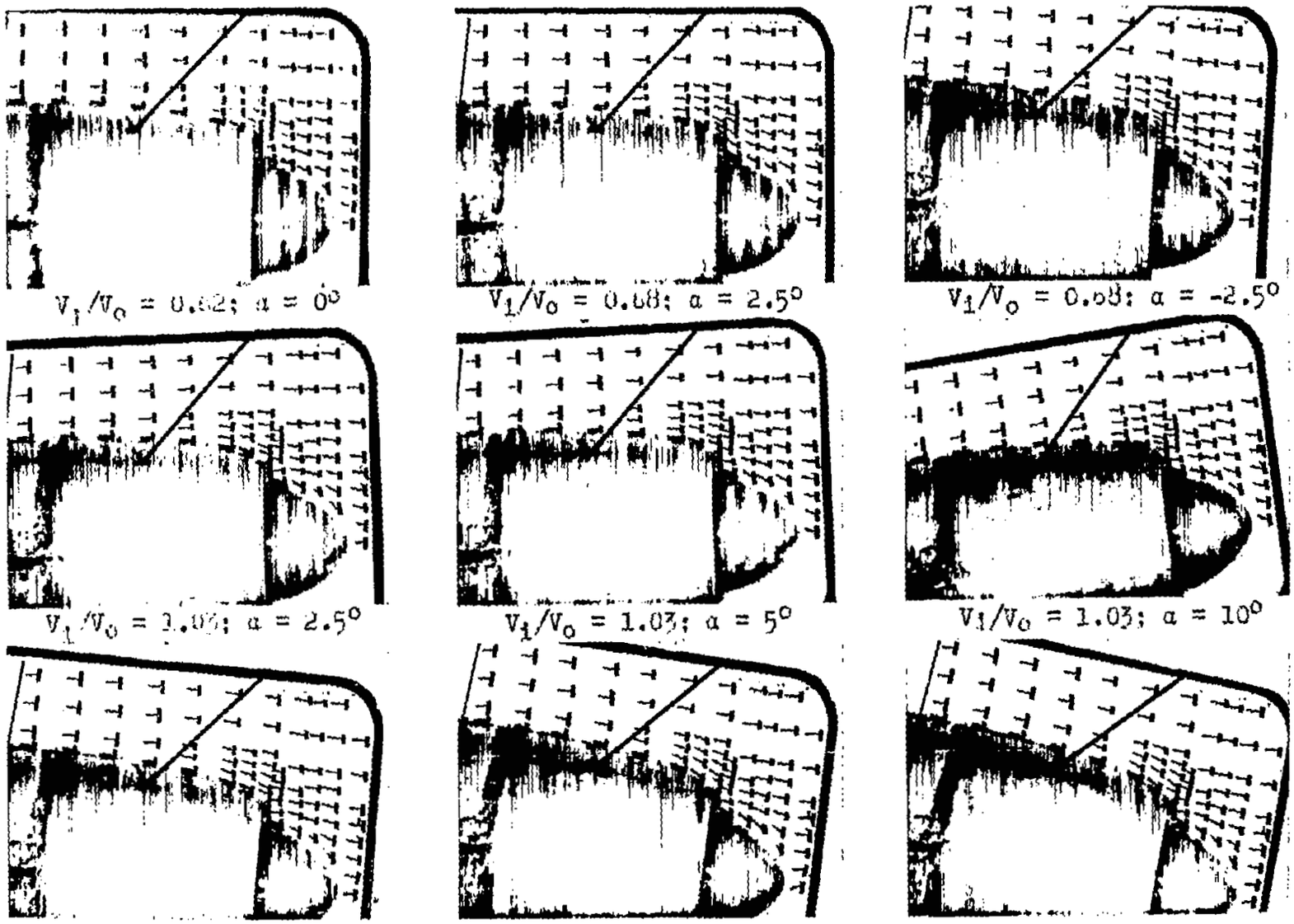

Figure 6.- Tuft photographs of NACA 1-70-100 cowling with NACA 1-50-040 spinner.

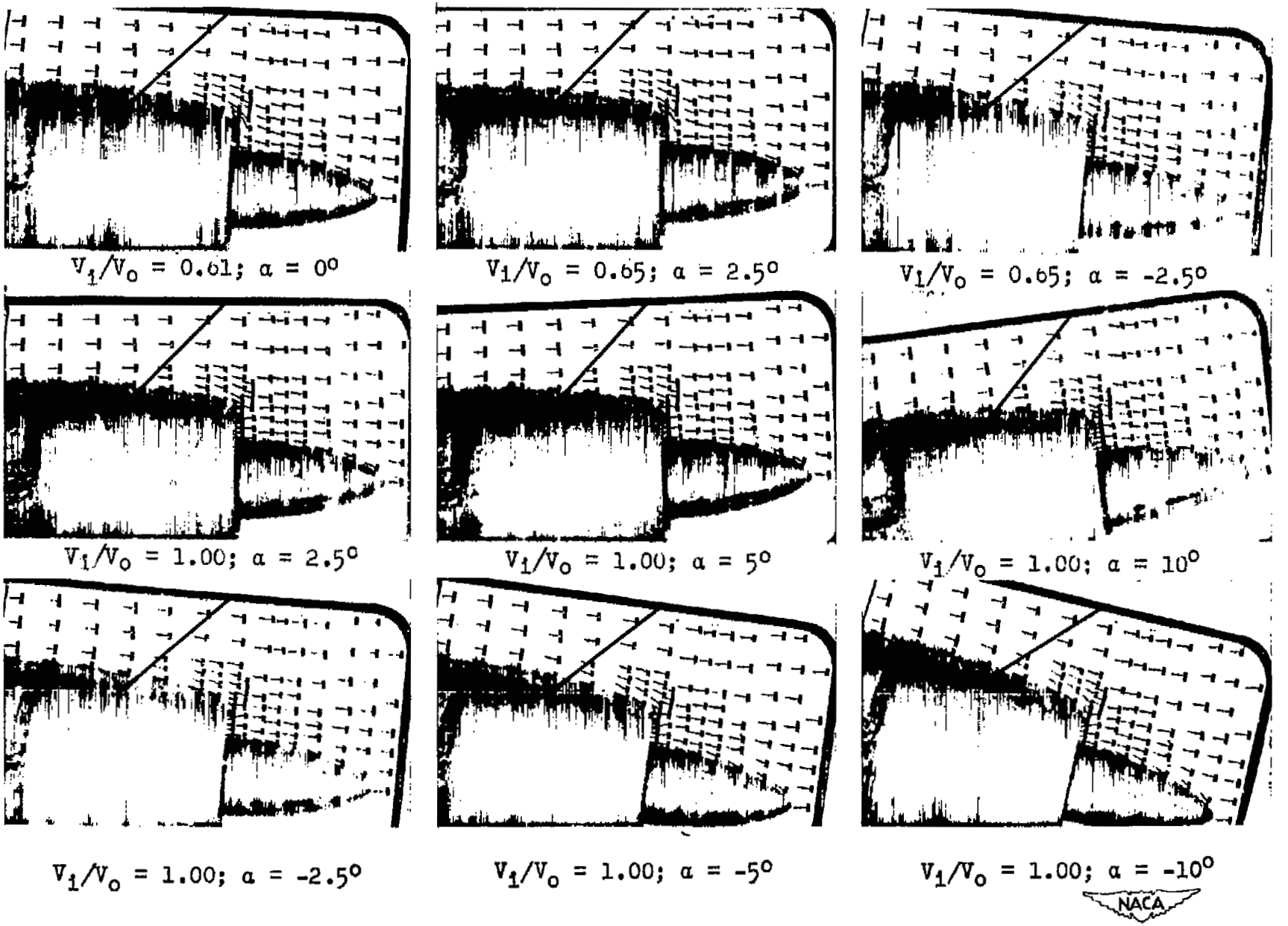

Figure 7.- Tuft photographs of NACA 1-70-100 cowling with NACA 1-40-080 spinner.

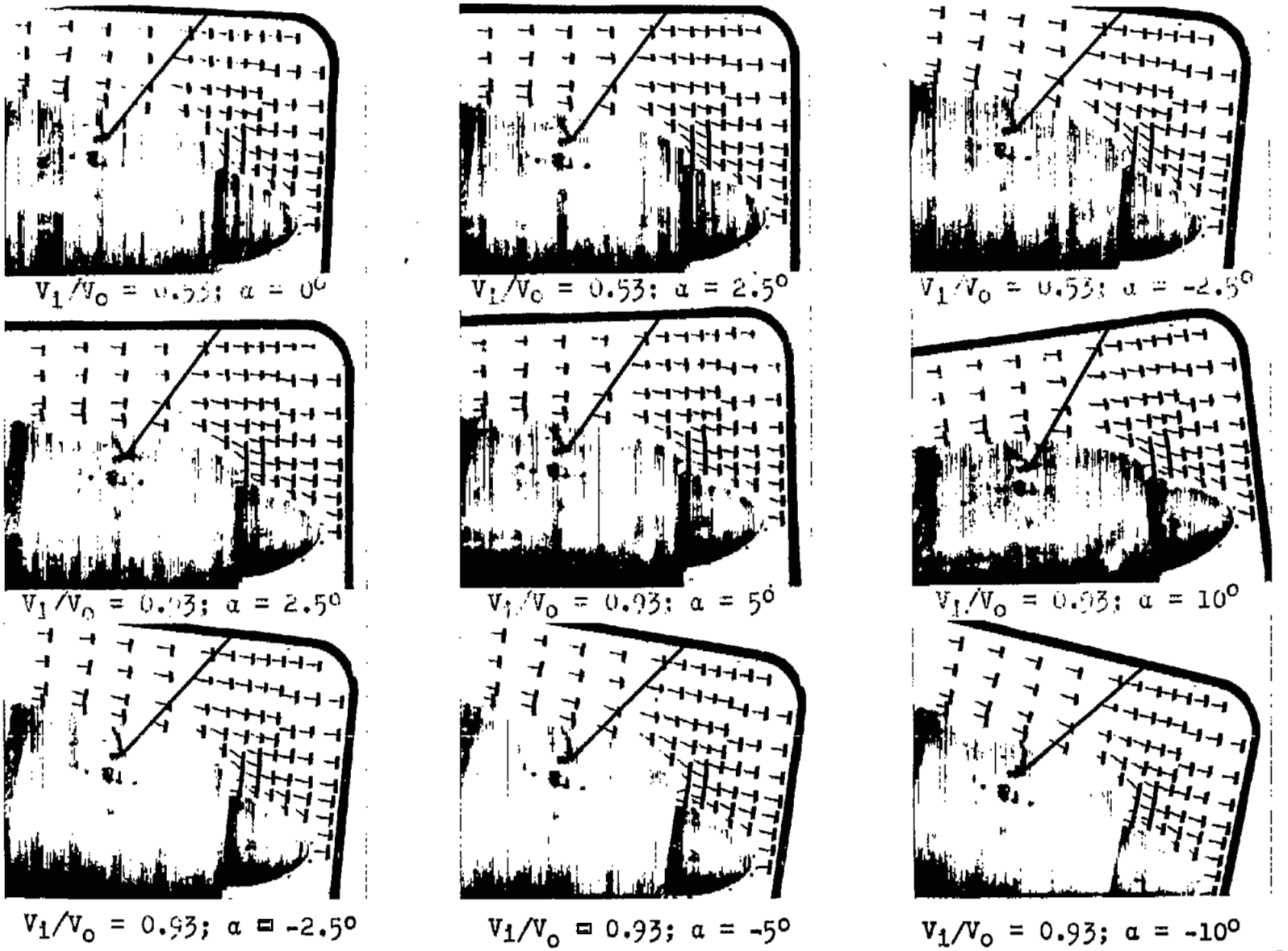

Figure 8.- Tuft photographs of NACA 1-55-100 cowling with NACA 1-40-040 spinner.

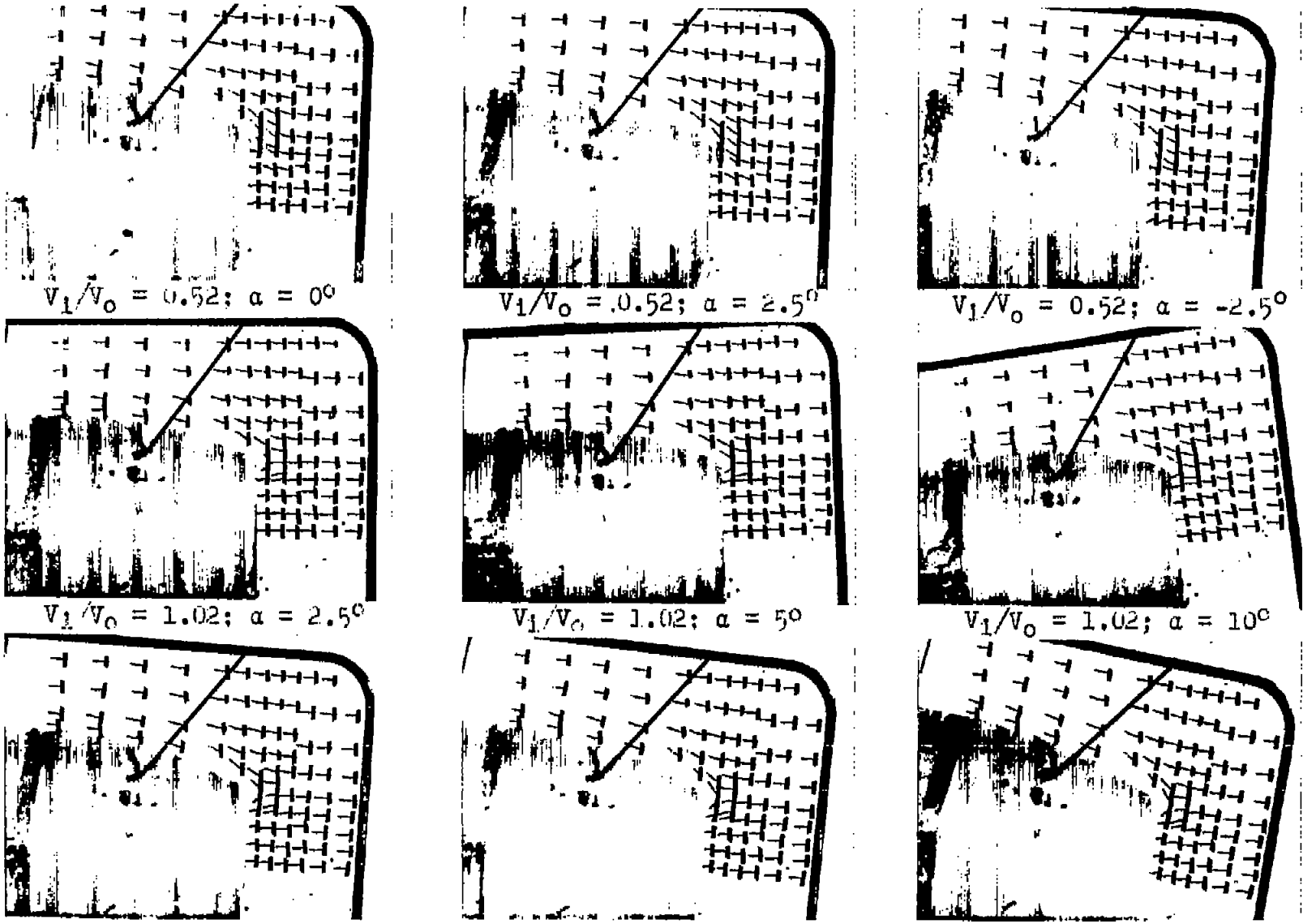

Figure 9.- Tuft photographs of NACA 1-55-100 cowling with no spinner.

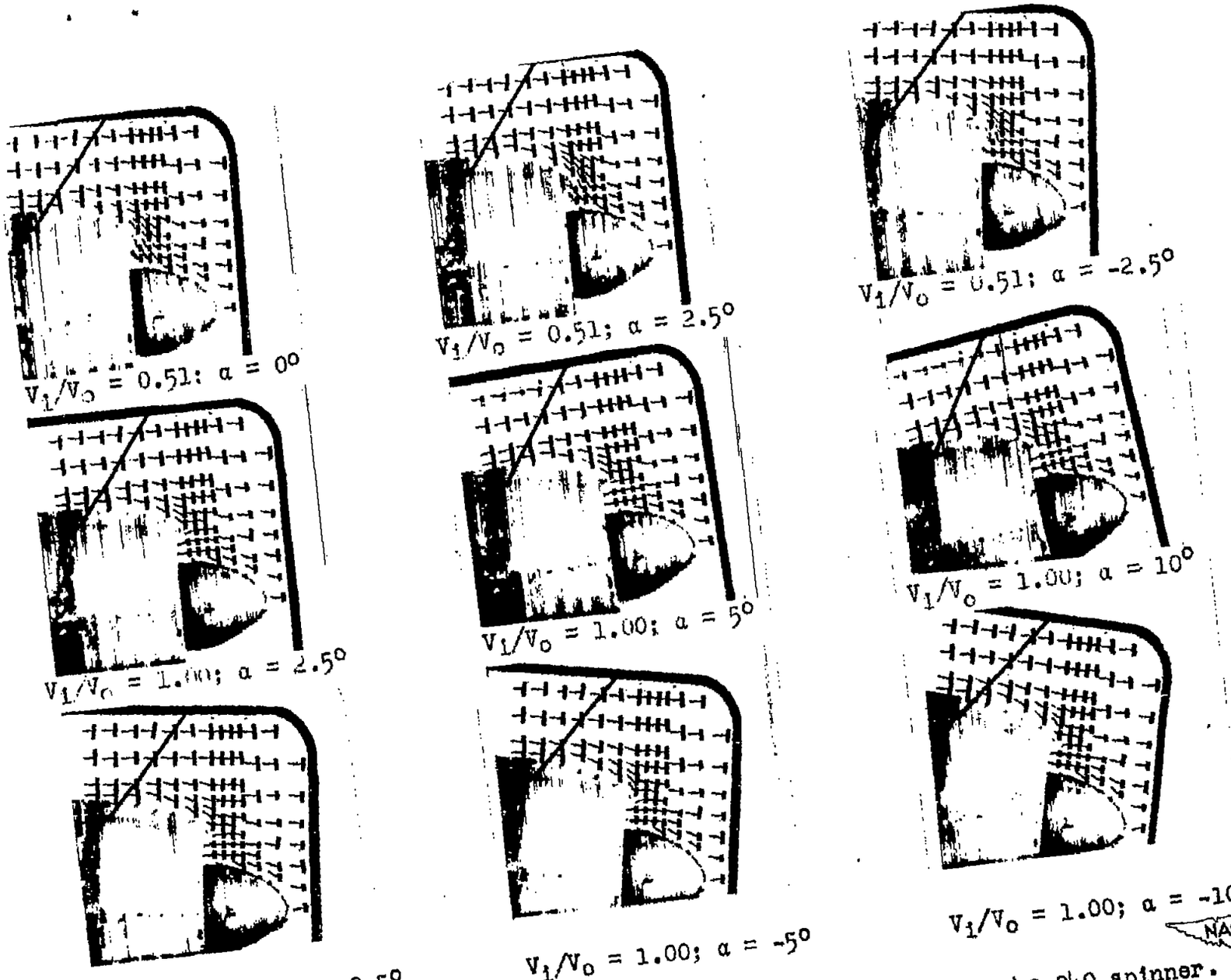

Figure 10.- Tuft photographs of NACA 1-70-050 cowling with NACA 1-40-040 spinner.

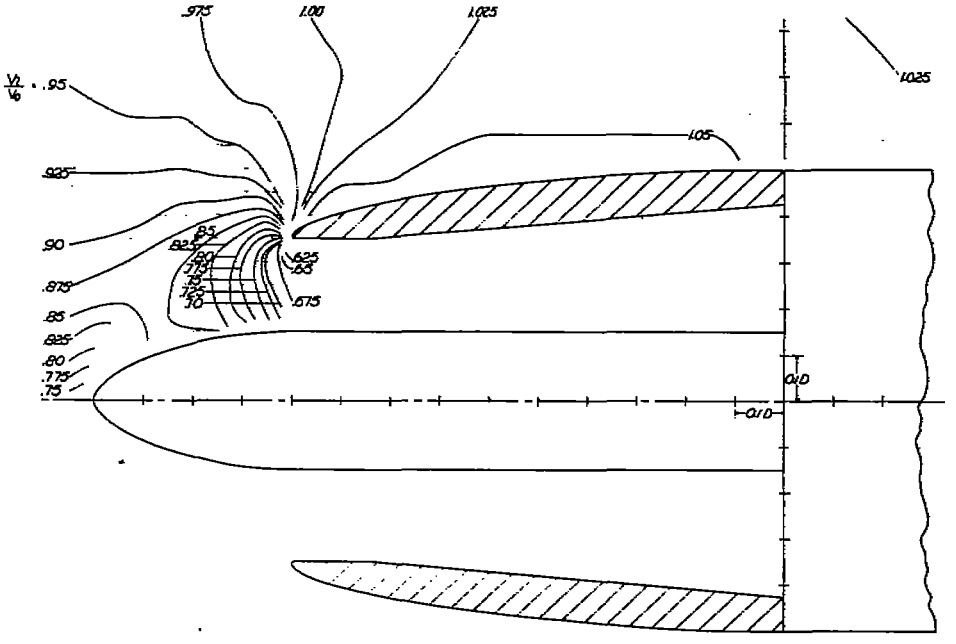

speed-ratio contours

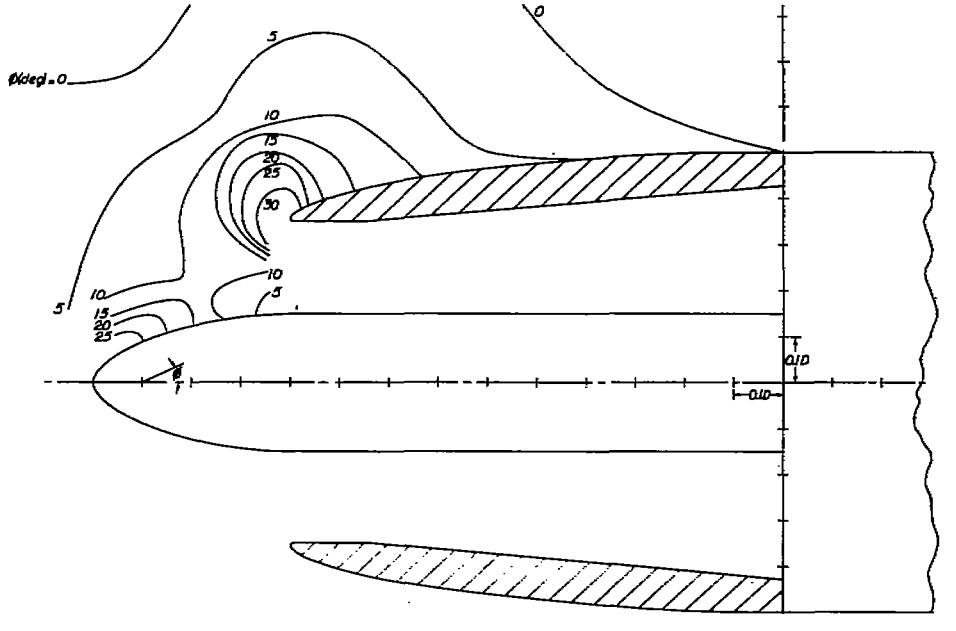

lines of constant flow angle

NACA

(a) $V_l/V_0 = 0.58$; $\alpha = 0°$.

Figure 11.-Speed and direction of flow in vicinity of NACA 1-70-100 cowling with NACA 1-30-040 spinner.

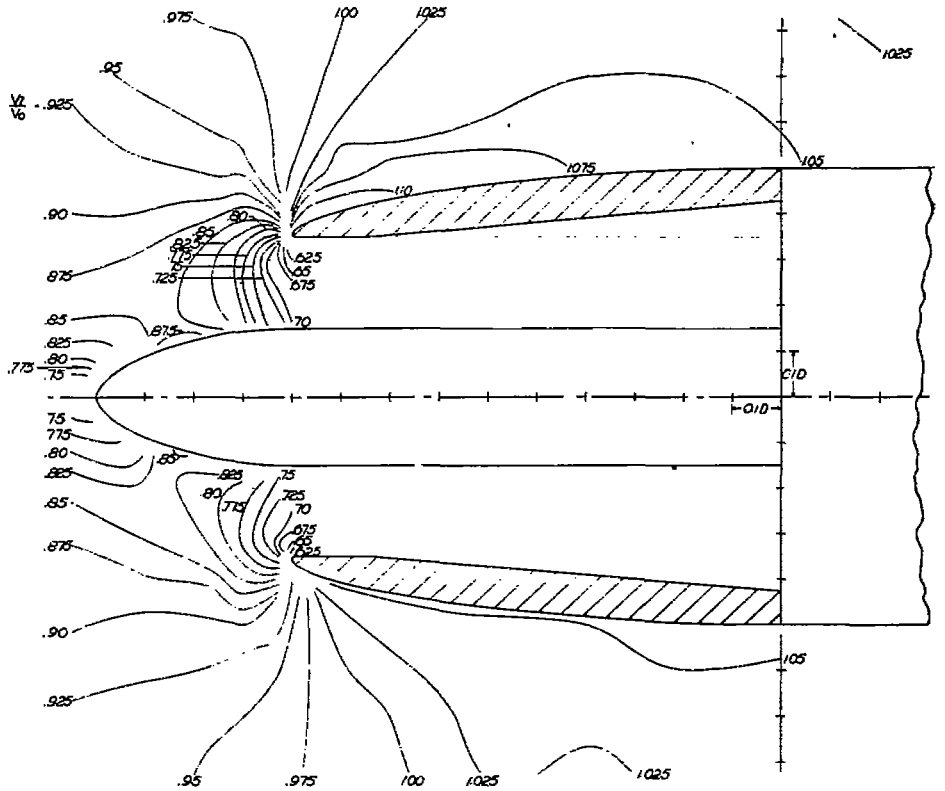

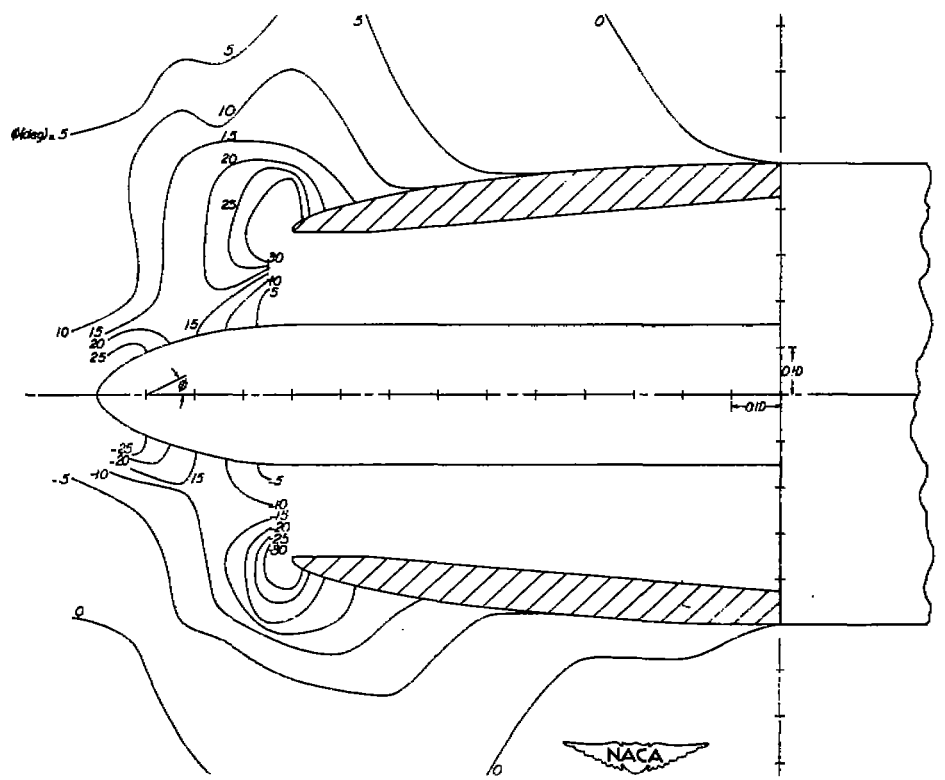

(b) $V_l/V_0 = 0.60$; $\alpha = 2.5°$.

Figure 11.- Continued.

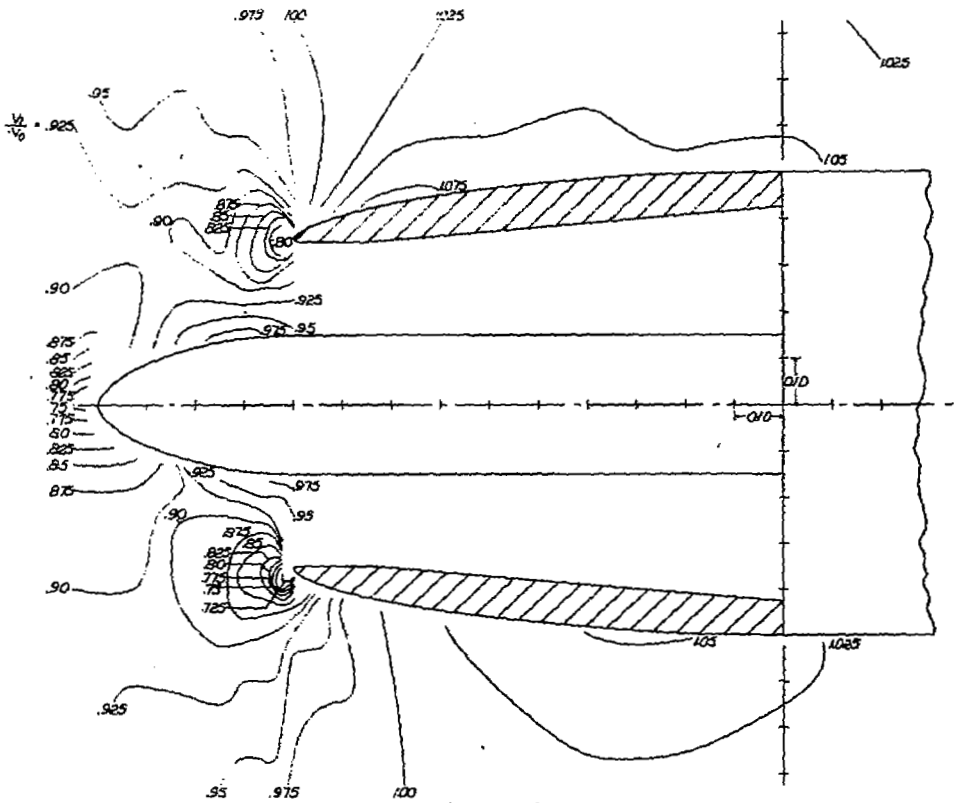

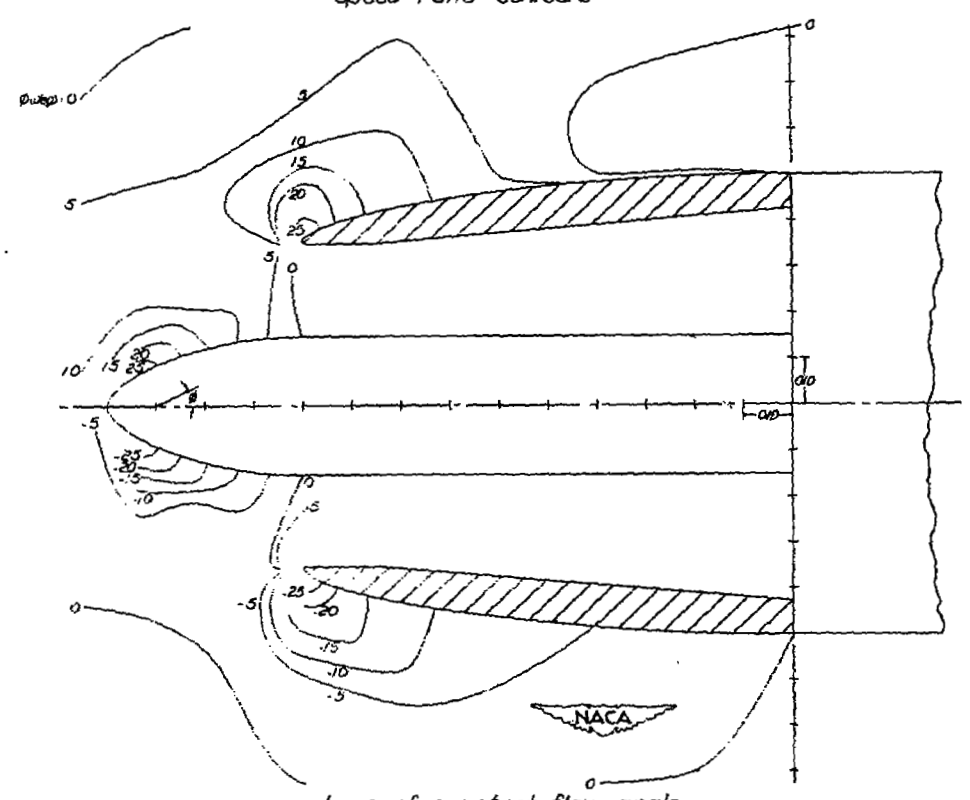

(c) $V_l/V_o = .091$; $\alpha = 25°$.

Figure 11.- Continued.

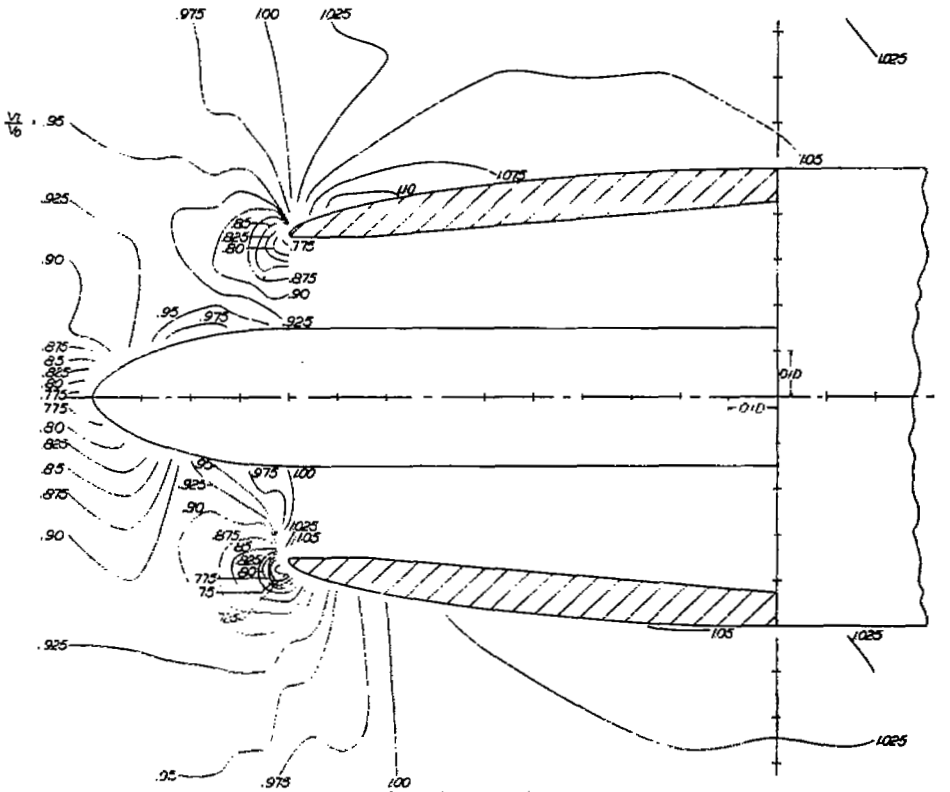

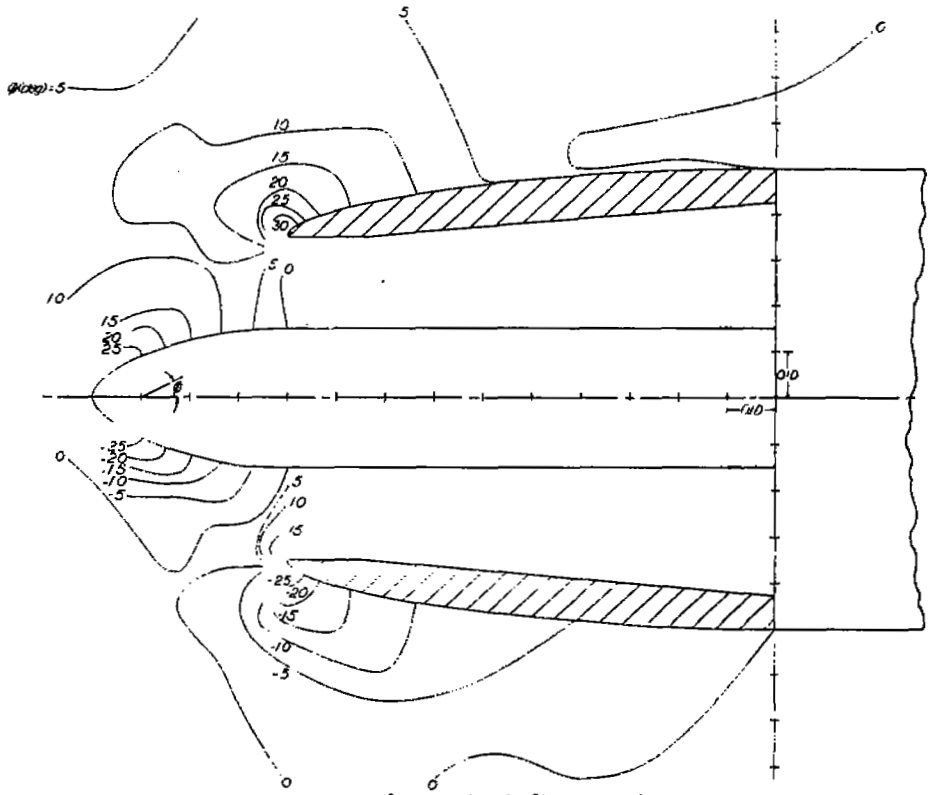

(d) $V_l/V_0 = 0.91$; $\alpha = 5°$.

Figure 11.-Continued.

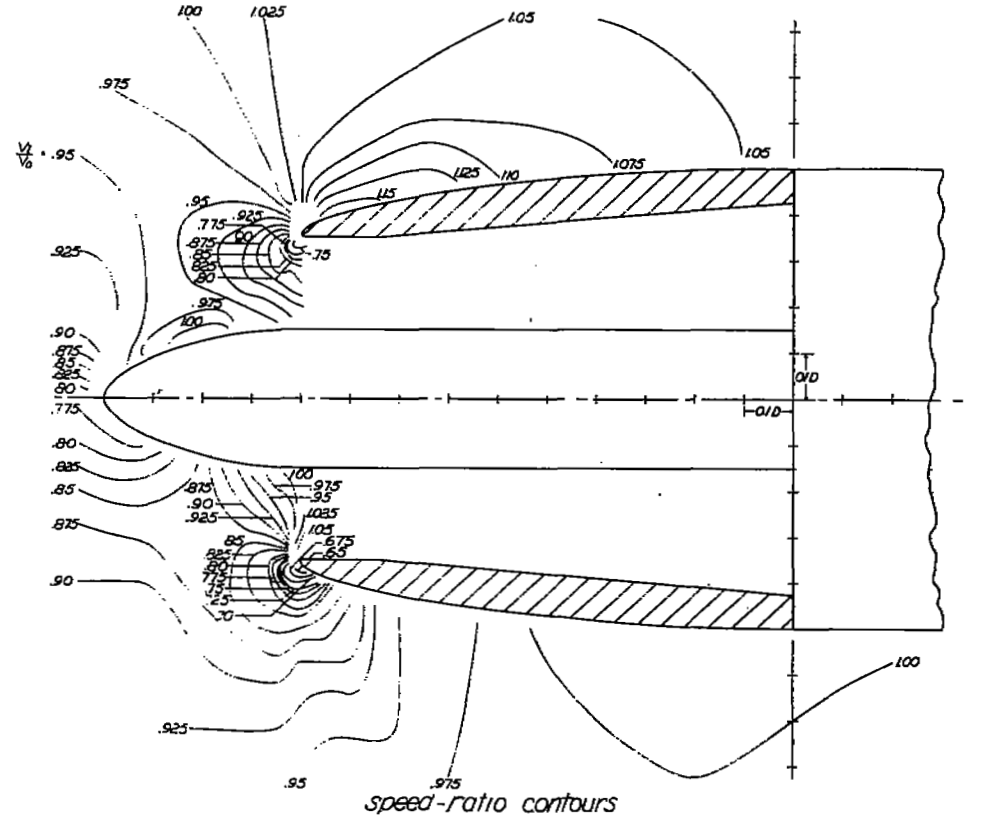

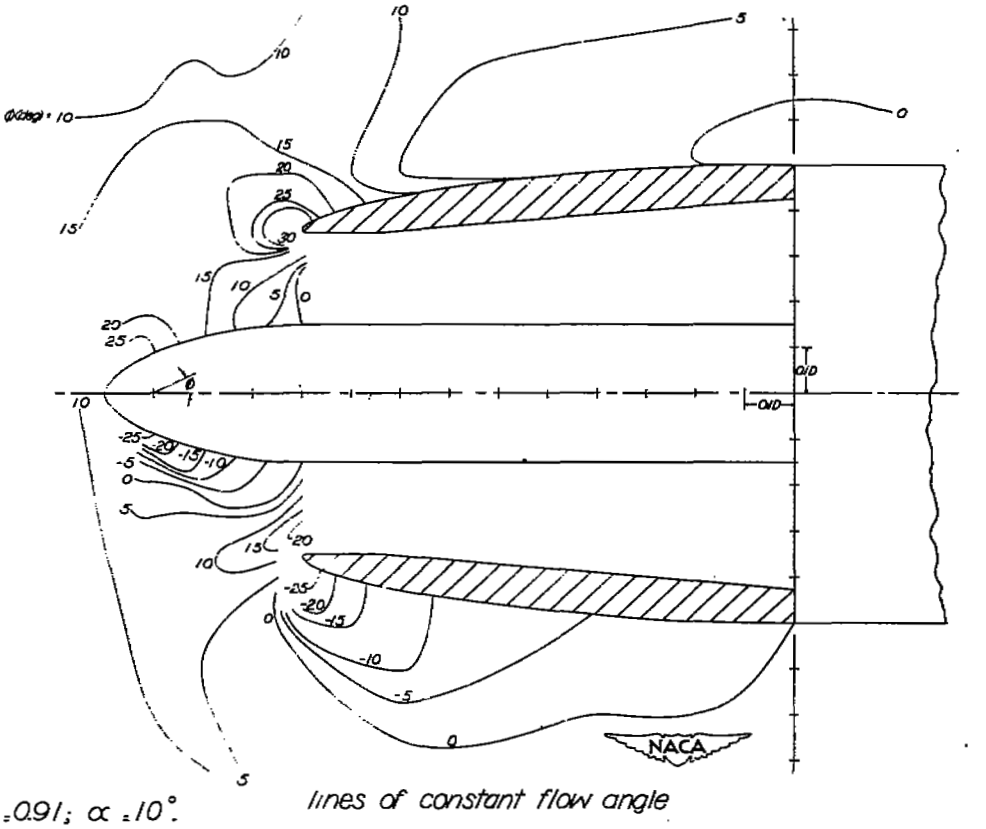

(e) $V_l/V_0 = 0.91$; $\alpha = 10°$.

Figure 11.- Concluded.

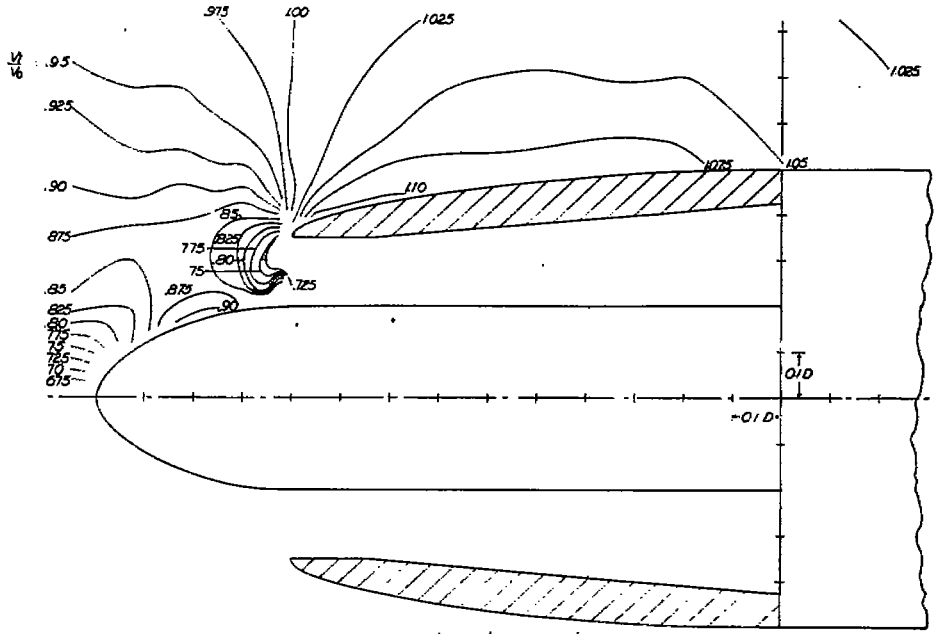

speed-ratio contours

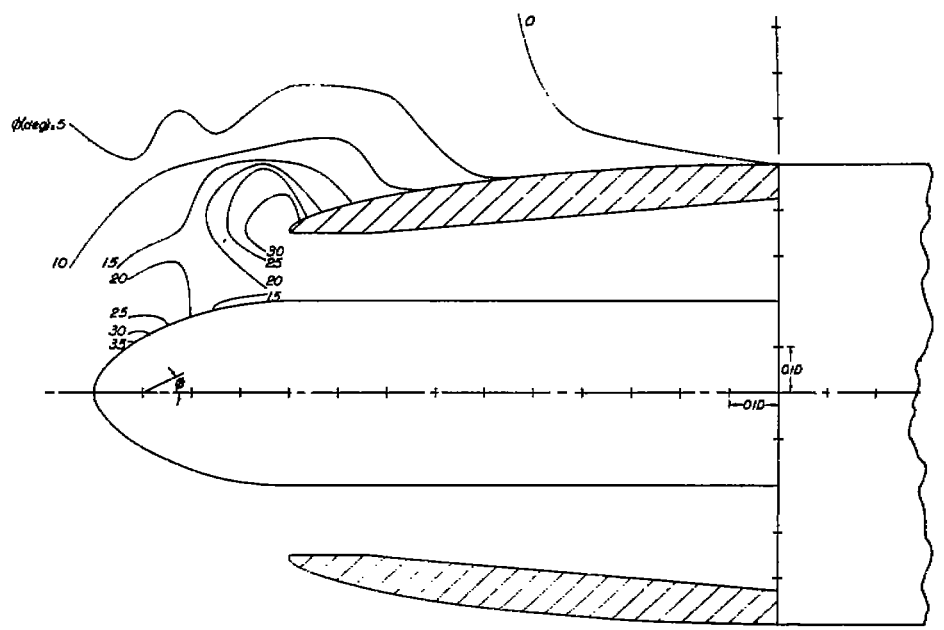

lines of constant flow angle NACA

(a) $V_l/V_0 = 0.63$; $\alpha = 0°$.

Figure 12.-Speed and direction of flow in vicinity of NACA 1-70-100 cowling with NACA 1-40-040 spinner.

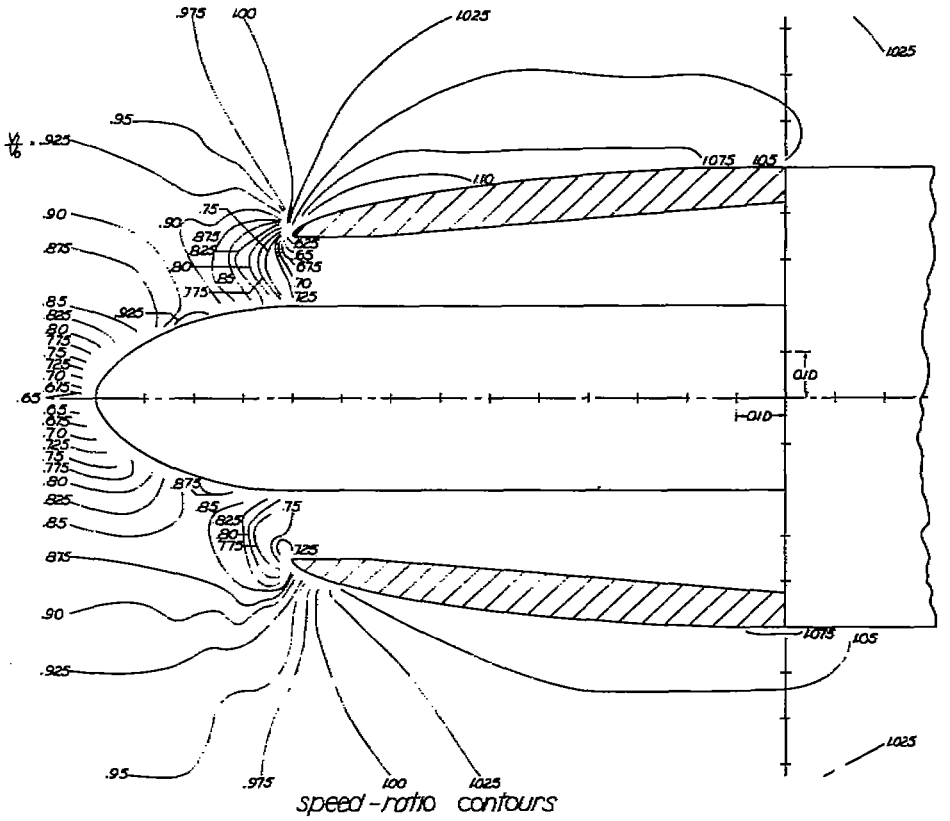

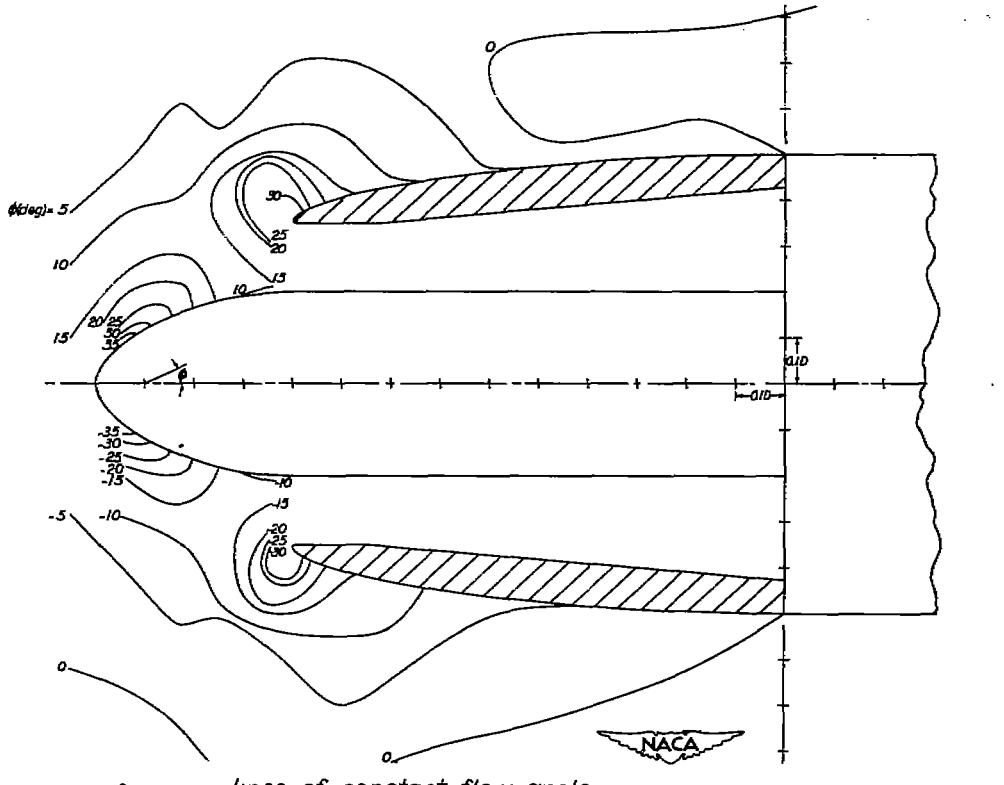

(b) $V_l/V_0 = .066$; $\alpha = 25°$

Figure 12.-Continued.

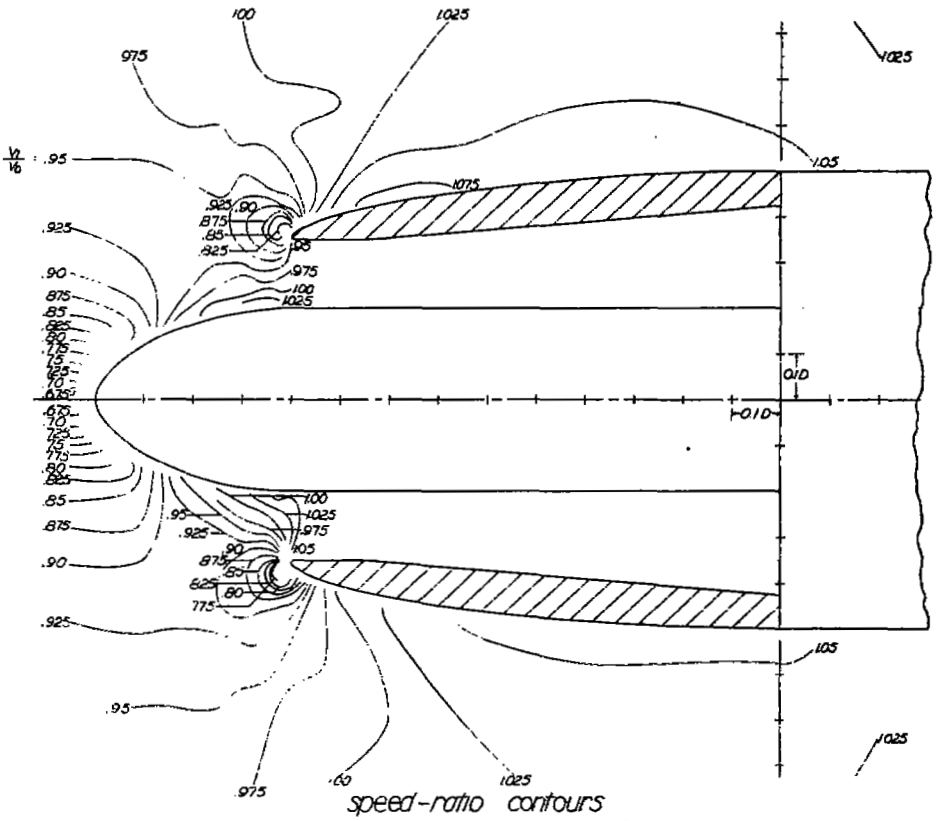

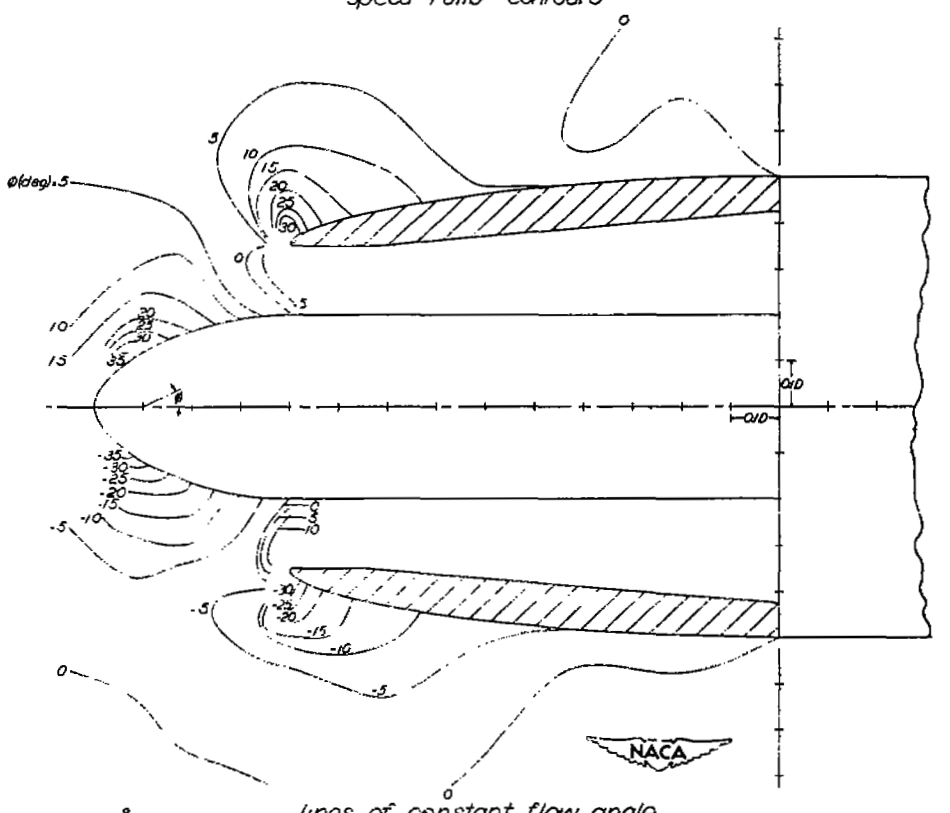

(c) $V_l/V_0 = 0.99$; $\alpha = 2.5°$.

Figure 12.-Continued.

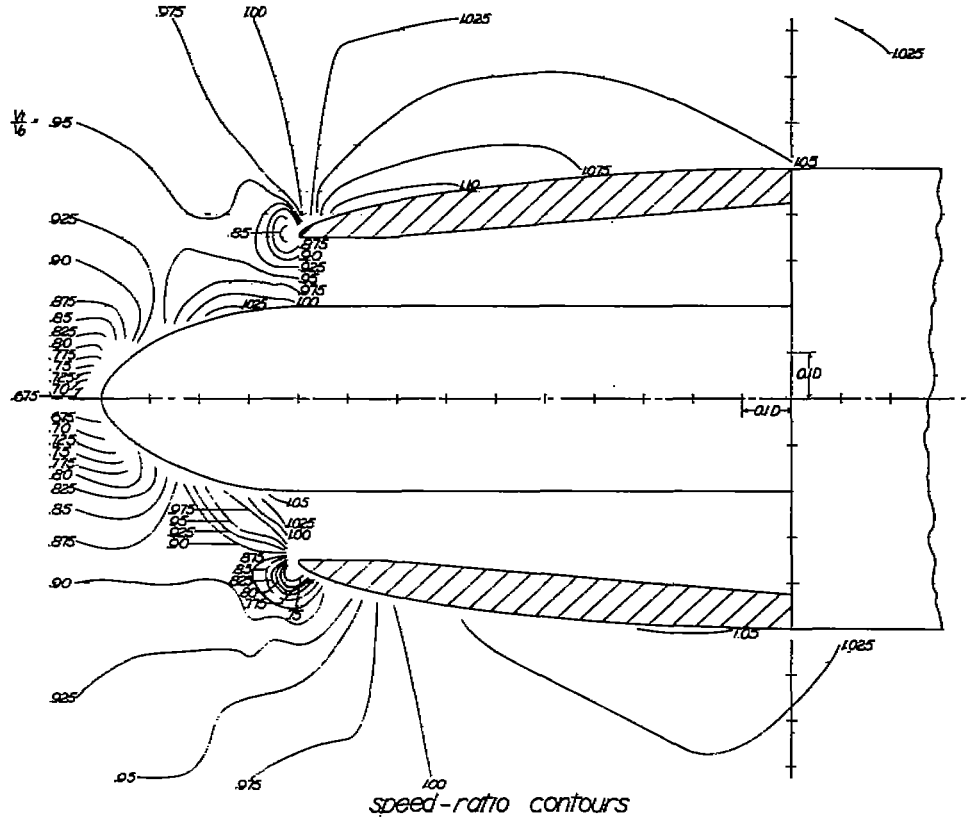

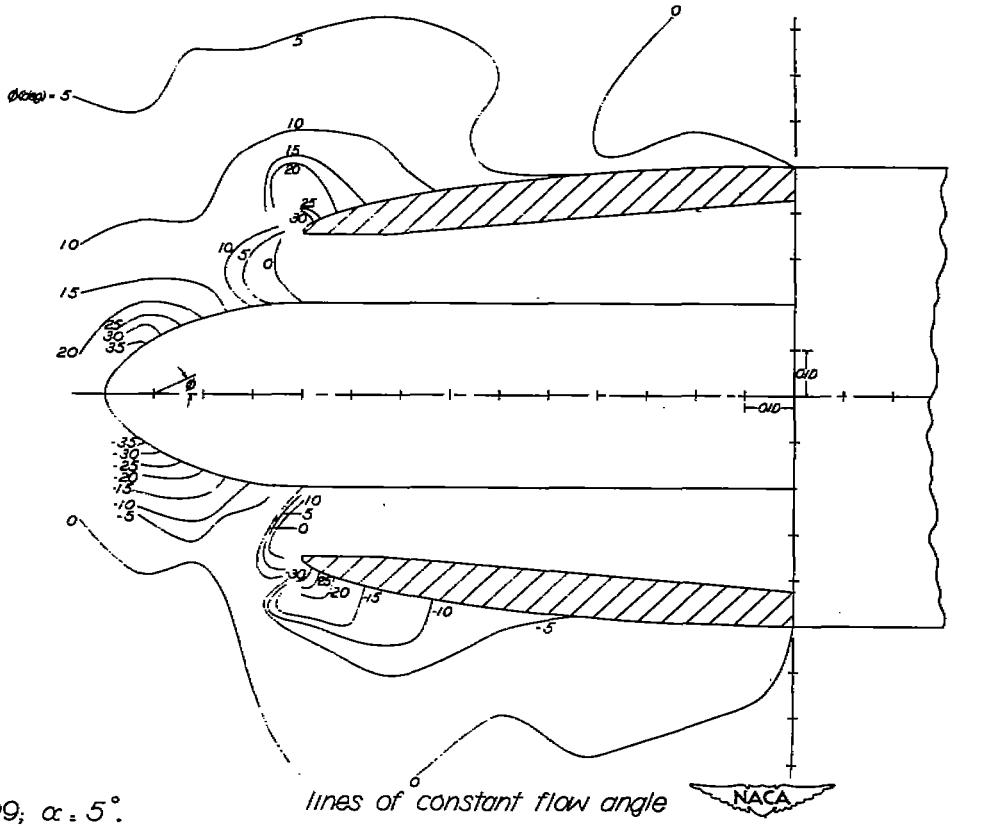

(d) $V_l/V_0 = .099$; $\alpha = 5°$.

Figure 12.-Continued.

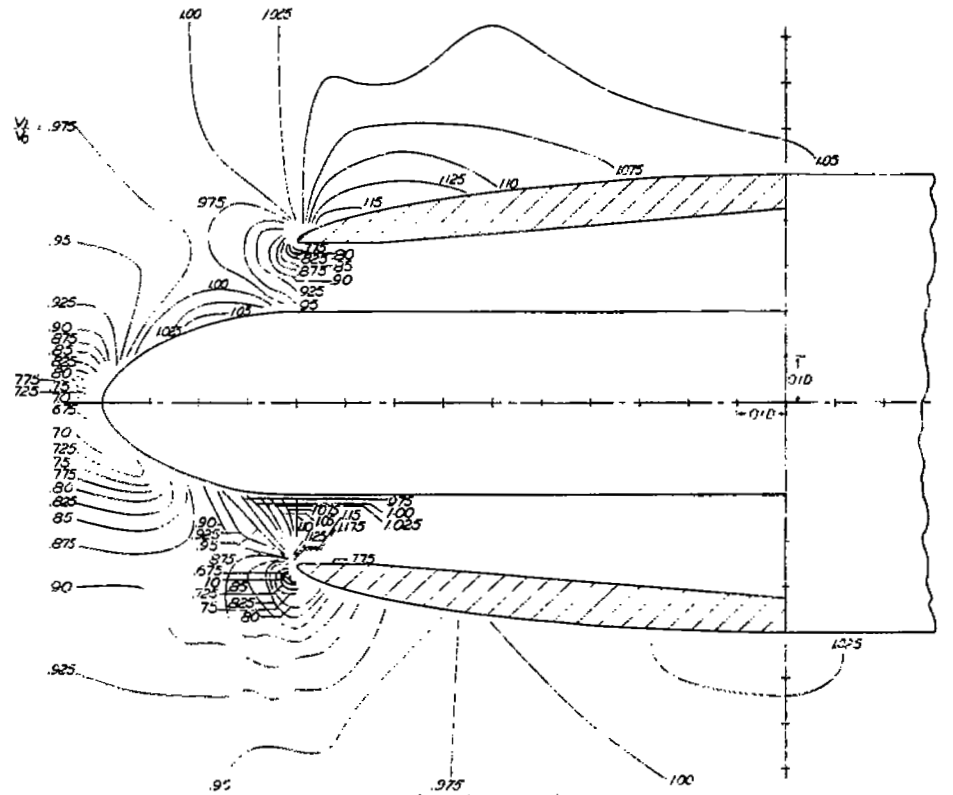

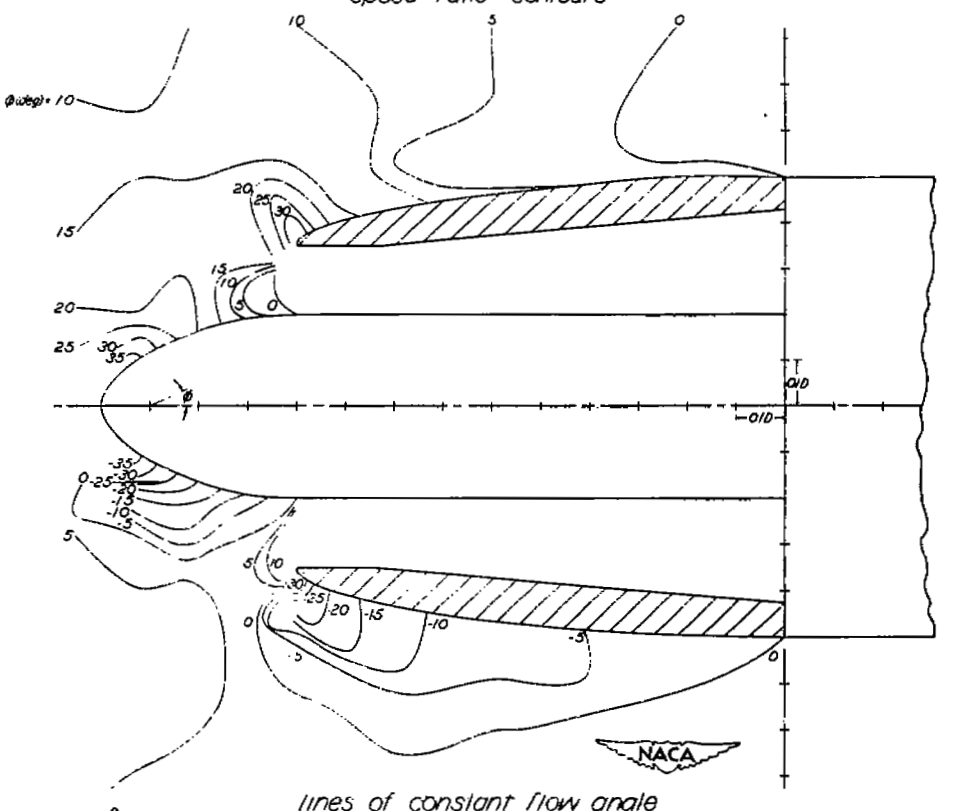

(e) $V_l/V_0 = .099$; $\alpha = 10°$.

Figure 12.- Concluded.

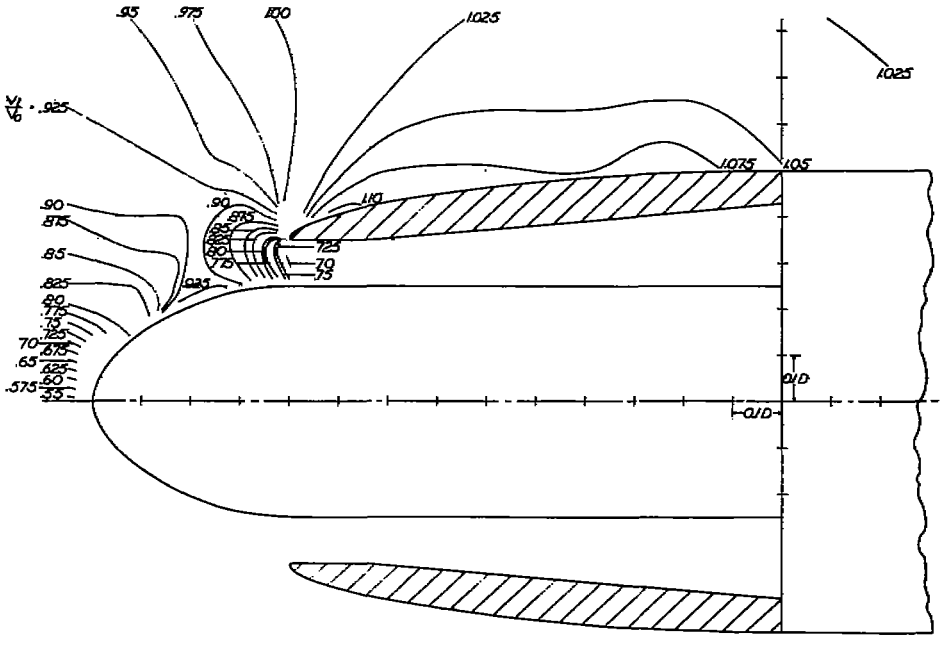

speed-ratio contours

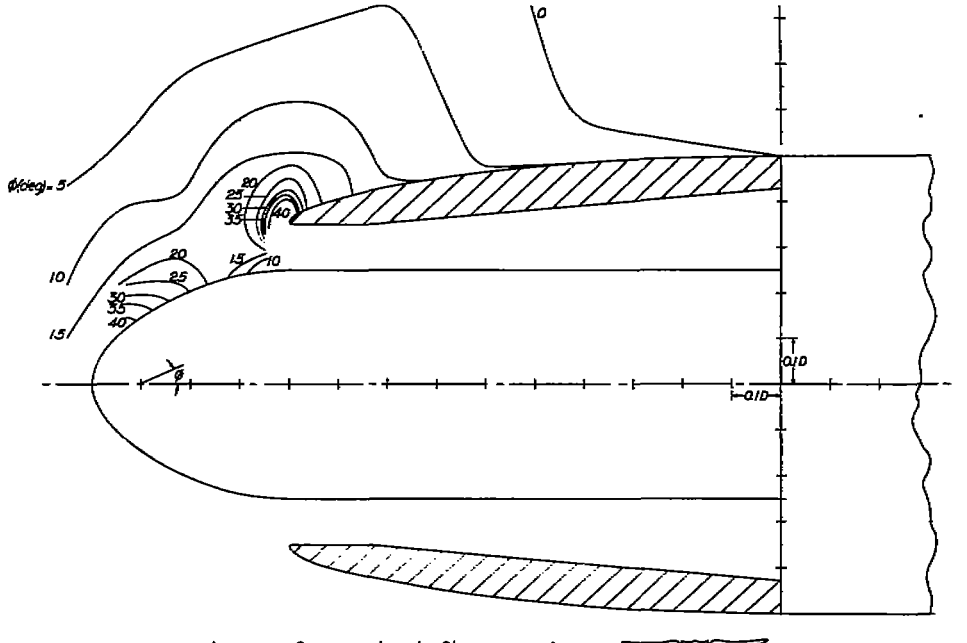

lines of constant flow angle NACA

(a) $V_i/V_0 = 0.62$; $\alpha = 0°$.

Figure 13.-Speed and direction of flow in vicinity of NACA 1-70-100 cowling with NACA 1-50-040 spinner.

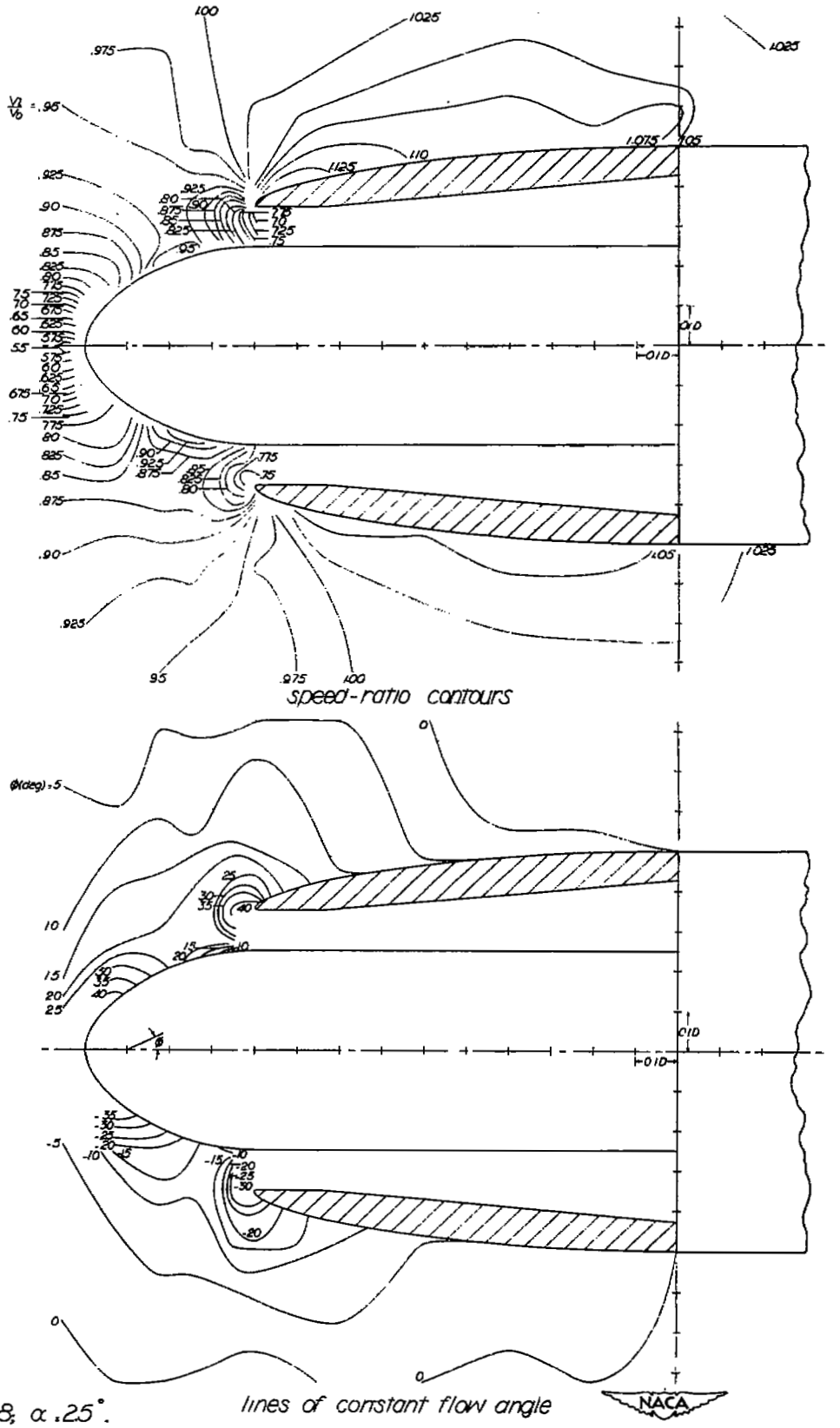

(b) $V_i/V_0 = 0.68$; α .25°.

Figure 13.-Continued.

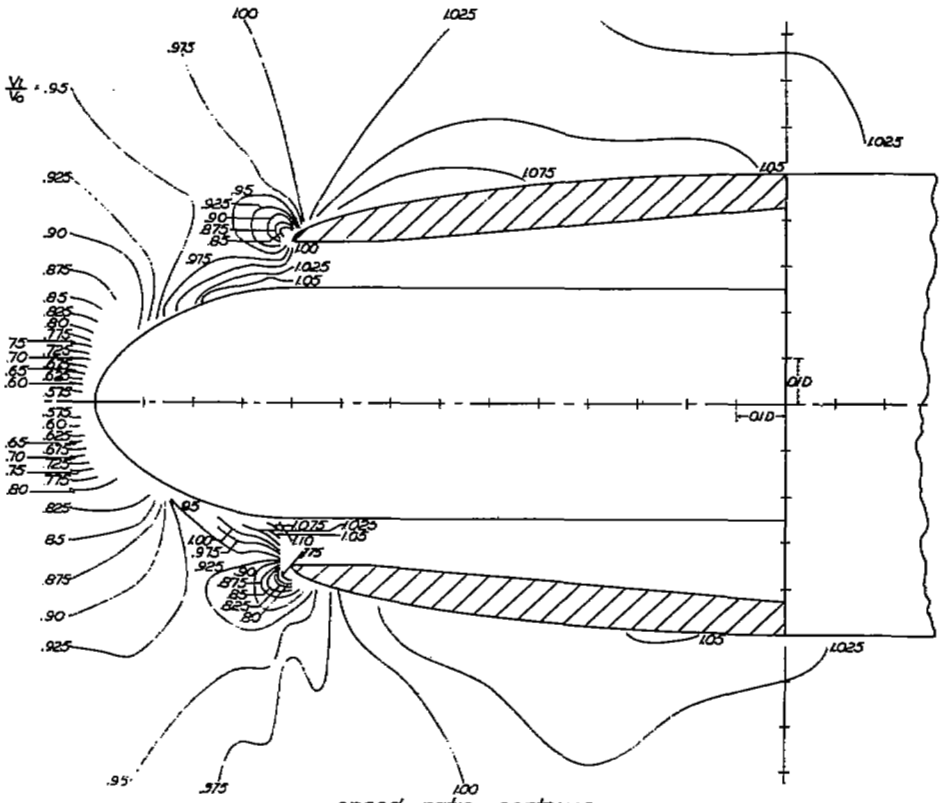

speed-ratio contours

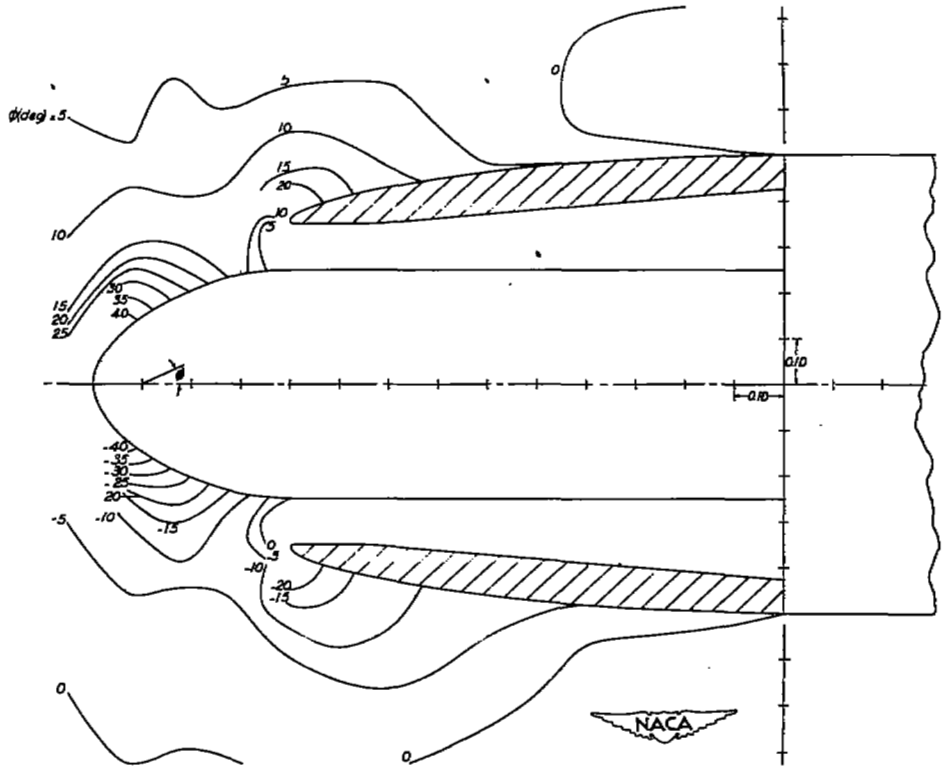

lines of constant flow angle

(c) $V_l/V_0 = 1.03$; $\alpha = 2.5°$.

Figure 13.-Continued.

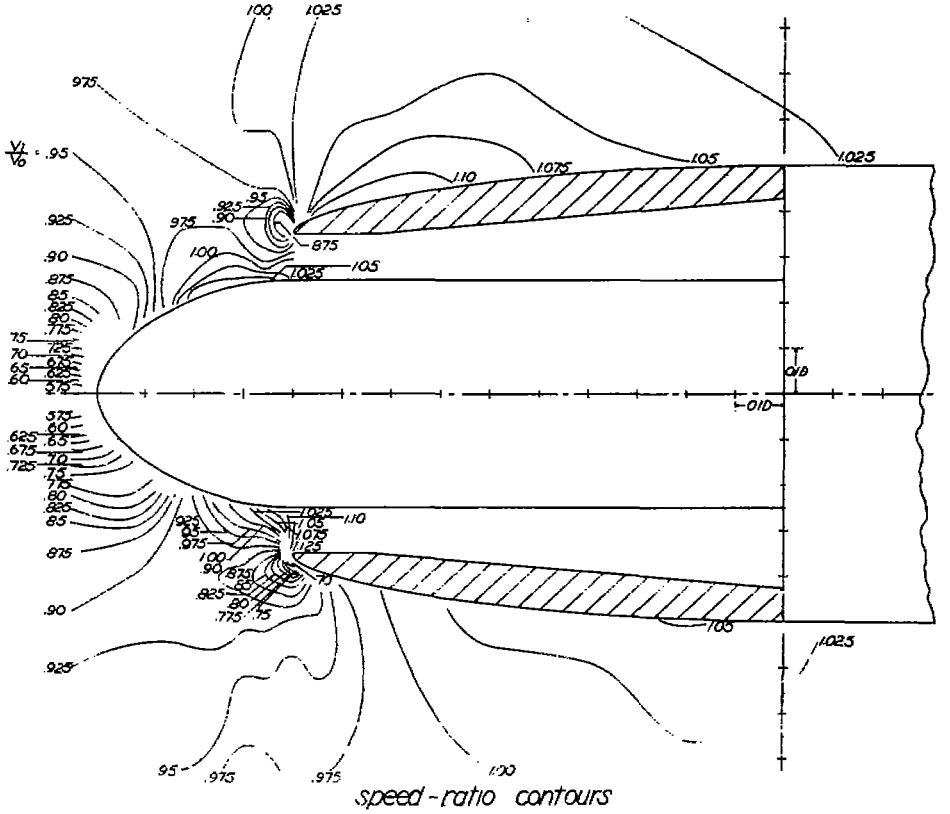

Speed-ratio contours

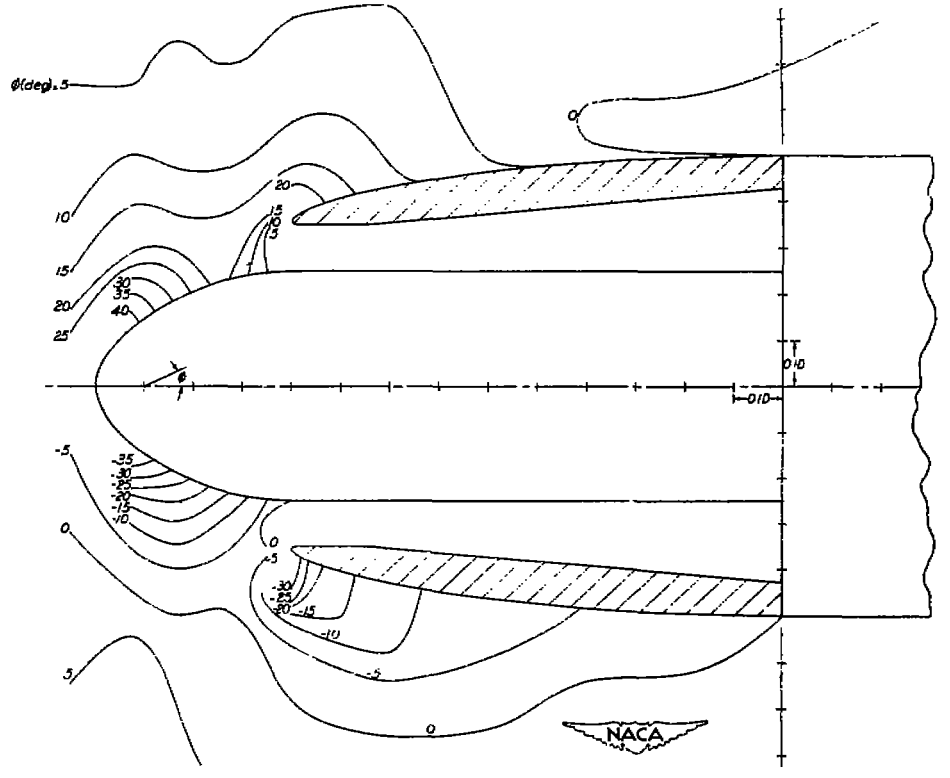

Lines of constant flow angle

(d) $V_i/V_o = 1.03$; $\alpha = 5°$.

Figure 13.- Continued.

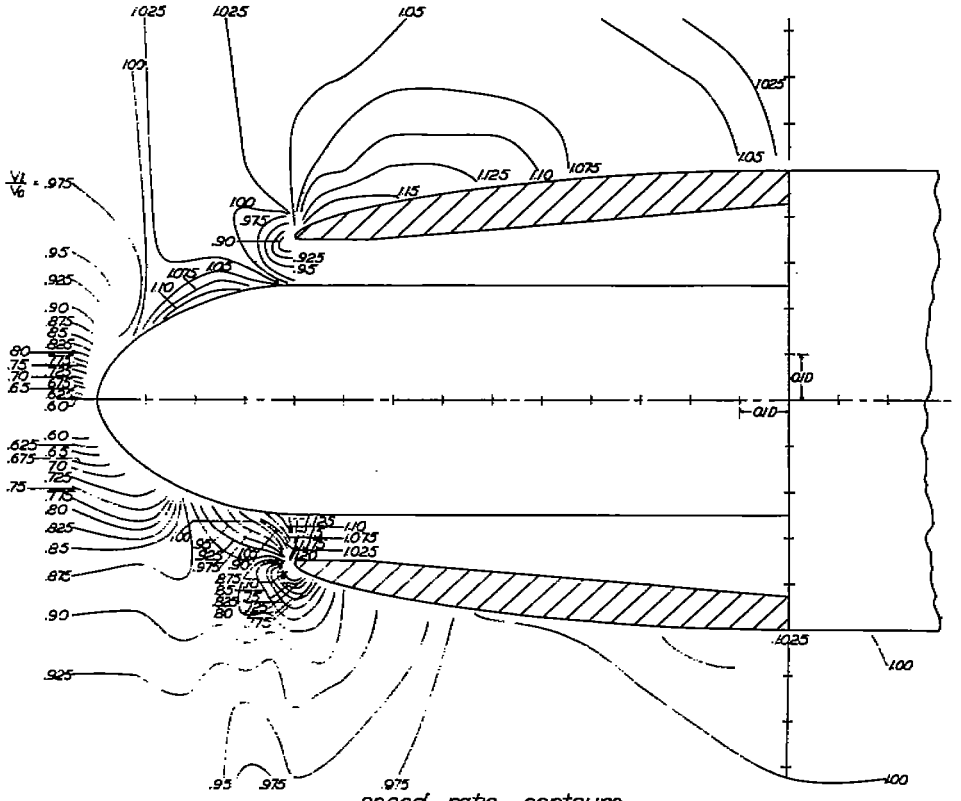

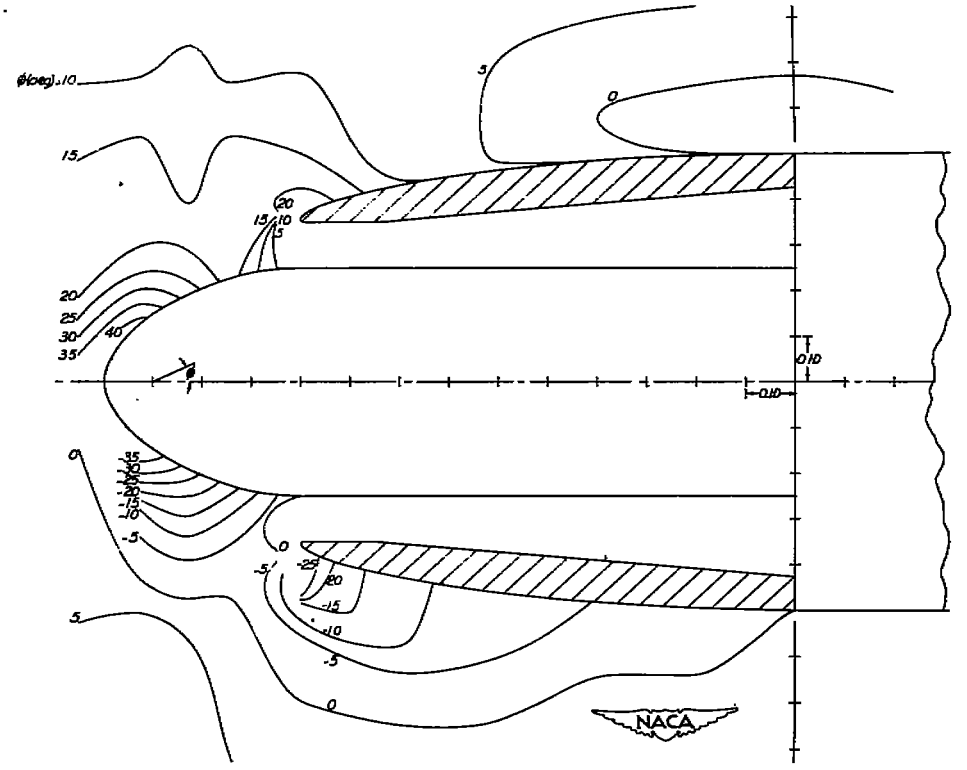

(e) $V_l/V_0 = 1.03$; $\alpha = 10°$.

Figure 13.-Concluded.

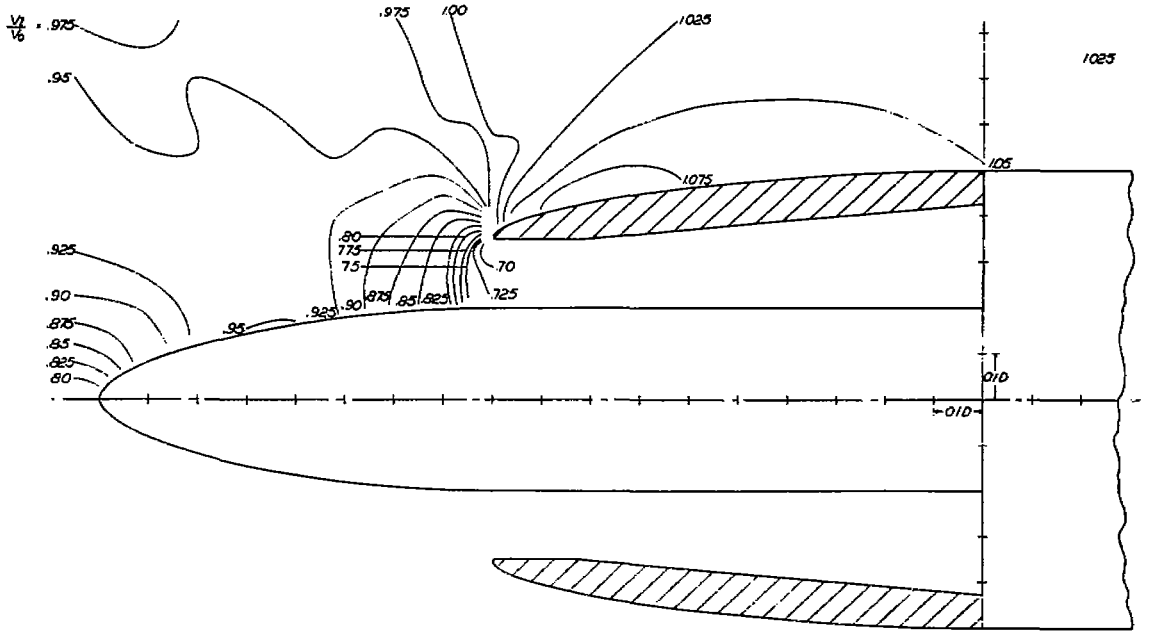

speed-ratio contours

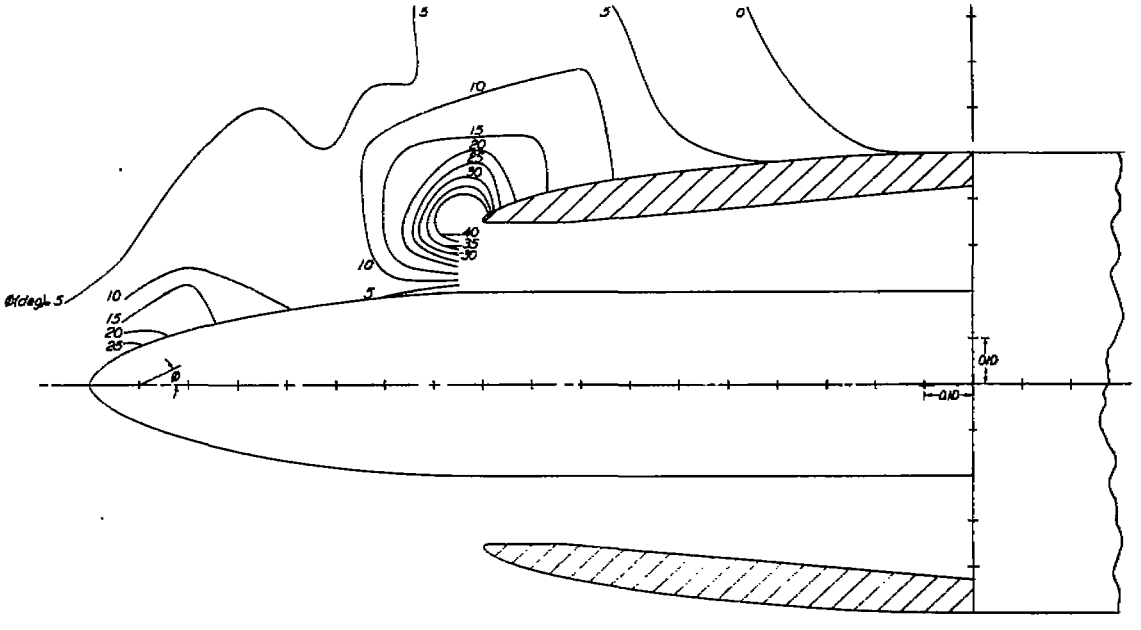

lines of constant flow angle

(a) $V_l/V_0 = 0.61$; $\alpha = 0°$.

Figure 14.-Speed and direction of flow in vicinity of NACA 1-70-100 cowling with NACA 1-40-080 spinner.

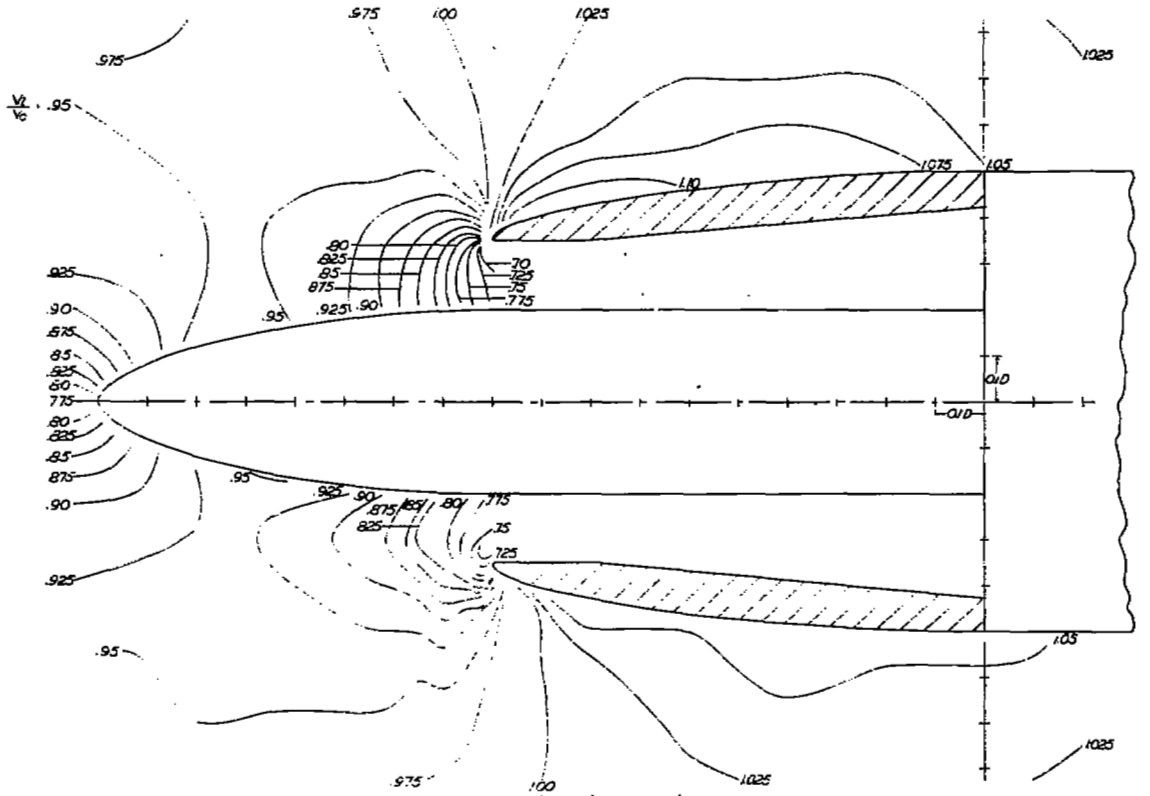

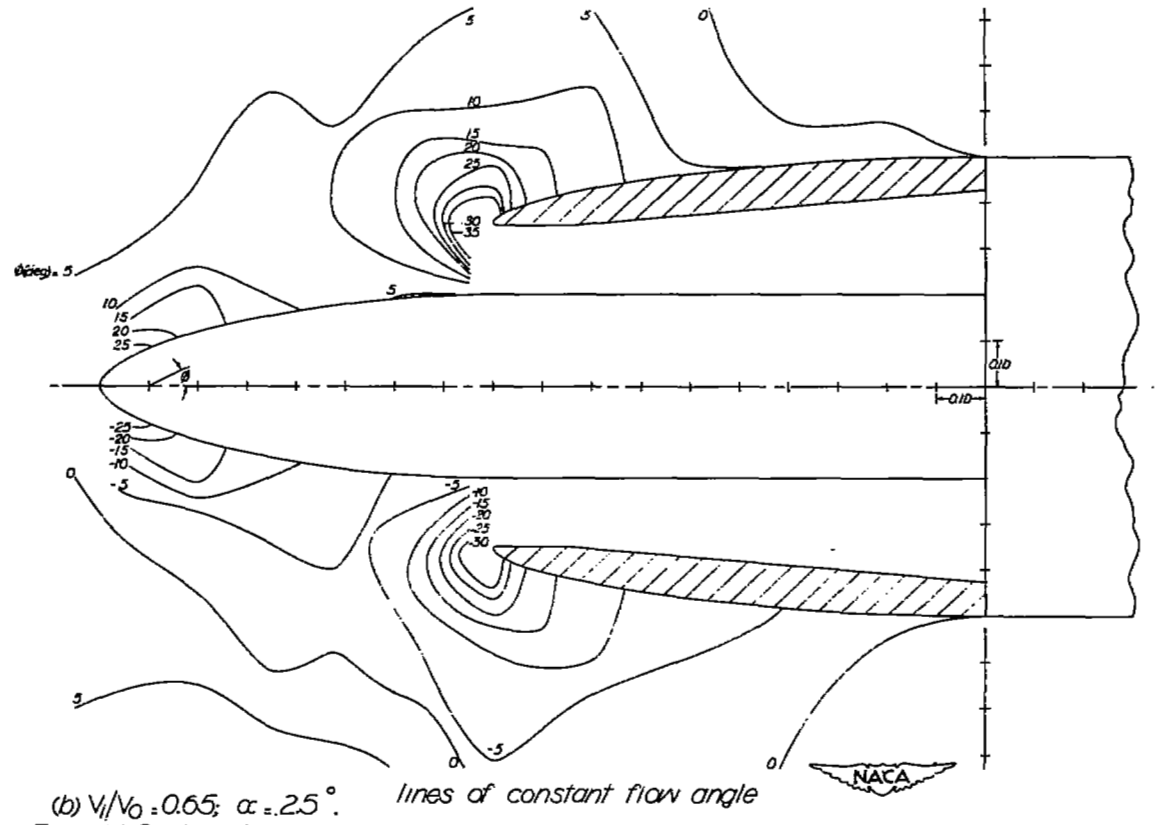

(b) $V_l/V_0 = 0.65$; $\alpha = .2.5°$.

Figure 14.-Continued.

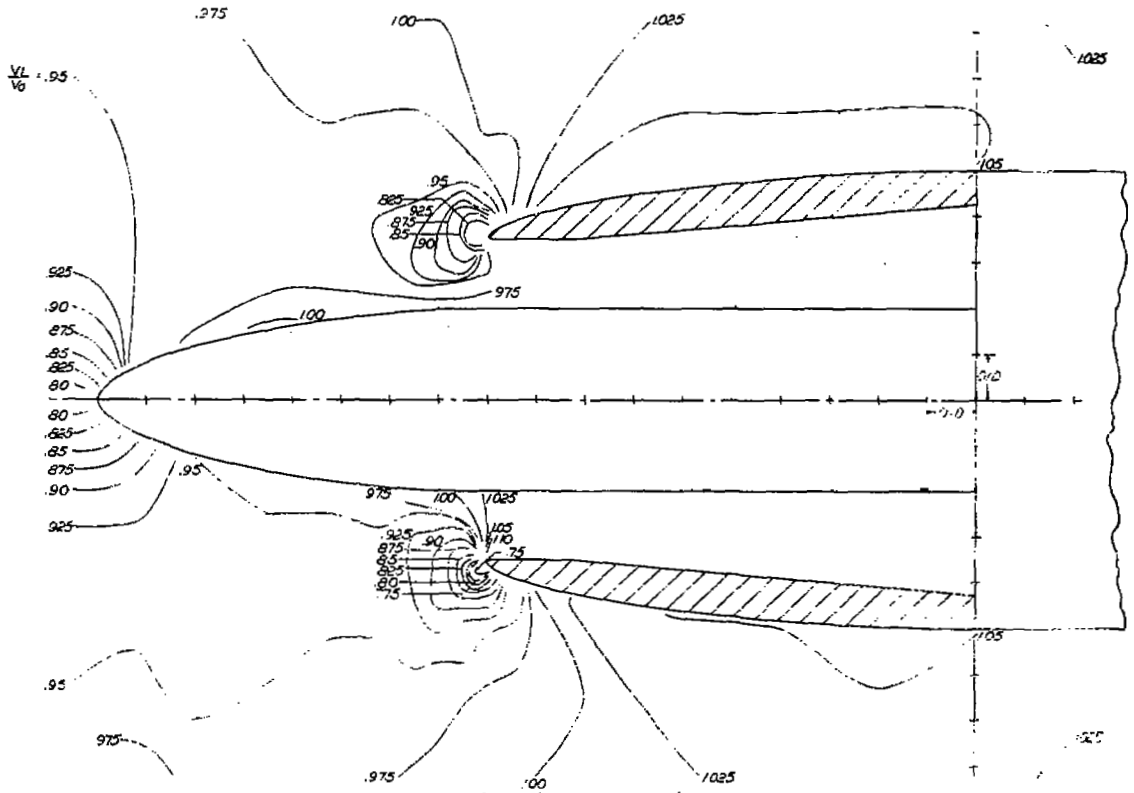

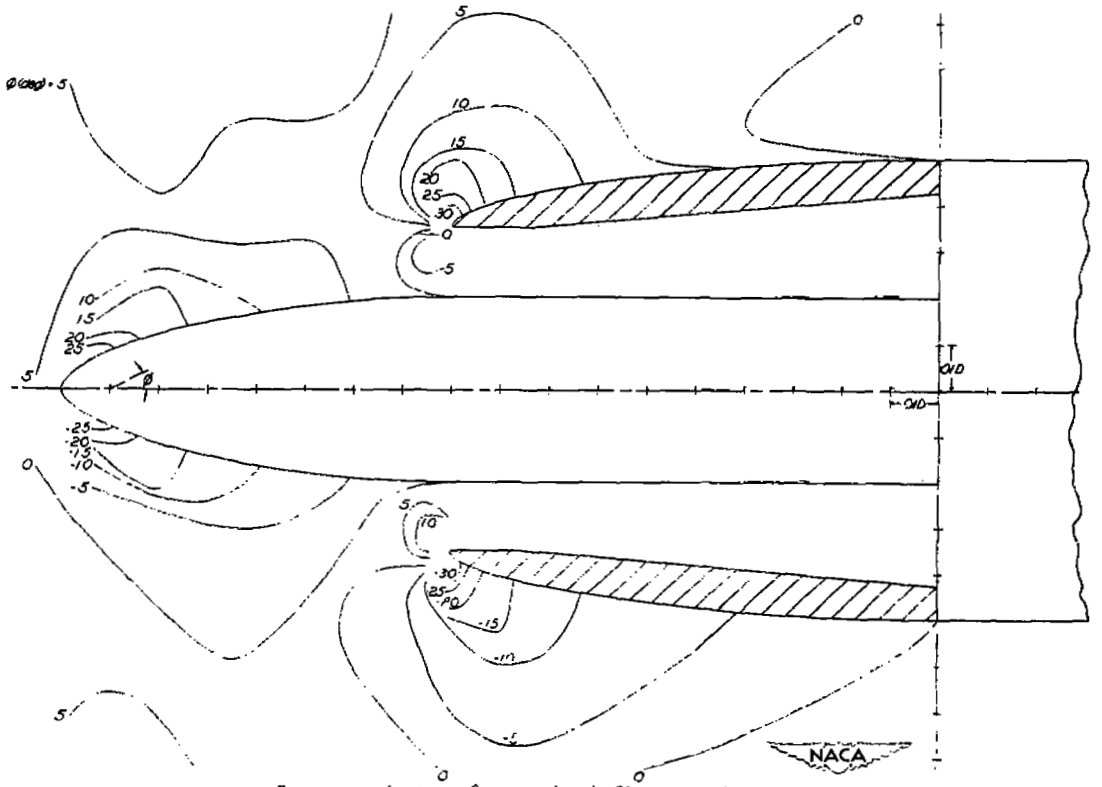

(c) $V_1/V_0 = 1.00$; $\alpha = 2.5°$.

Figure 14.-Continued.

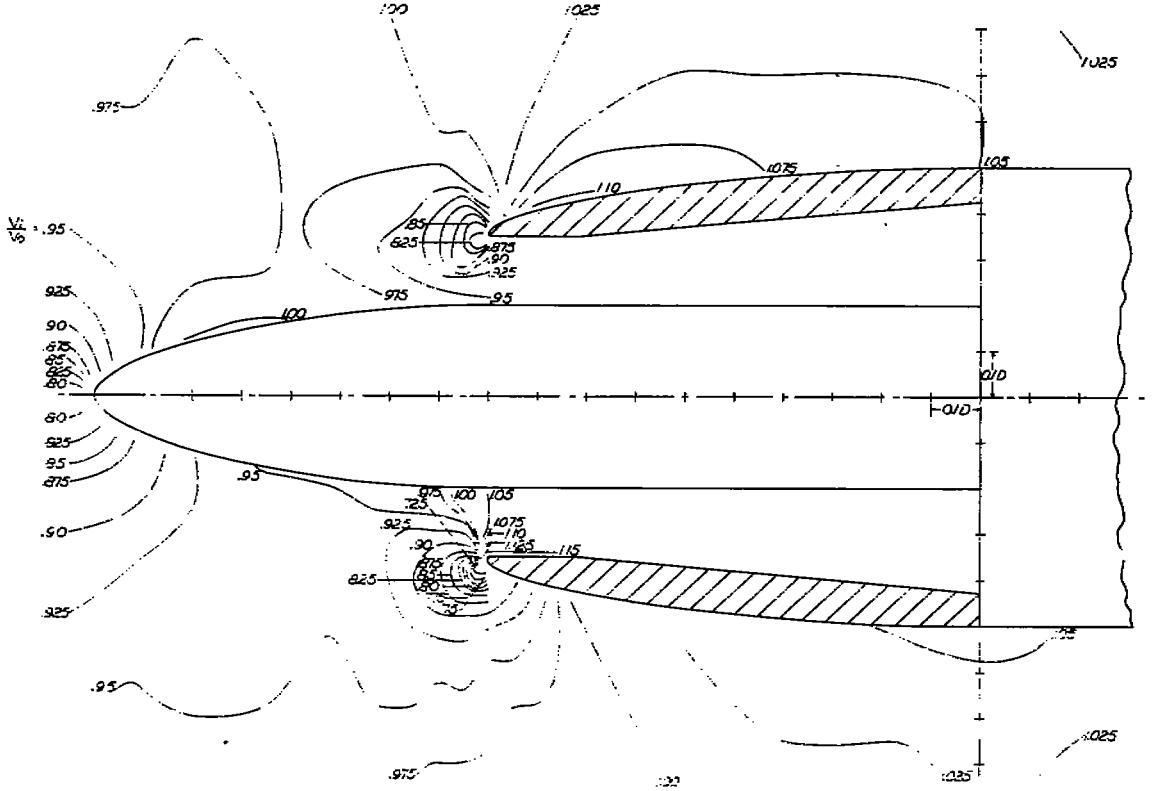

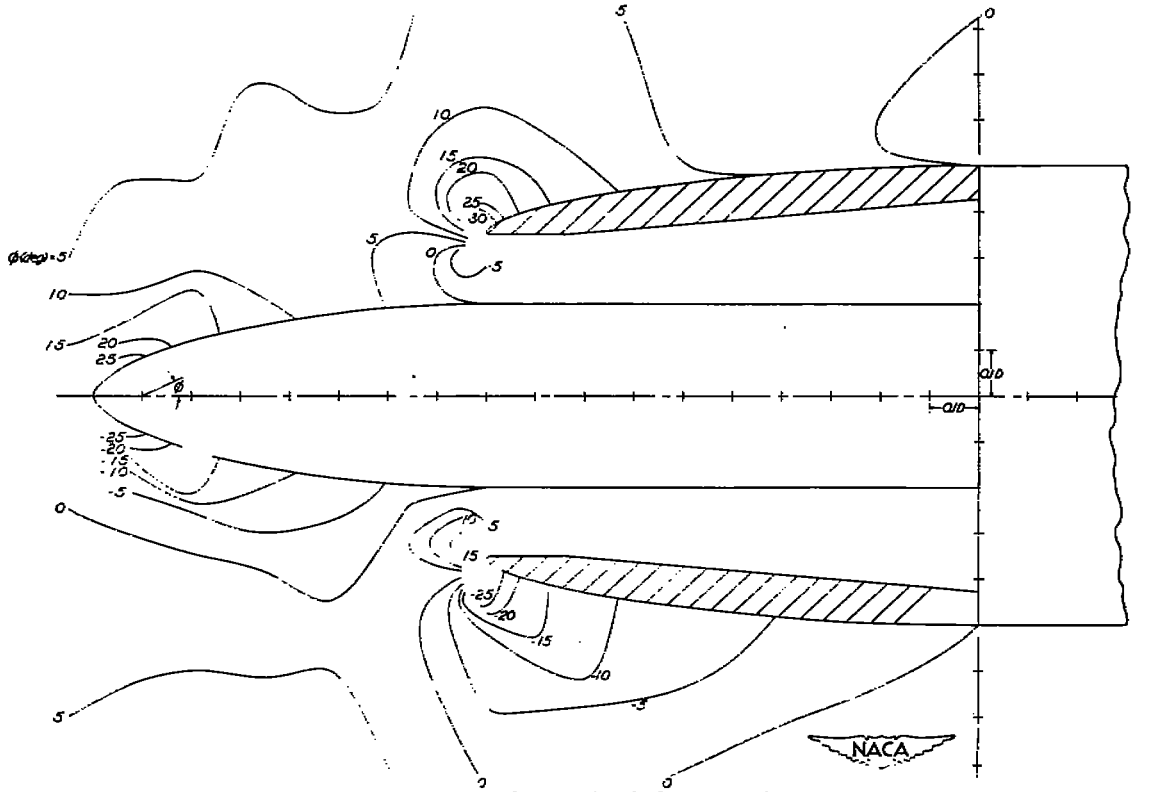

(d) $V_l/V_0 = 1.00$; $\alpha = 5°$

Figure 14.- Continued.

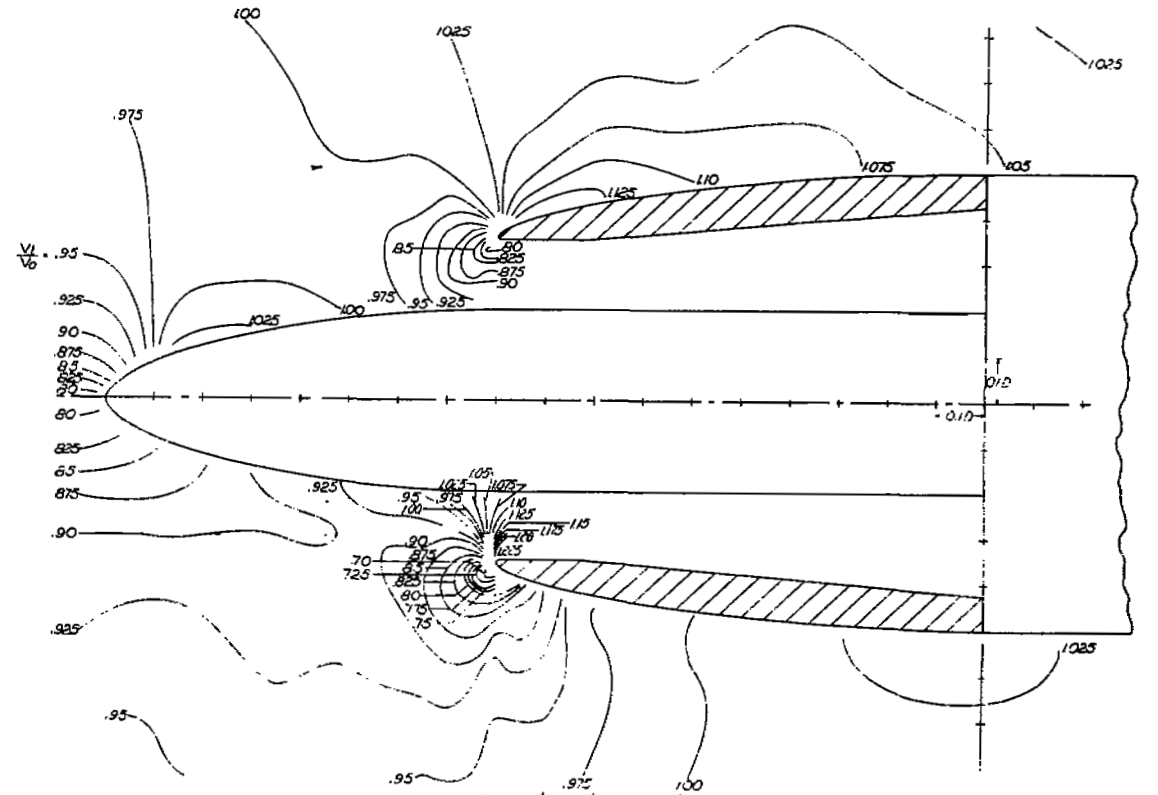

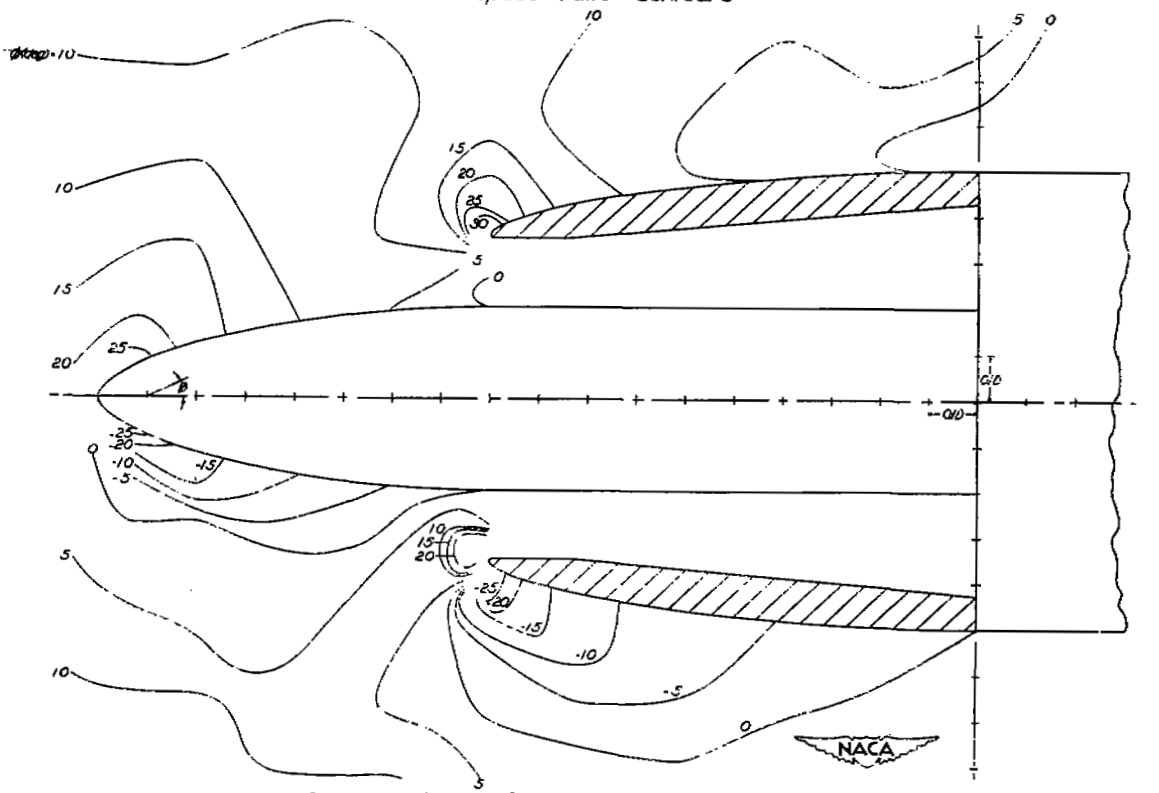

(e) $V_l/V_0 = 1.00$; $\alpha = 10^\circ$.

Figure 14.- Concluded.

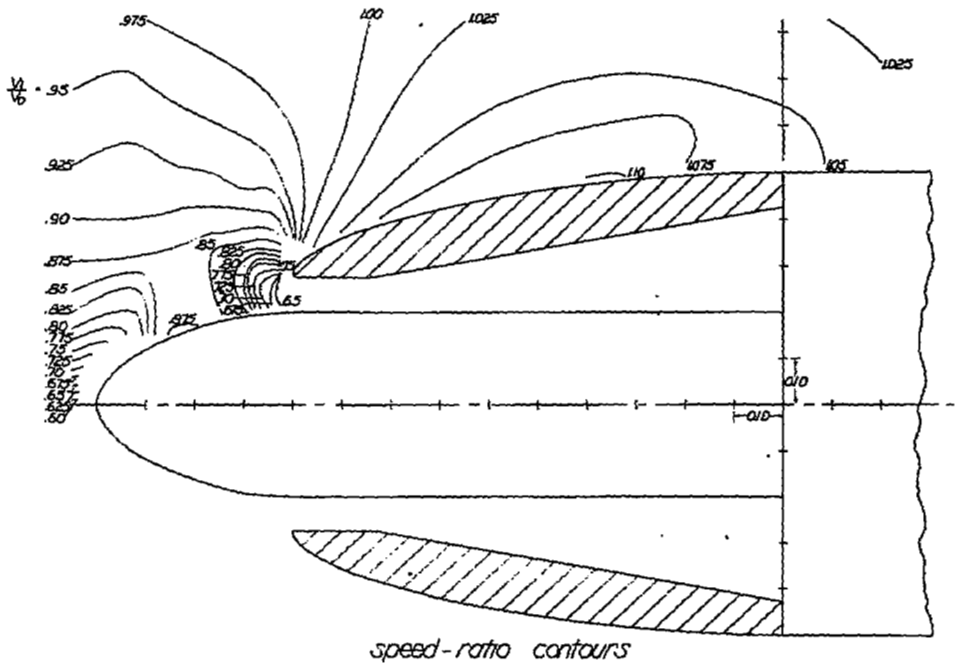

speed-ratio contours

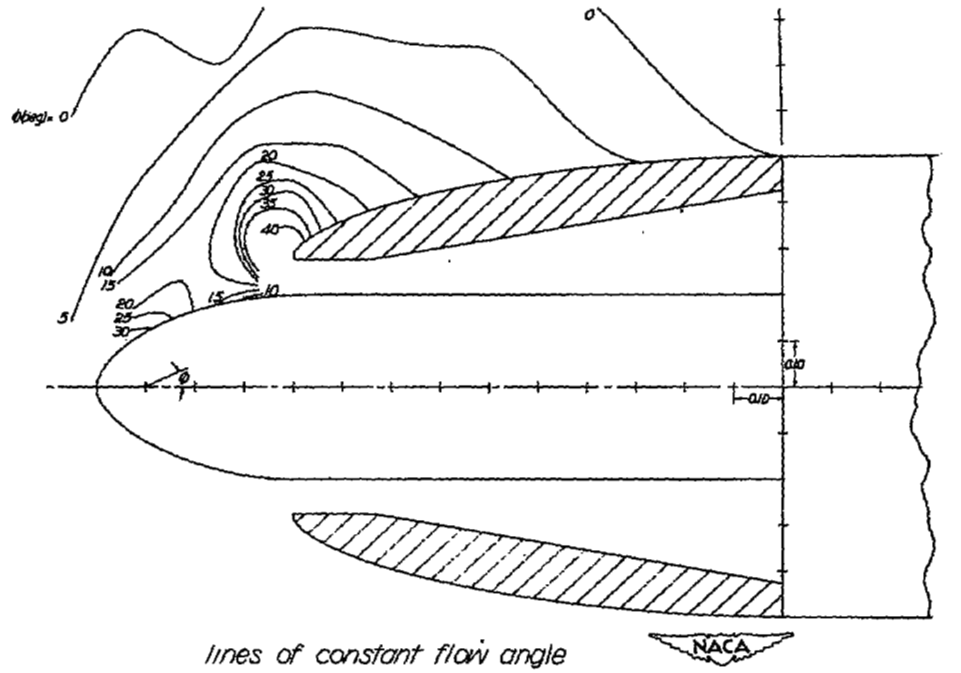

lines of constant flow angle

(a) $V_1/V_0 = 0.53$; $\alpha = 0°$.

Figure 15.- Speed and direction of flow in vicinity of NACA 1-55-100 cowling with NACA 1-40-040 spinner.

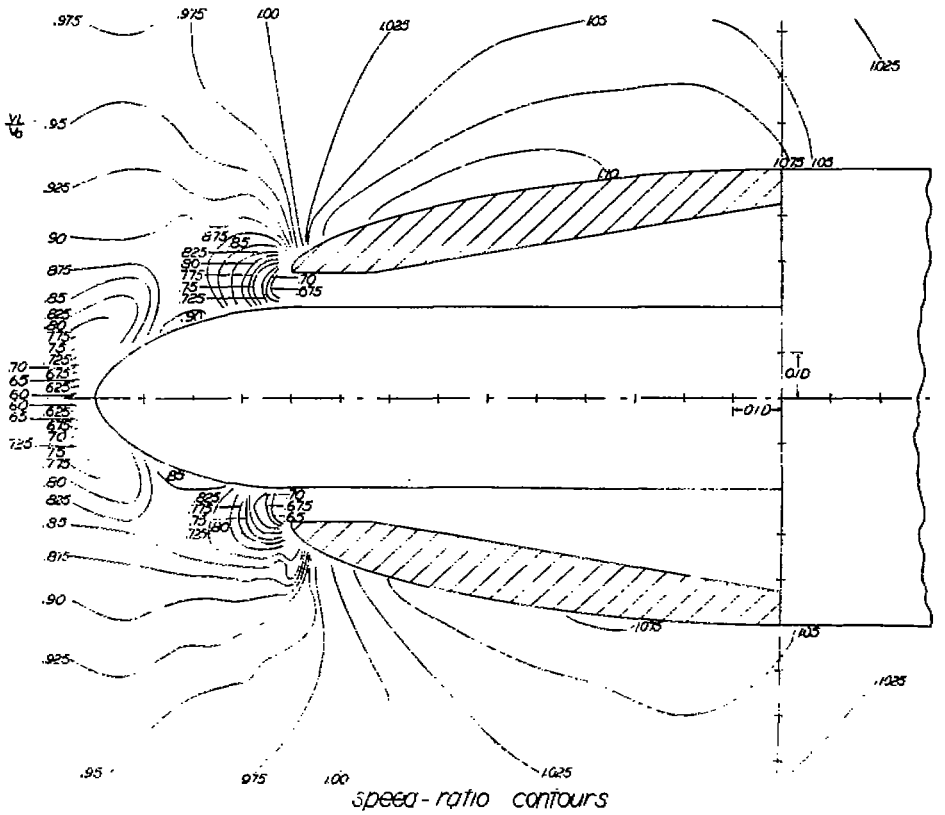

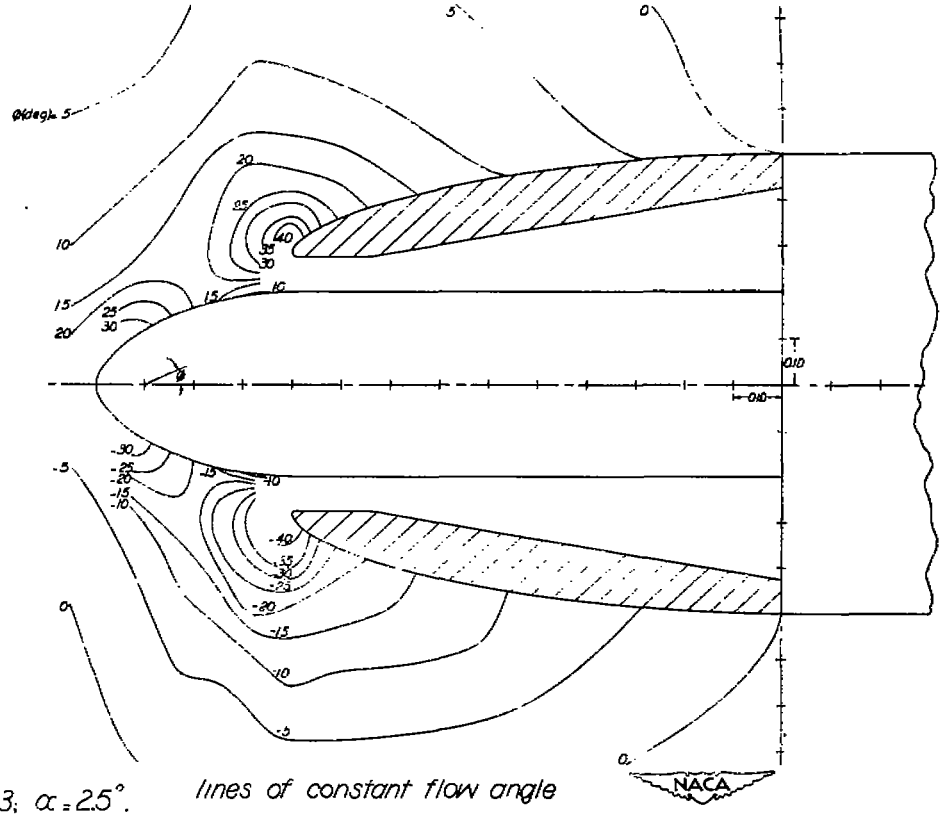

(b) $V_l/V_0 = 0.53$; $\alpha = 2.5°$.

Figure 15.-Continued.

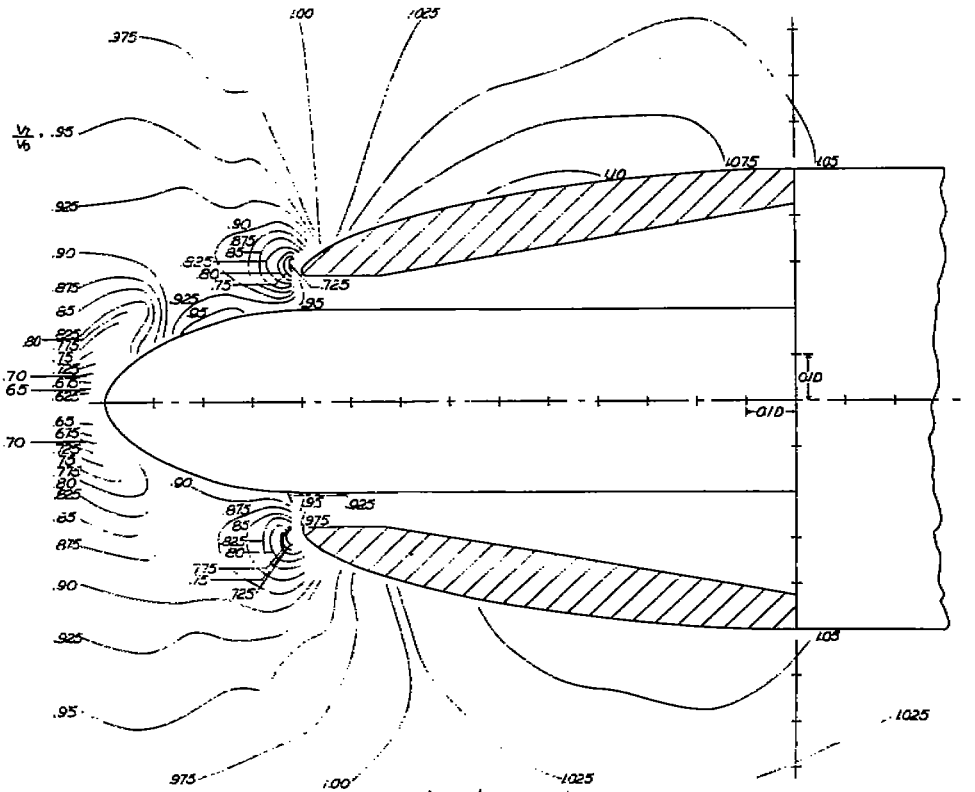

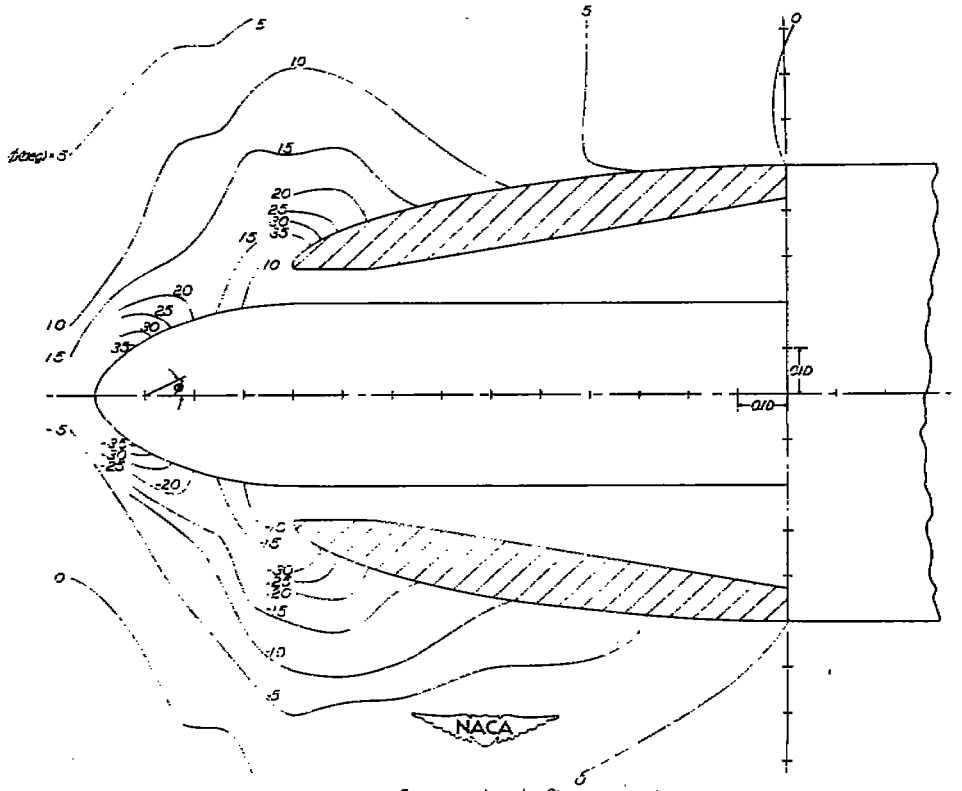

(c) $V_i/V_0 = 0.93$; $\alpha = 2.5°$.

Figure 15.-Continued.

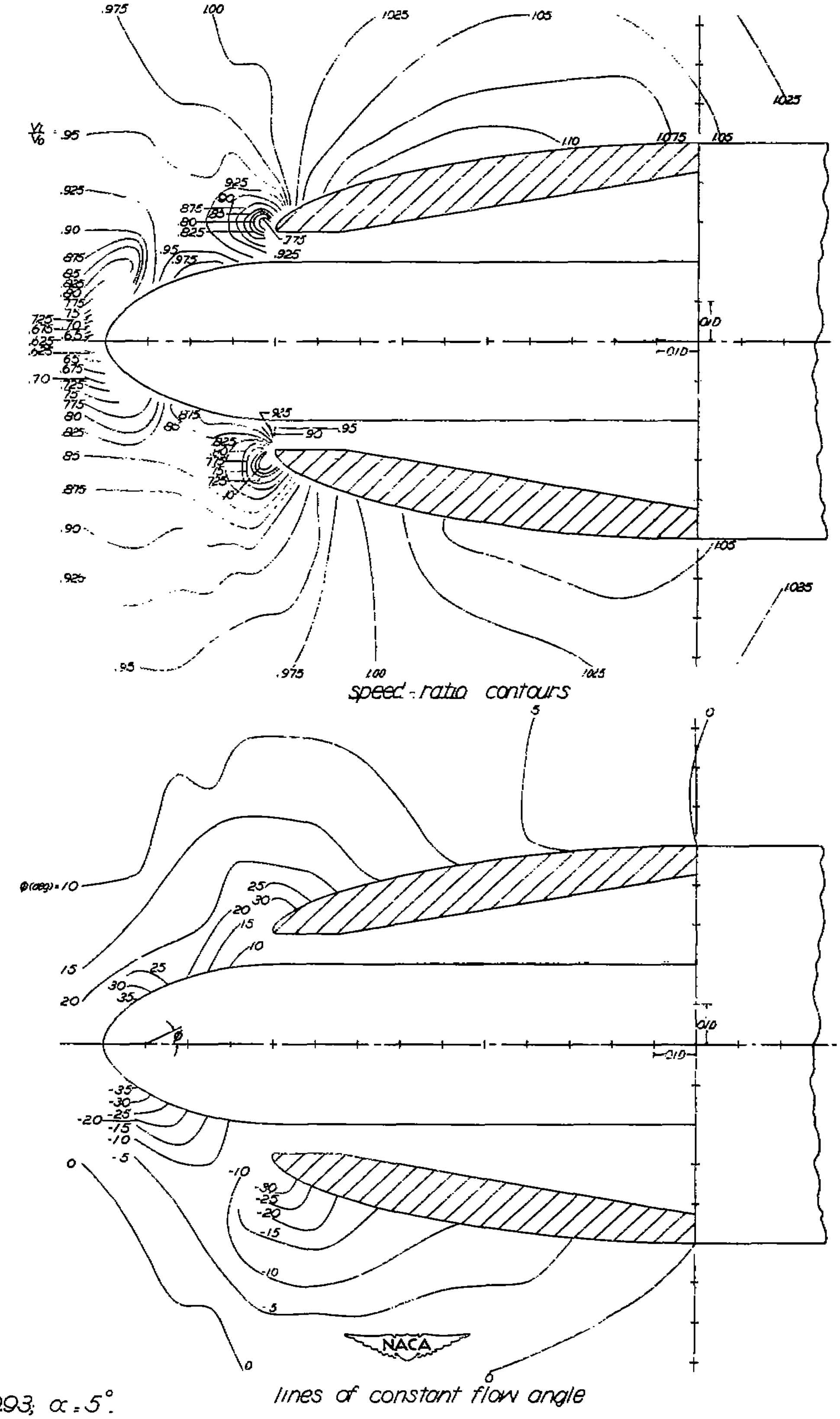

(a) $V_i/V_0 = 0.93$; $\alpha = 5^{\circ}$.
Figure 15.- Continued.

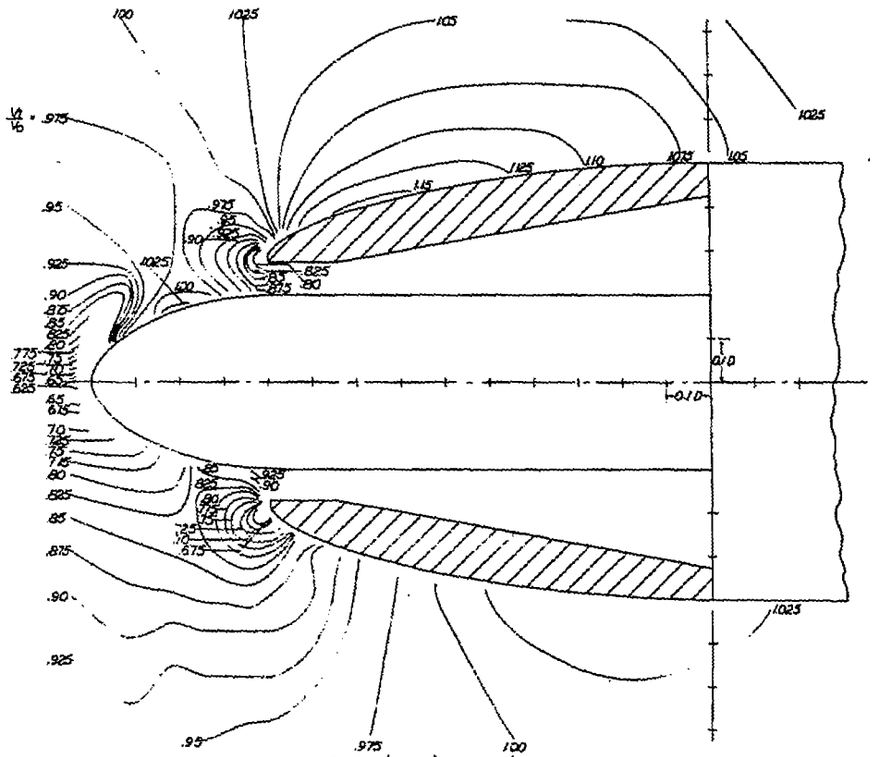

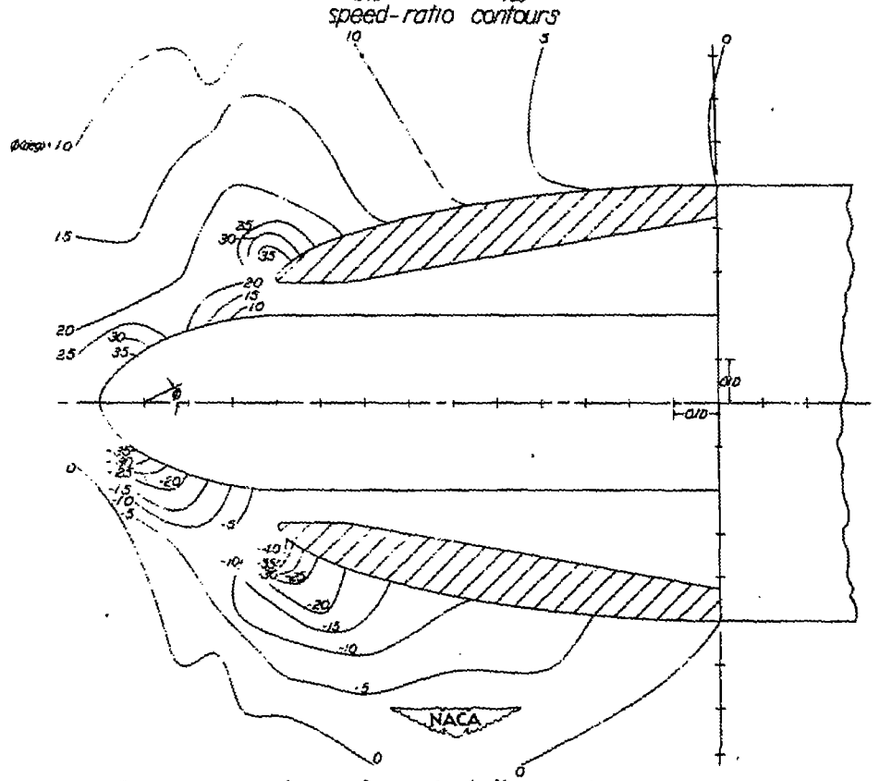

(e) V_l/V_0 ,093; α - 10°

Figure 15.-Concluded.

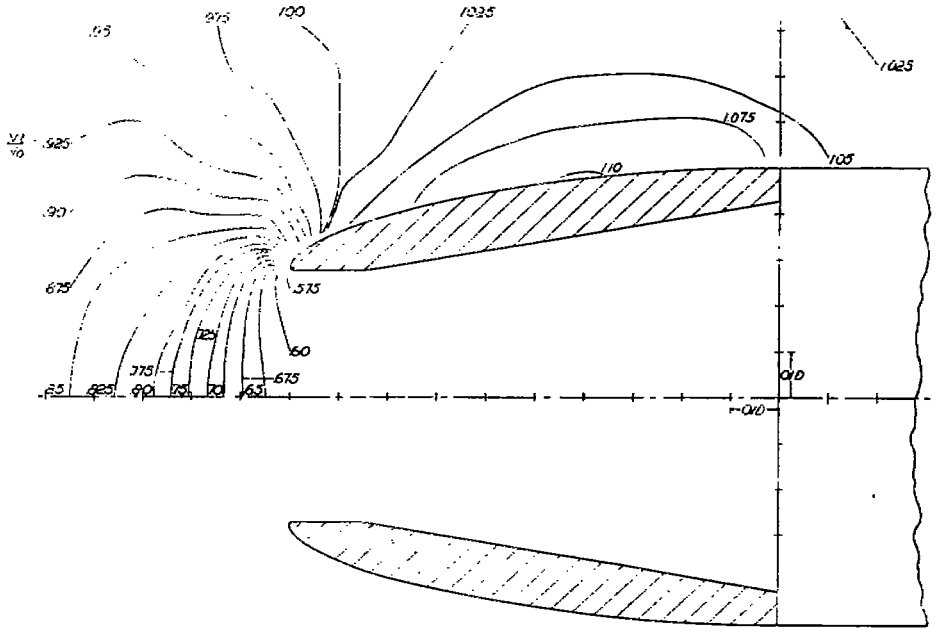

speed-ratio contours

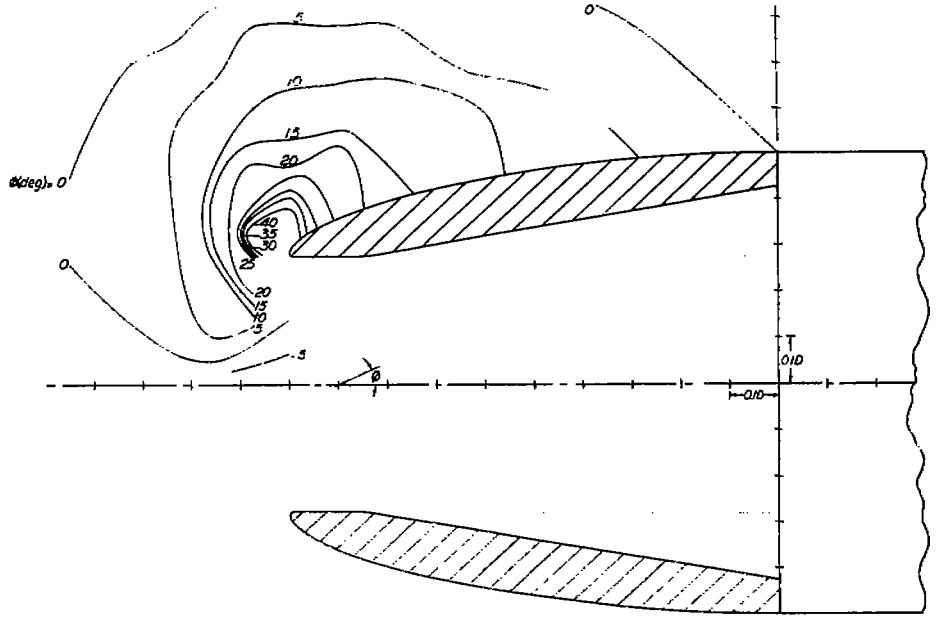

lines of constant flow angle

(a) $V_1/V_0 = 0.52$; $\alpha = 0°$.

Figure 16.-Speed and direction of flow in vicinity of NACA 1-55-100 cowling with no spinner.

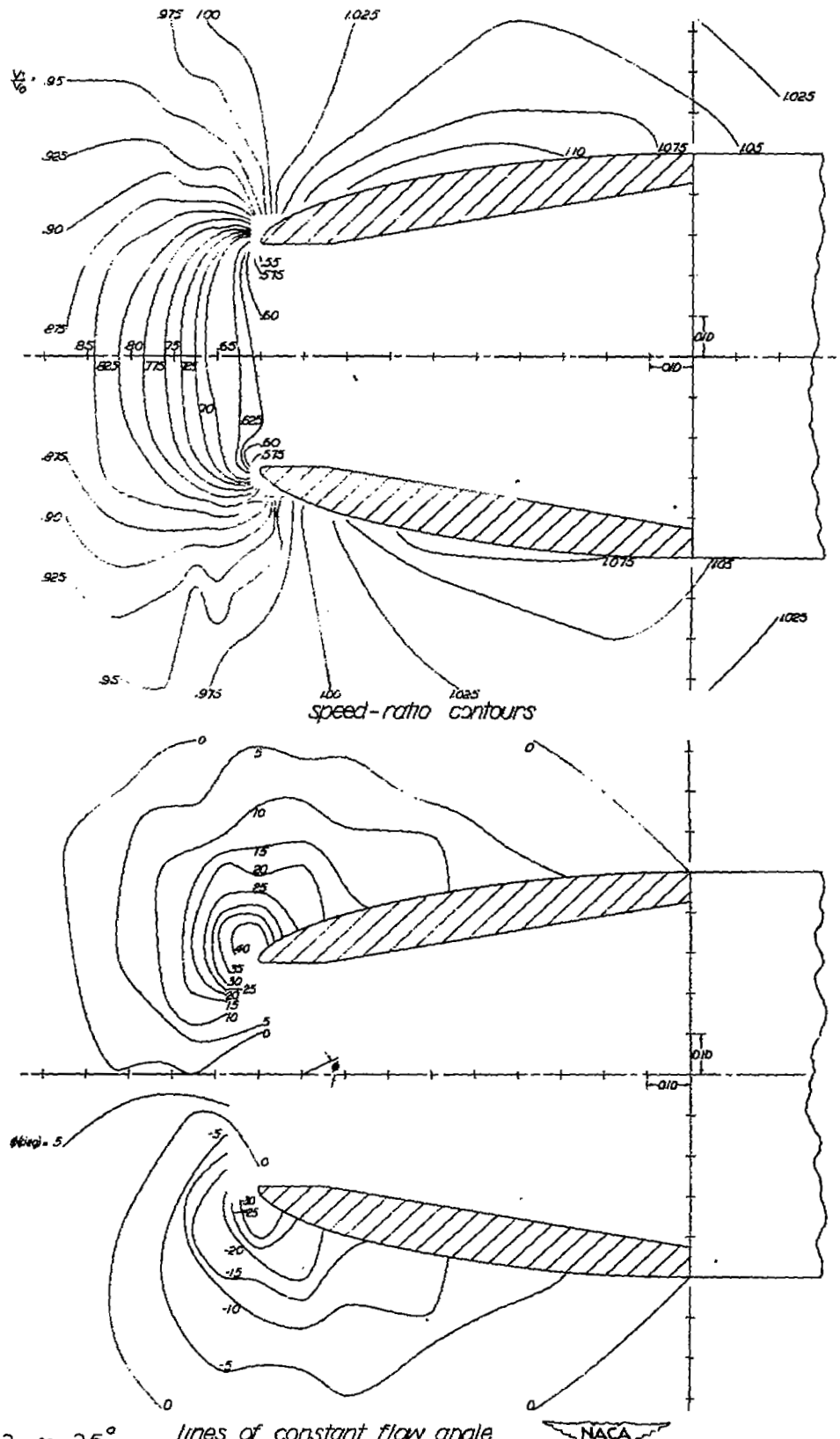

(b) $V_l/V_0 = 0.52$; $\alpha = 2.5°$

Figure 16.-Continued.

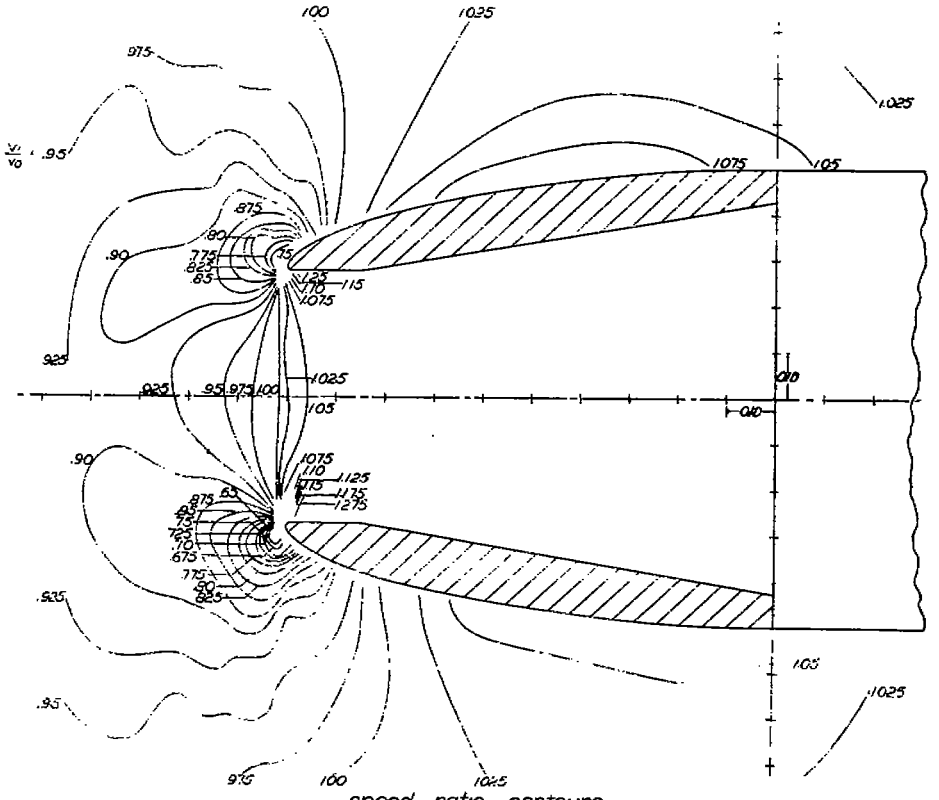

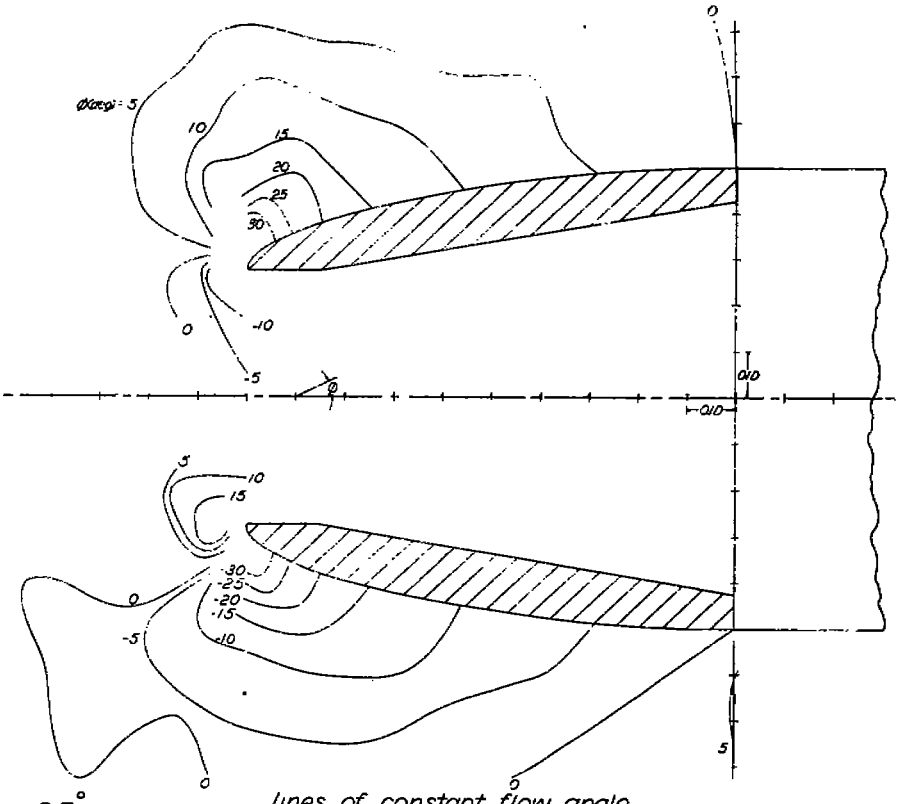

(c) $V_l/V_0 = 1.02$; $\alpha = 2.5°$.

Figure 16.-Continued.

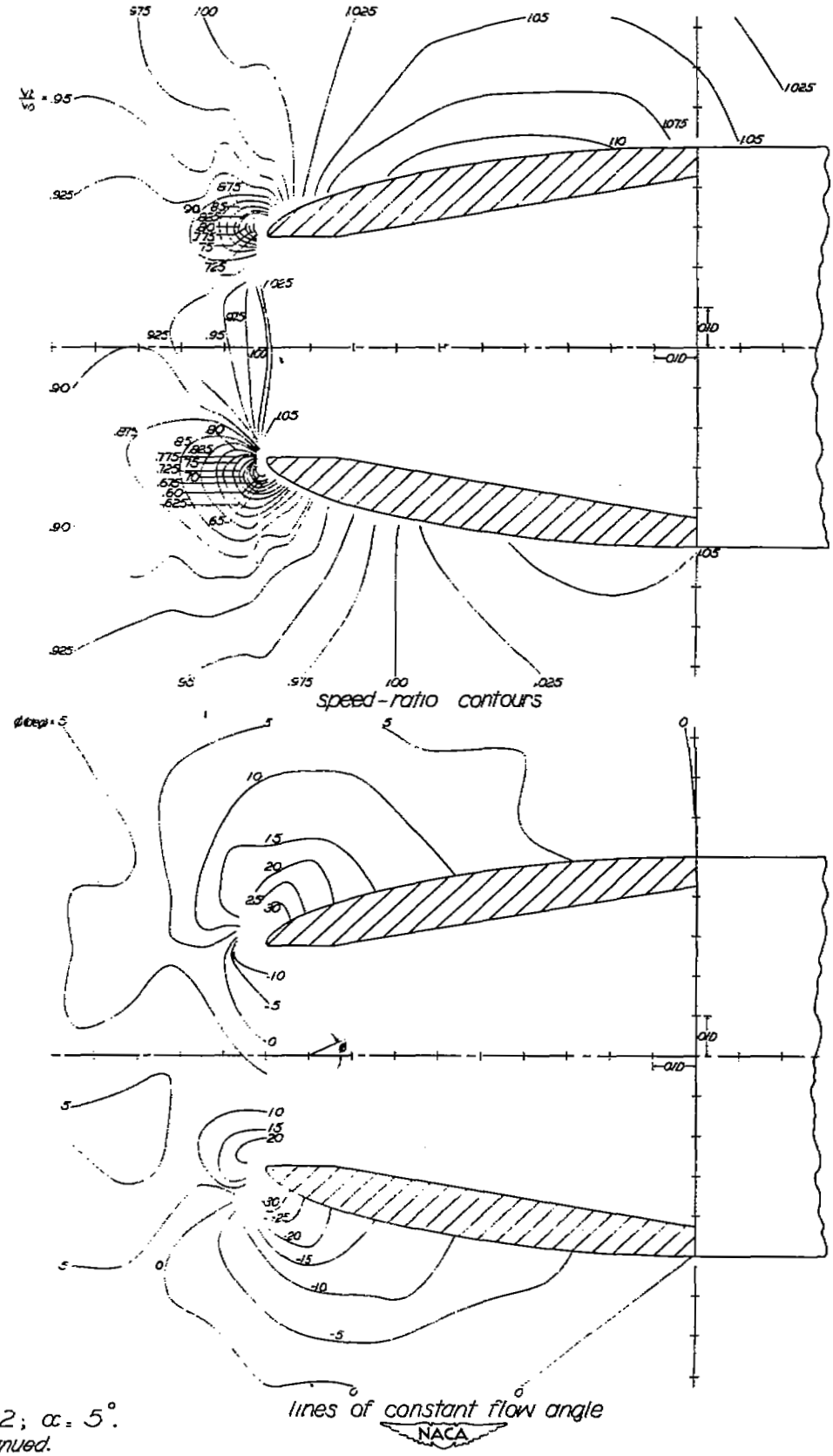

(d) $V_1/V_0 = 1.02$; $\alpha = 5°$.

Figure 16.-Continued.

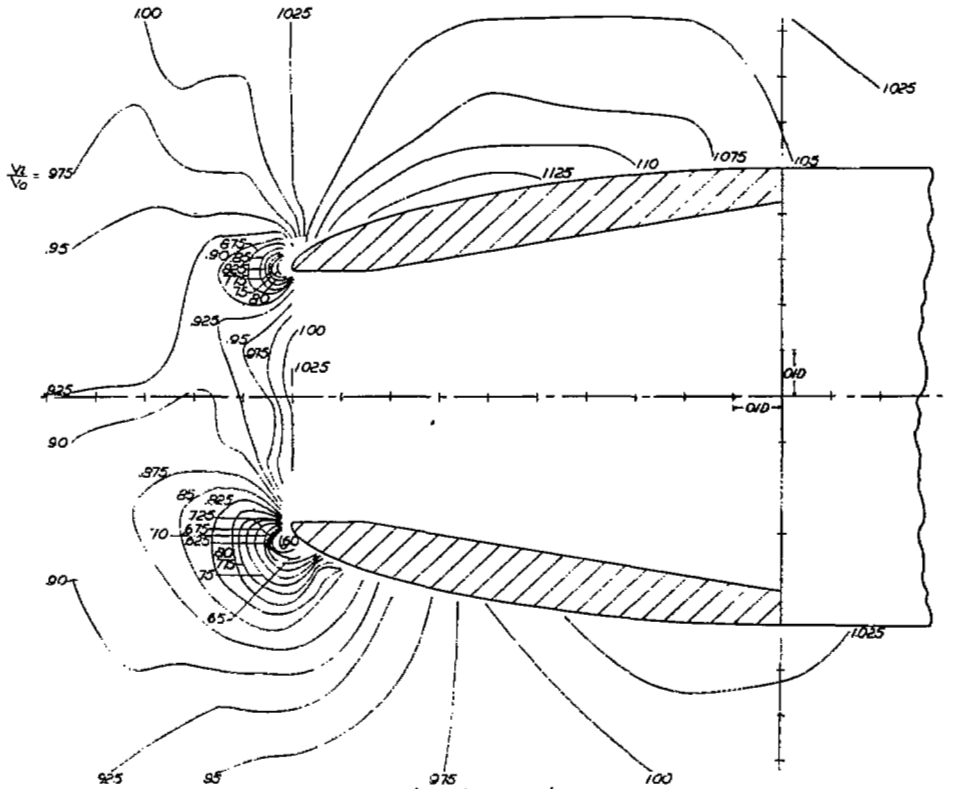

speed-ratio contours

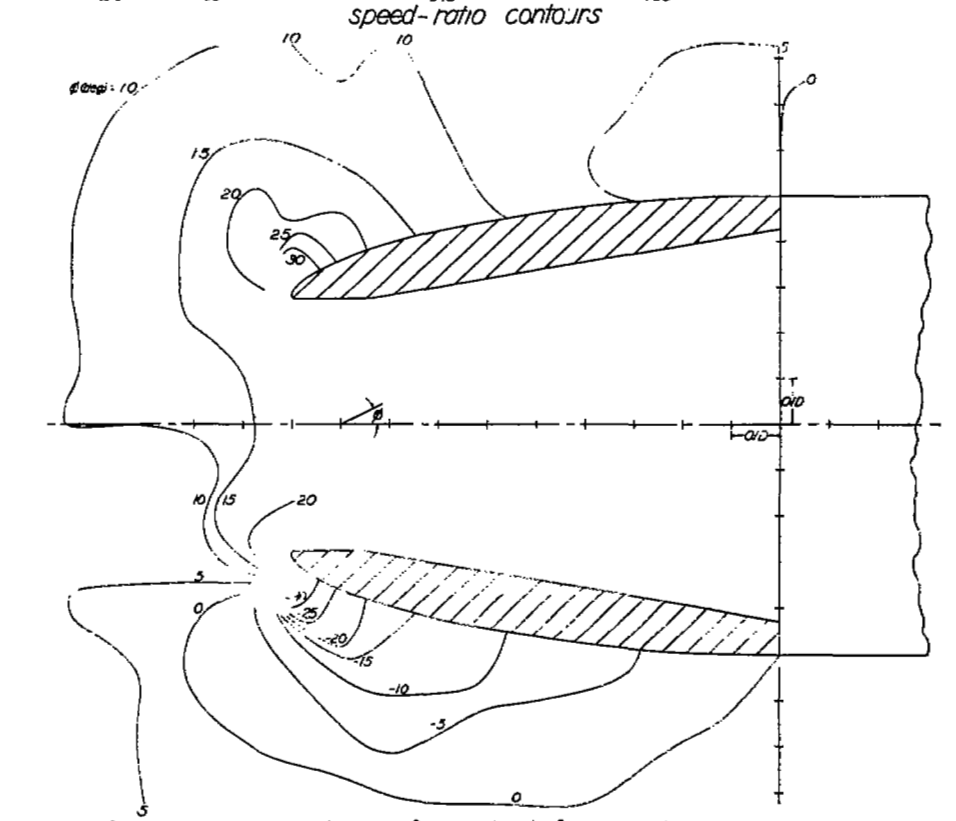

lines of constant flow angle

(e) $V_l/V_0 = 1.02$; $\alpha = 10°$

Figure 16.-Concluded.

NACA

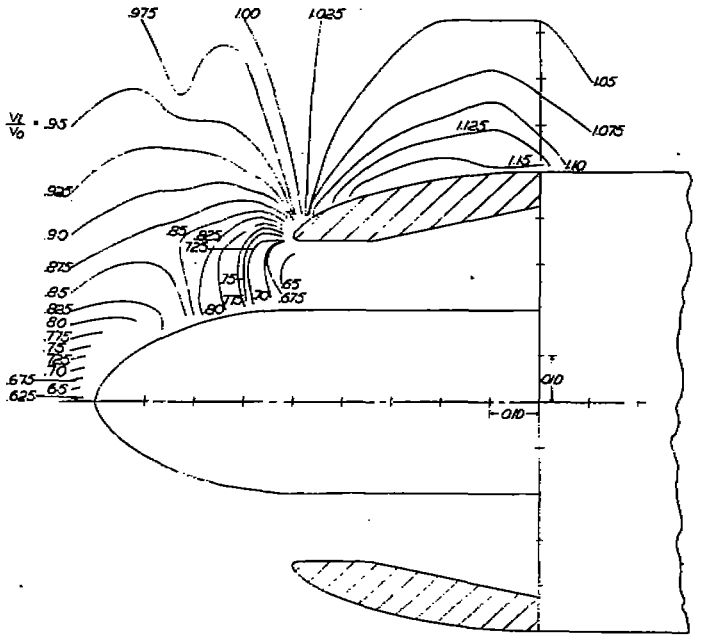

speed-ratio contours

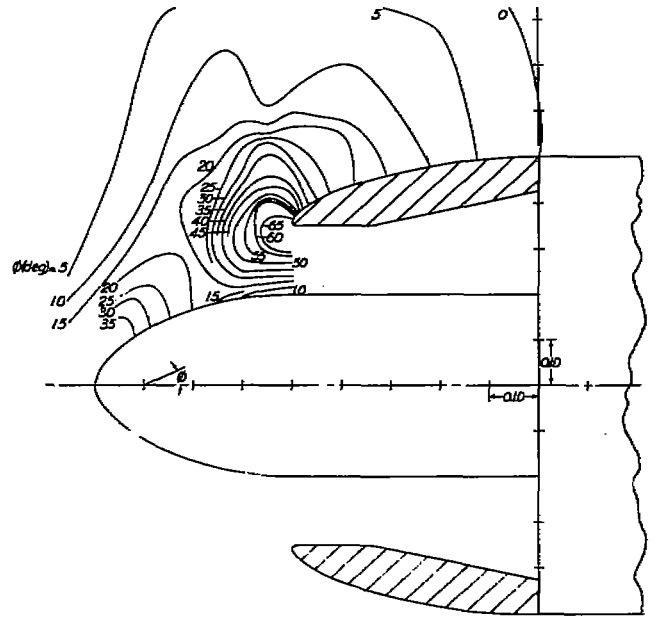

lines of constant flow angle

(a) $V_i/V_0 = 0.51$; $\alpha = 0°$.

Figure 17.-Speed and direction of flow in vicinity of NACA 1-70-050 cowling with NACA 1-40-040 spinner.

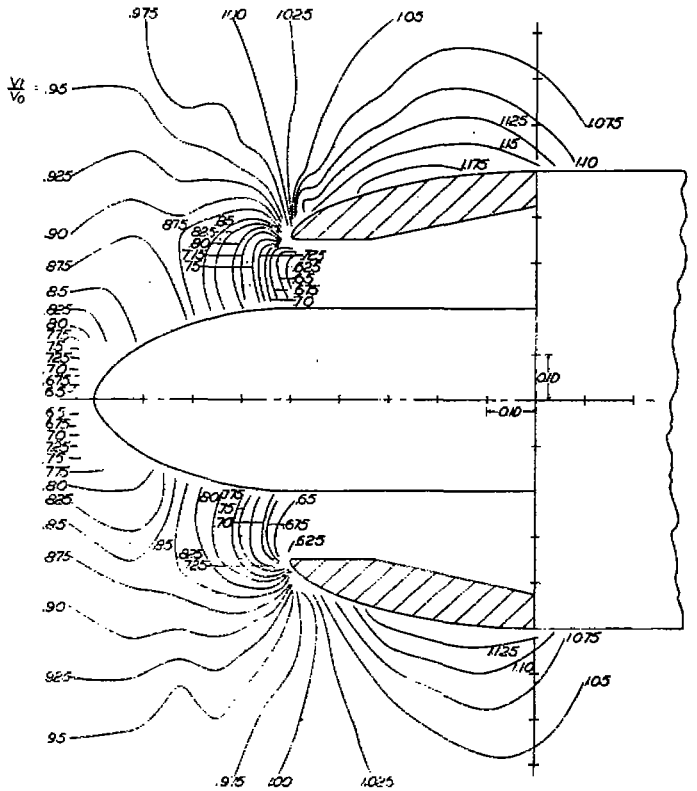

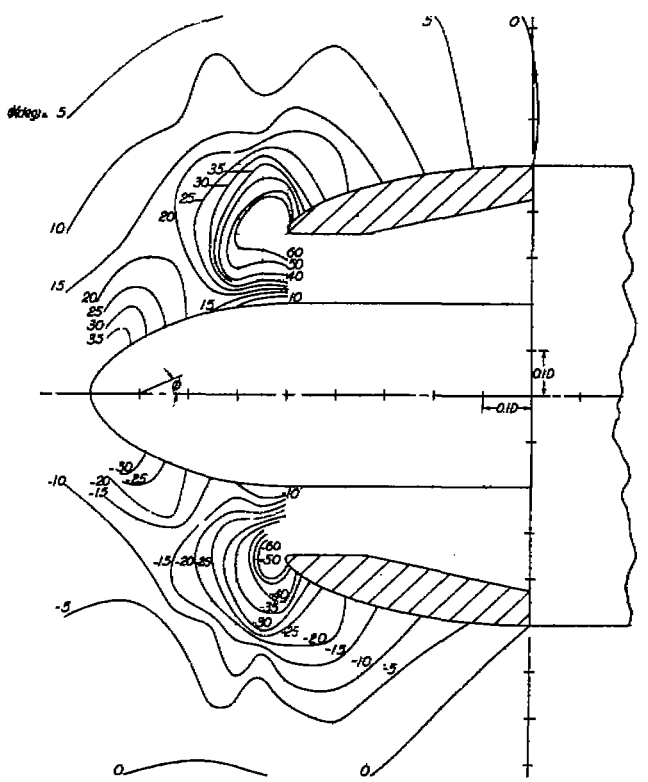

(b) $V_1/V_0 = 0.51$; $\alpha = 2.5°$

Figure 17.-Continued.

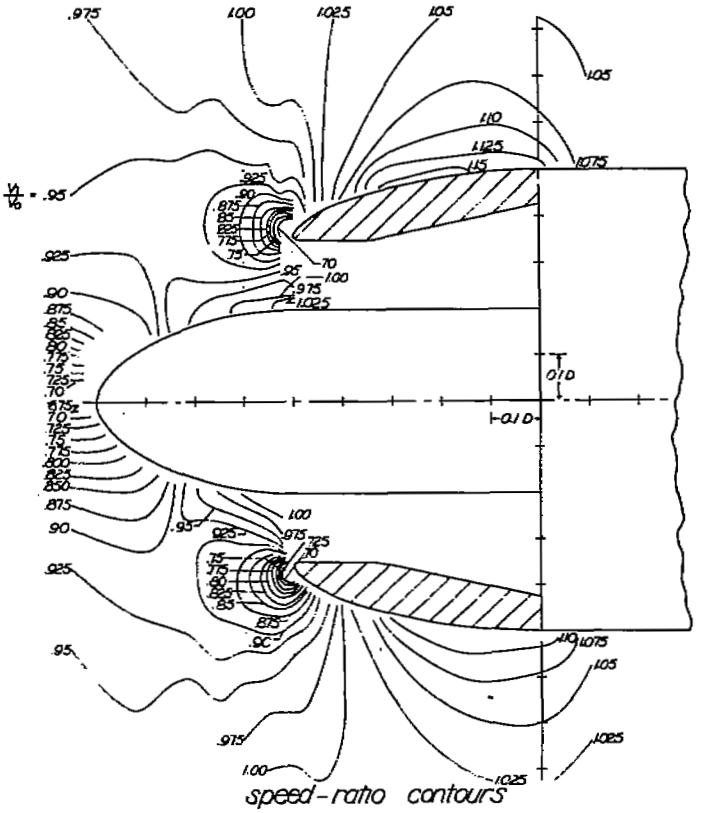

speed-ratio contours

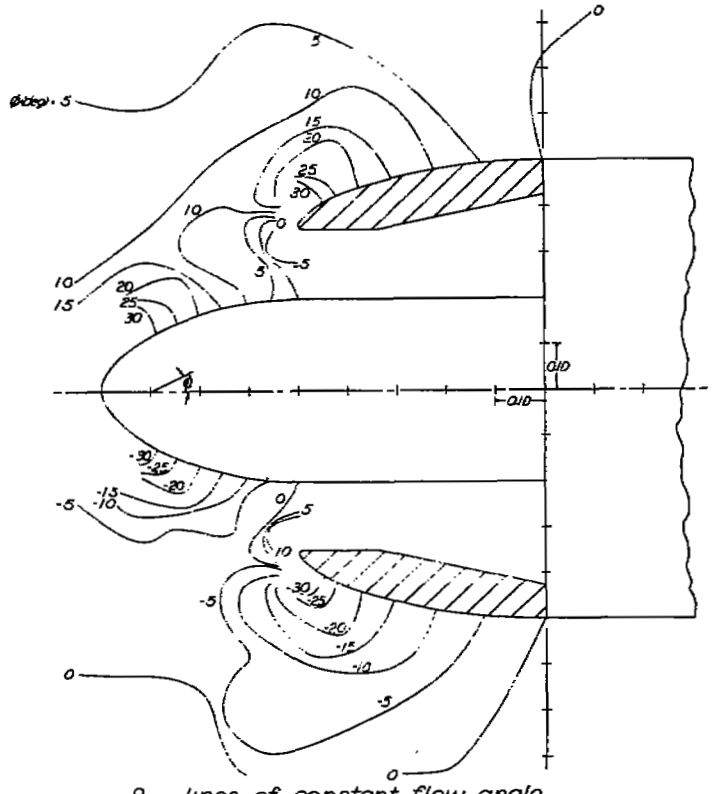

lines of constant flow angle

(c) $V_1/V_0 = 1.00$; $\alpha = 2.5°$.

Figure 17.- Continued.

NACA

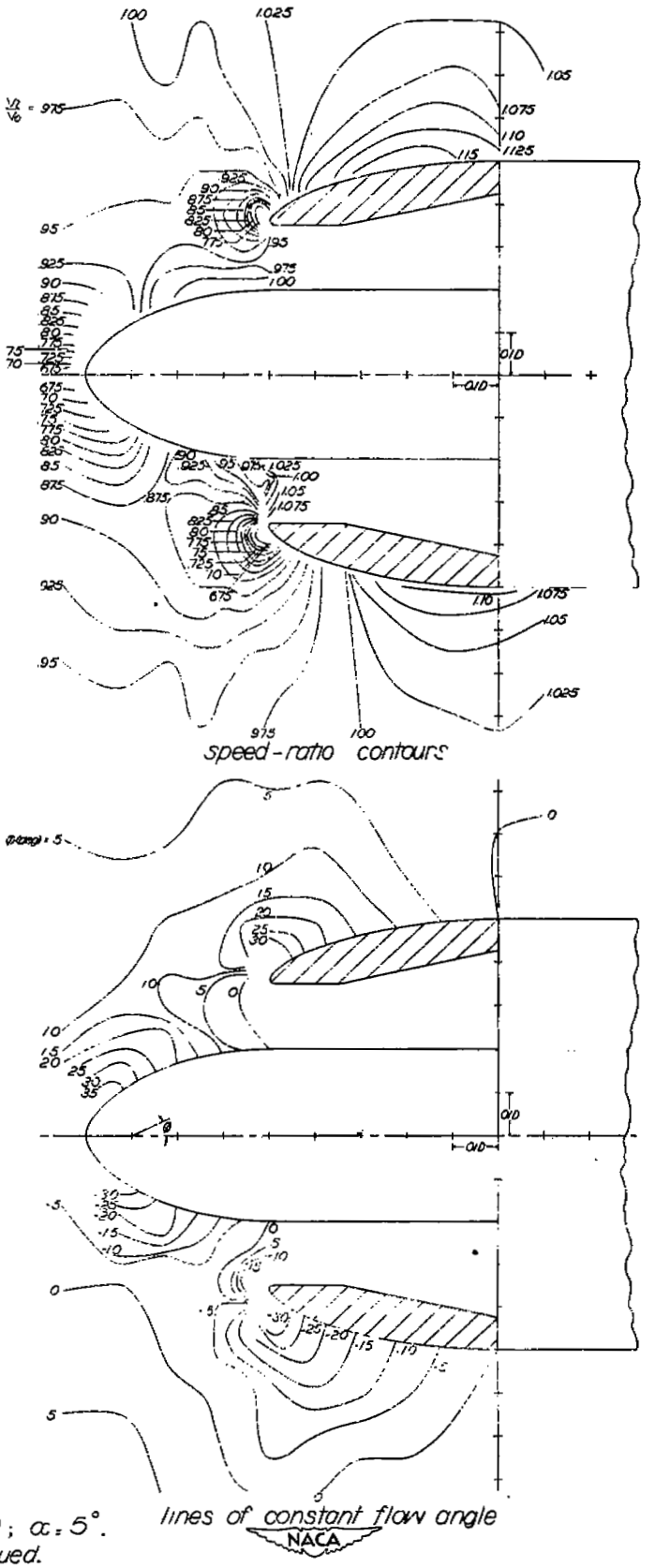

(d) $V_l/V_0 = 1.00$; $\alpha = 5°$.

Figure 17.-Continued.

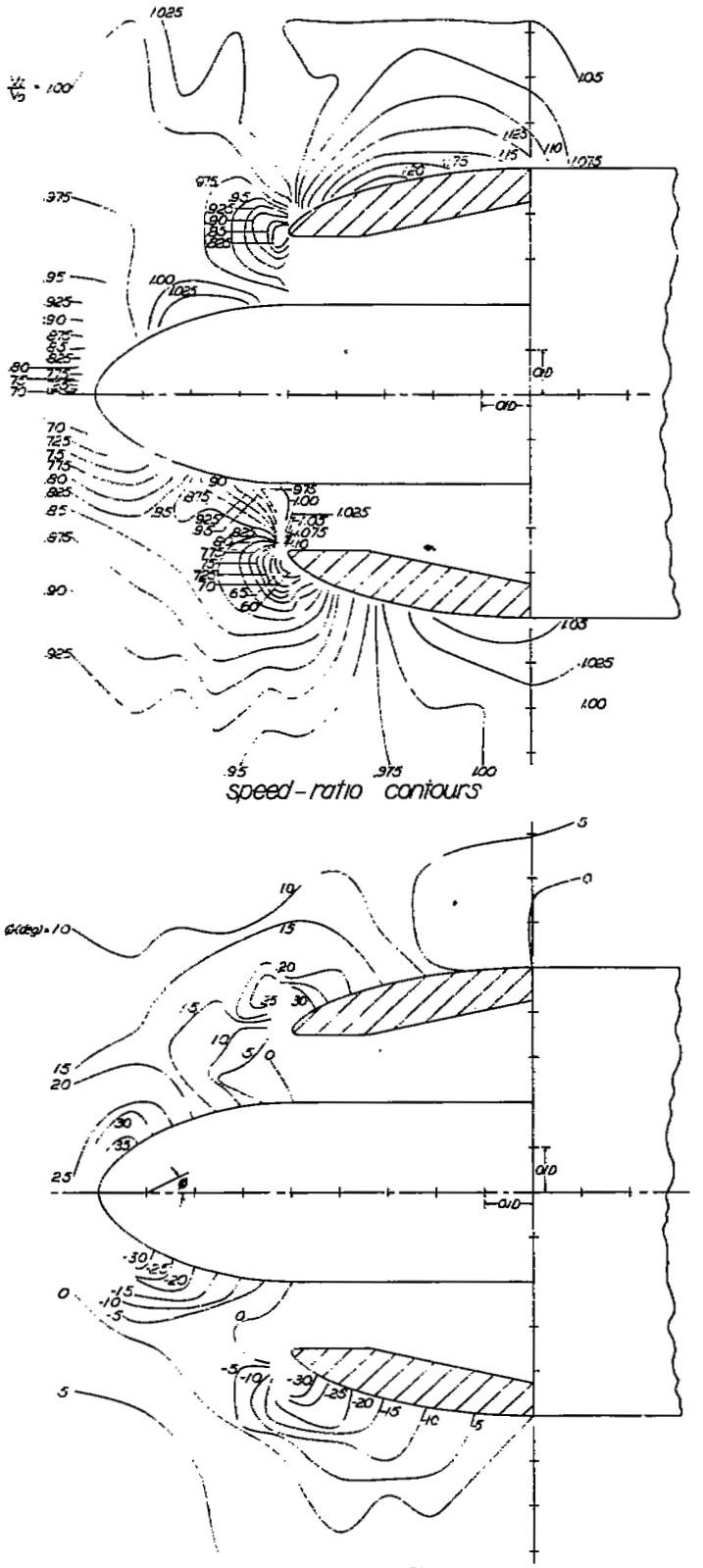

(e) $V_j/V_0 = 1.00$; $\alpha = 10°$.

Figure 17.- Concluded.

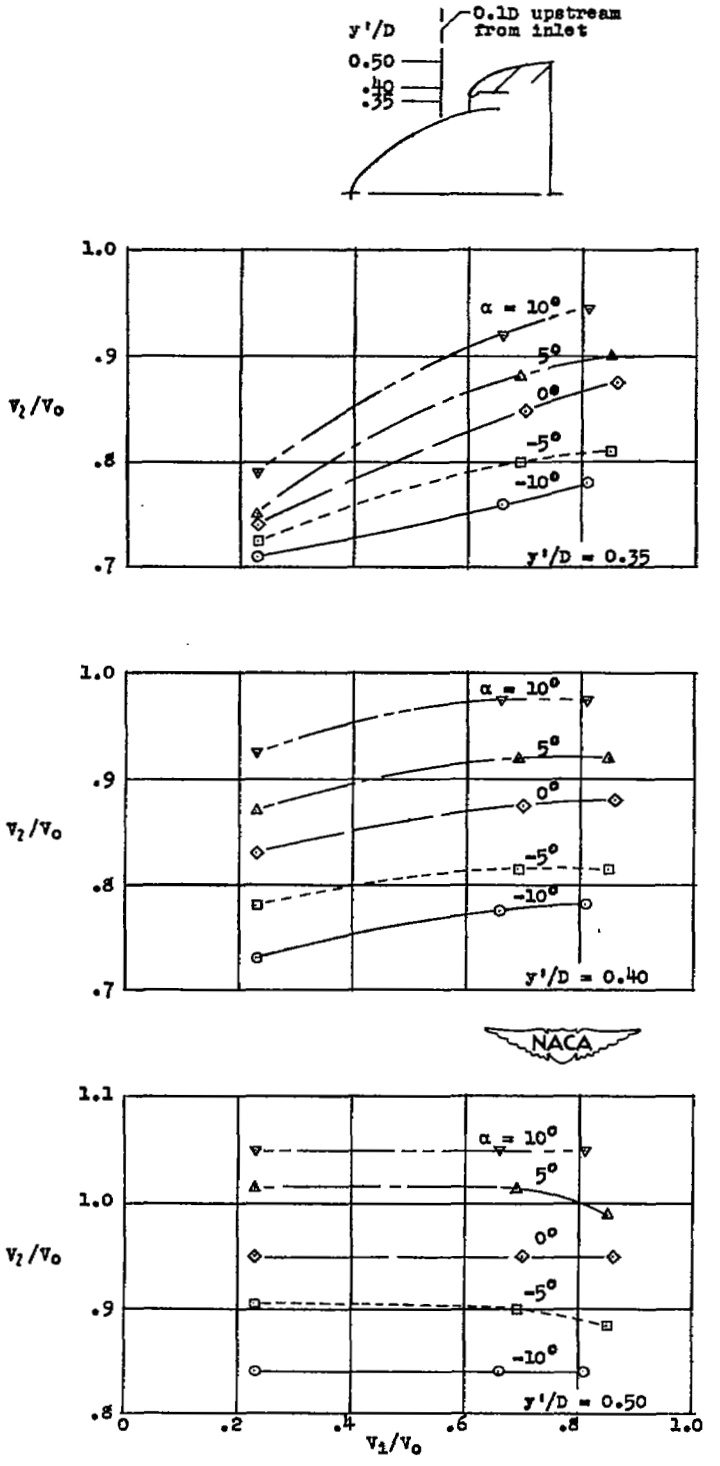

(a) Effect on local flow-speed ratios.

Figure 18.-Effect of changes in inlet-velocity ratio and angle of attack (from reference 1) on local flow-speed ratios and flow angles in propeller-shank region (0.1D upstream from inlet).

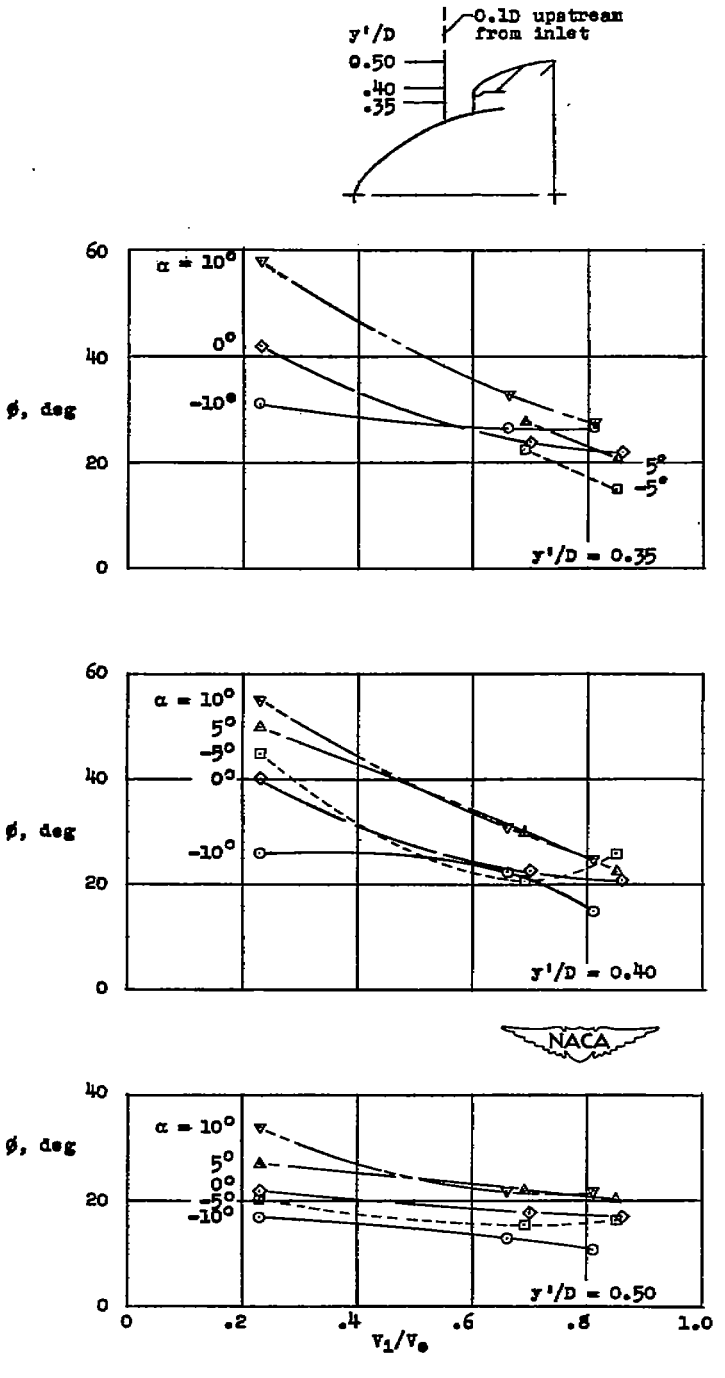

(b) Effect on local flow angles.

Figure 18.-Concluded.

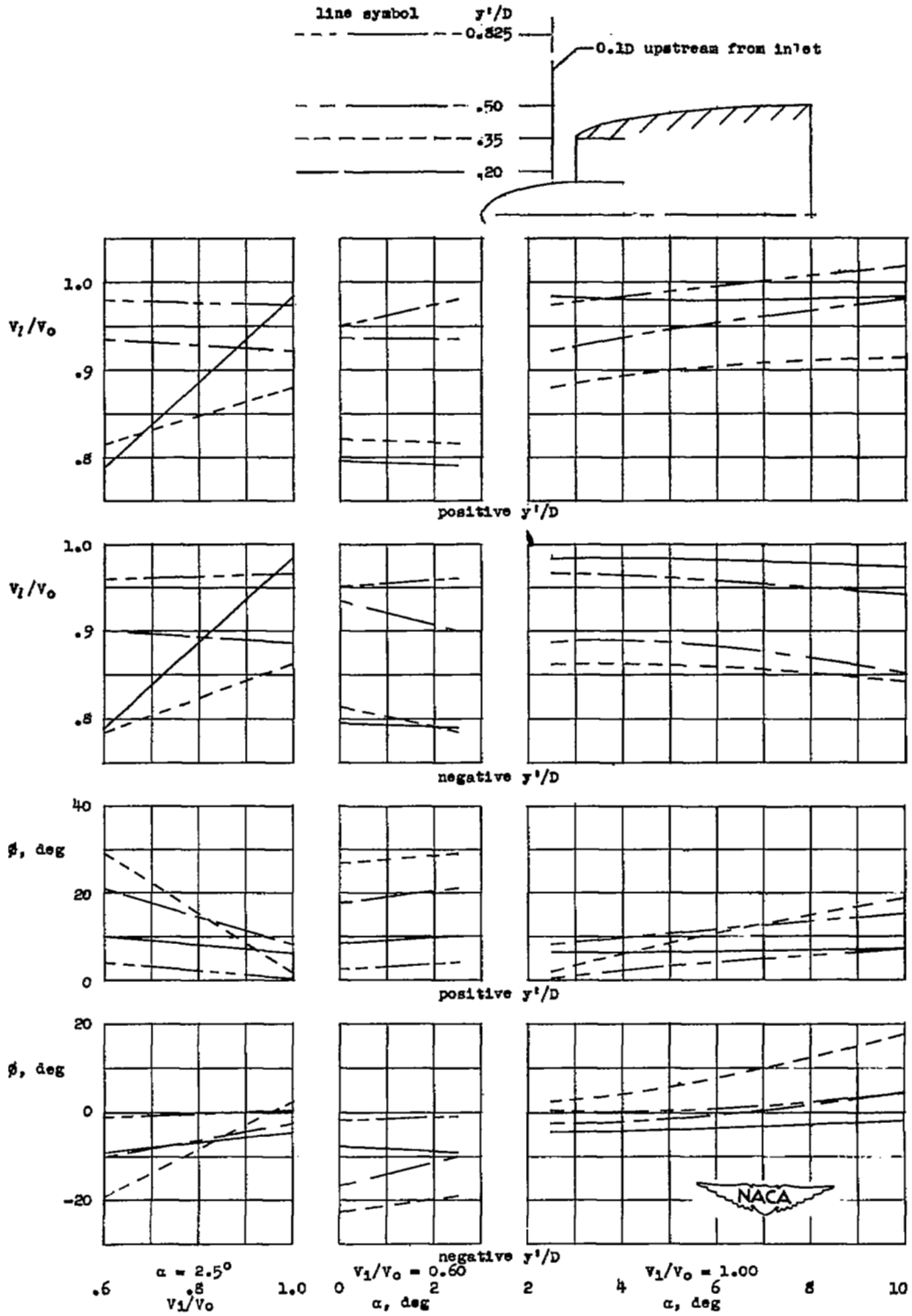

(a) NACA 1-70-100 cowling with NACA 1-30-040 spinner, 0.1D upstream from inlet.

Figure 19.-Effect of changes in angle of attack and inlet-velocity ratio on local flow-speed ratios and flow angles in the propeller-shank region.

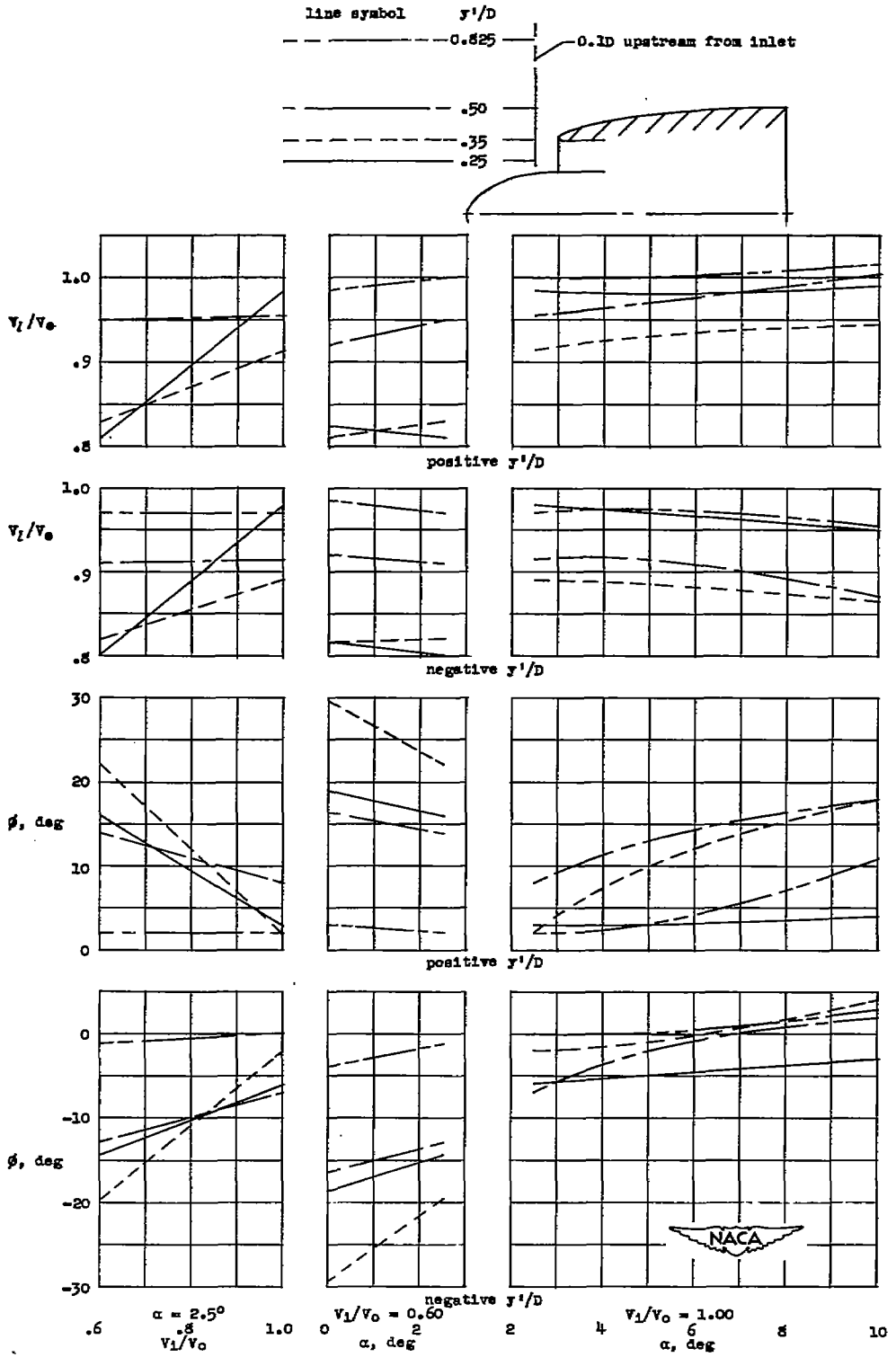

(b) NACA 1-70-100 cowling with NACA 1-40-040 spinner, 0.1D upstream from inlet.
Figure 19.-Continued.

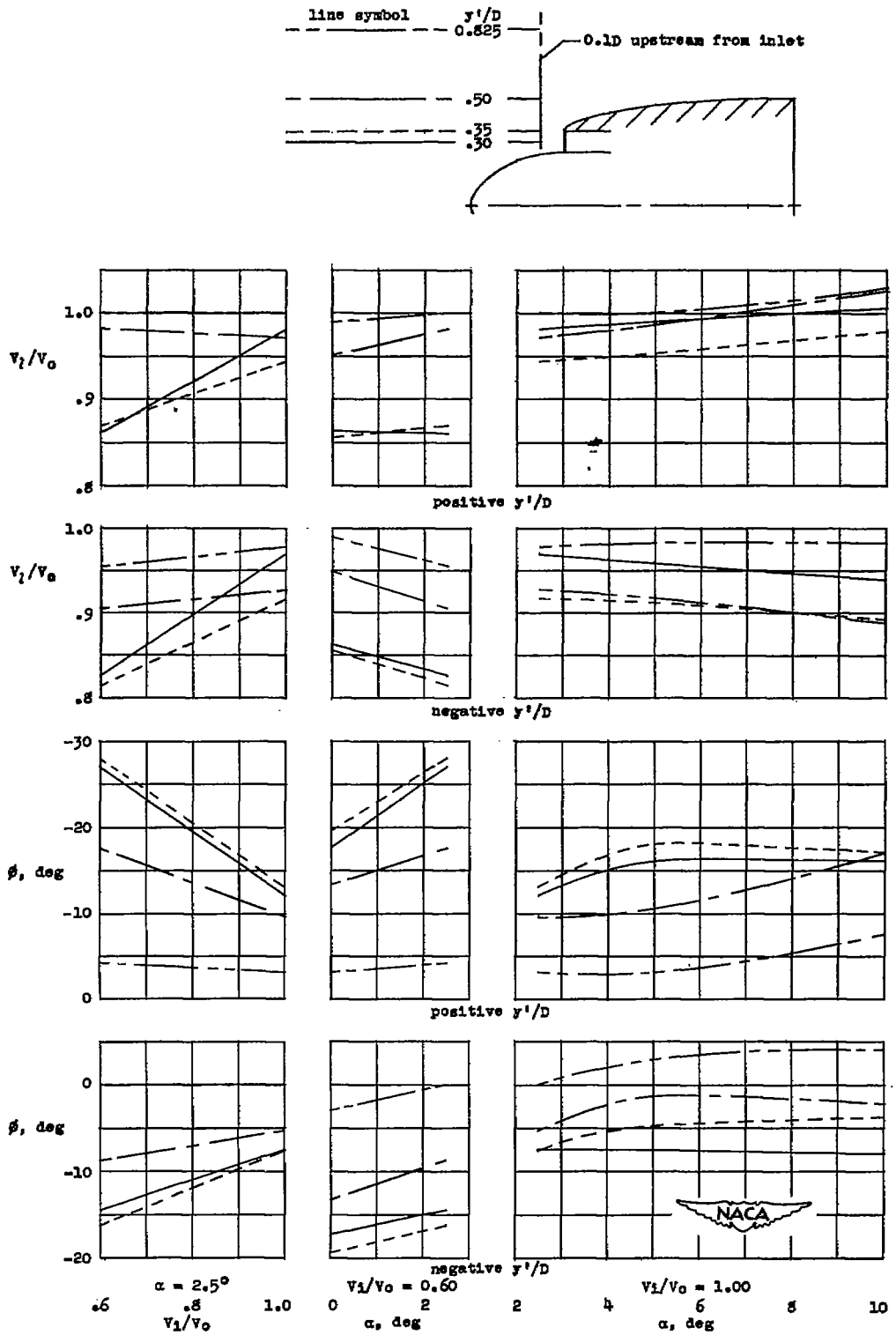

(c) NACA 1-70-100 cowling with NACA 1-50-040 spinner, 0.1D upstream from inlet.
Figure 19.-Continued.

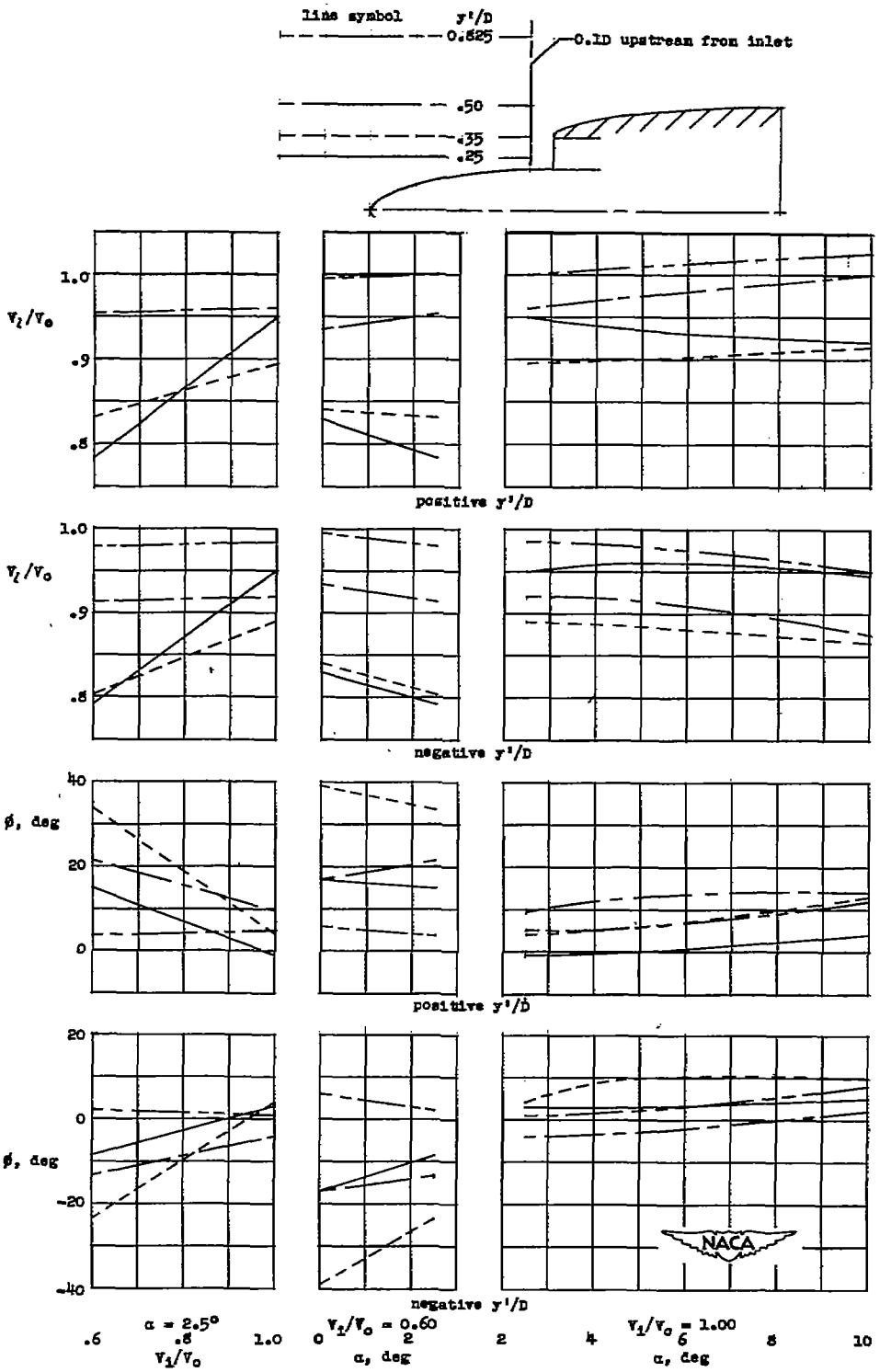

(d) NACA 1-70-100 cowling with NACA 1-40-050 spinner, 0.1D upstream from inlet.
Figure 19.-Continued.

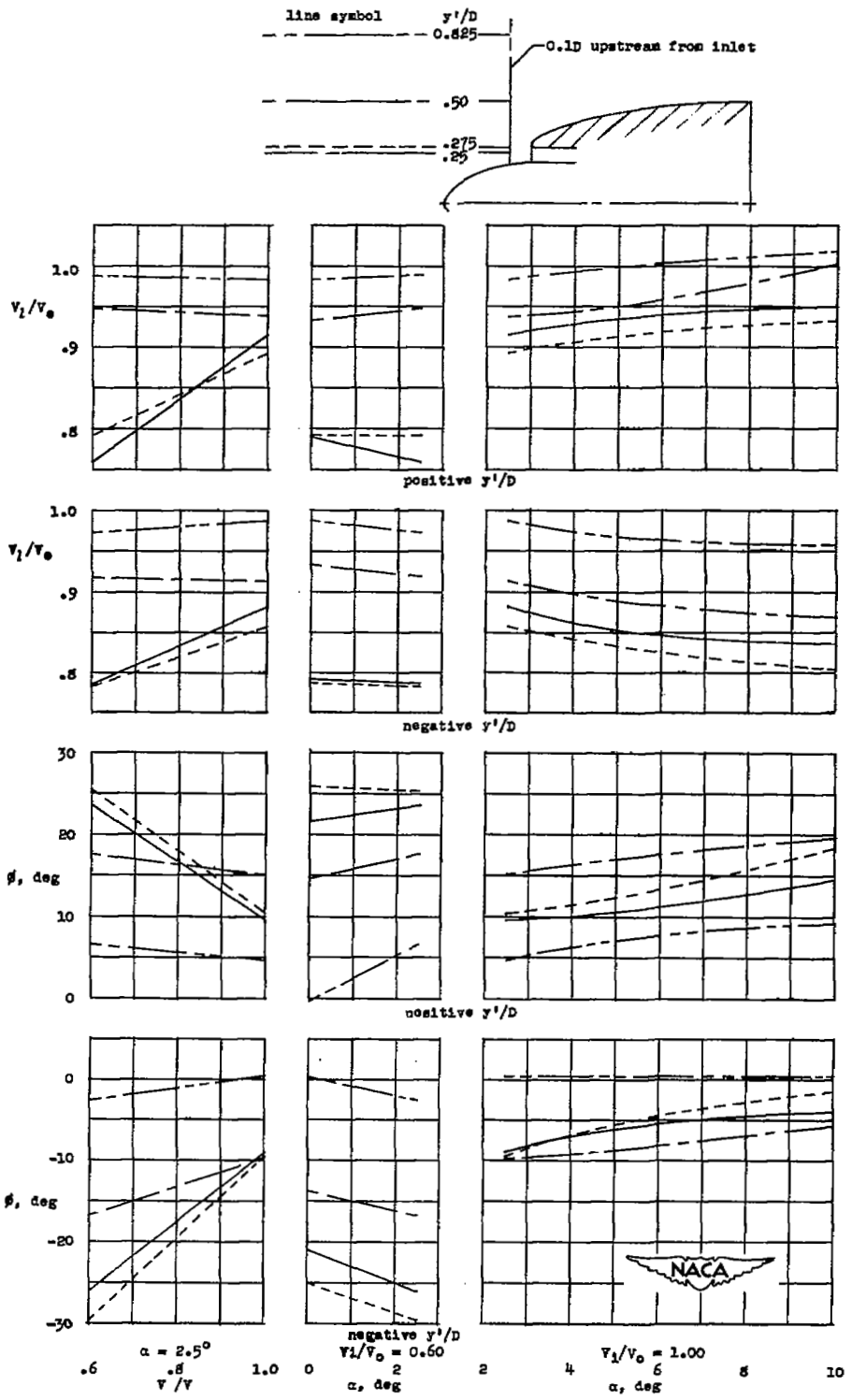

(c) NACA 1-55-100 cowling with NACA 1-40-040 spinner, 0.1D upstream from inlet.
Figure 19.-Continued.

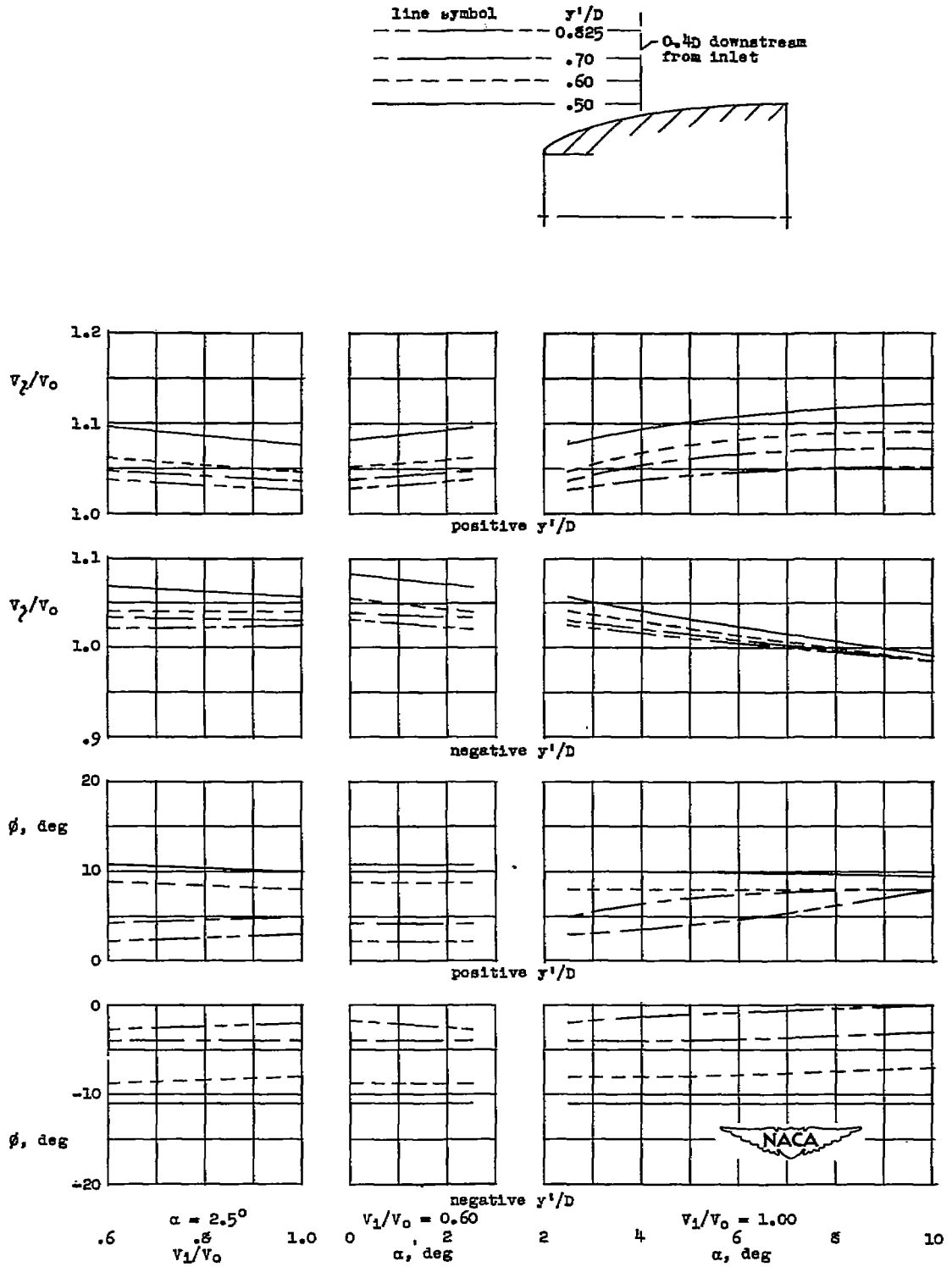

(f) NACA 1-55-100 cowling with no spinner, 0.4D downstream from inlet.
Figure 19.-Continued.

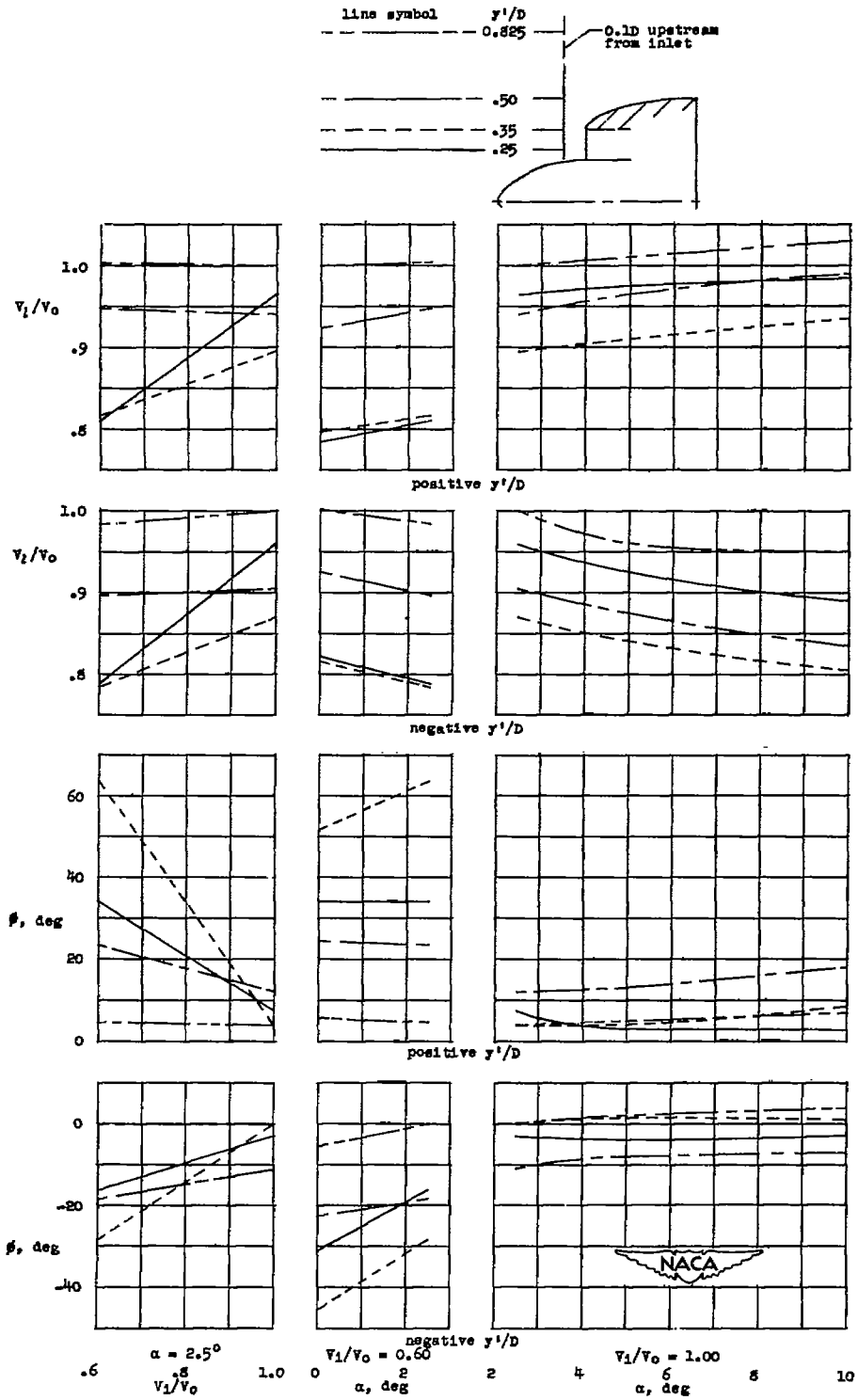

(g) NACA 1-70-050 cowling with NACA 1-40-040 spinner, 0.1D upstream from inlet.

Figure 19.-Concluded.

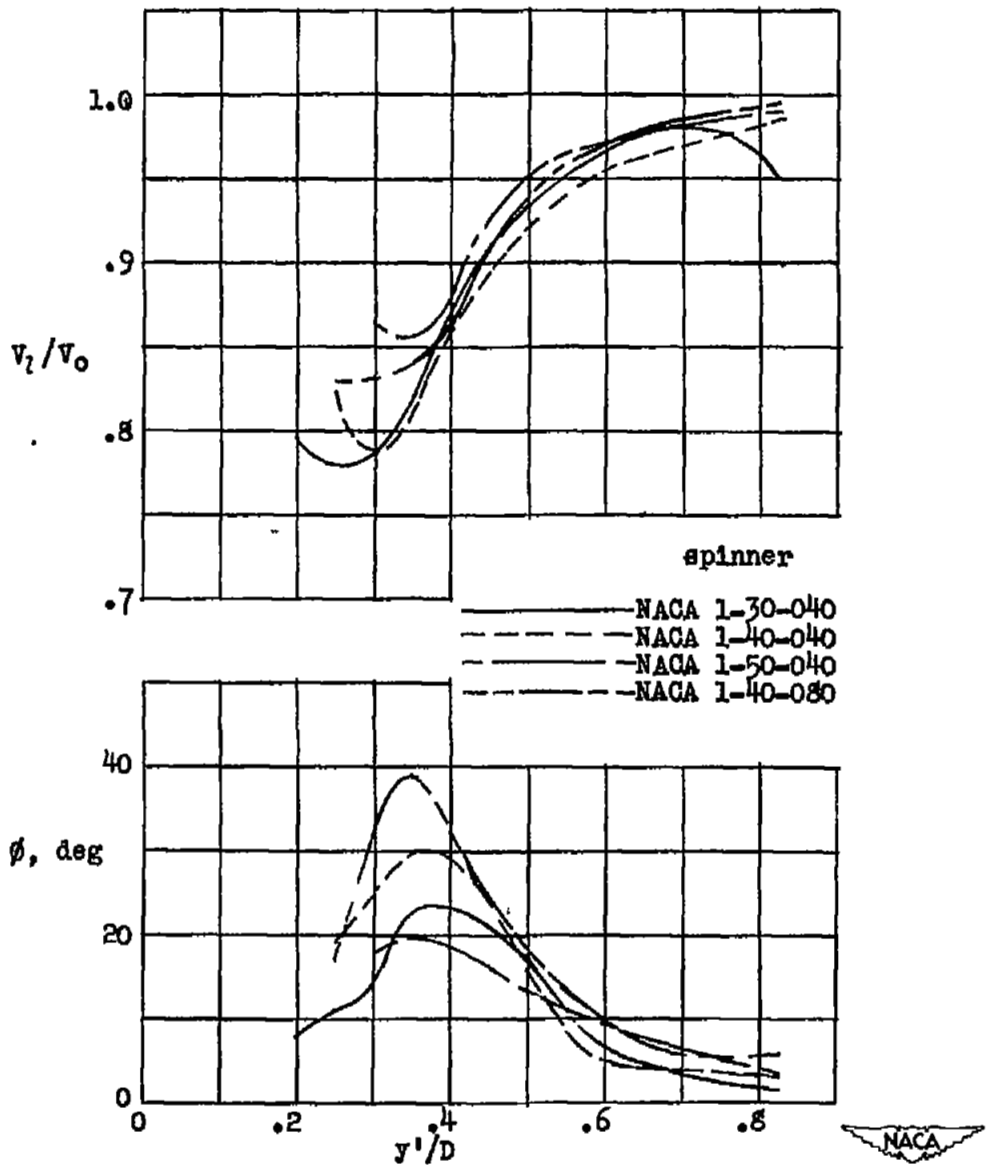

(a) $V_1/V_o = 0.60$; $\alpha = 0^\circ$.

Figure 20.-Effect of changes in spinner-diameter ratio and spinner-length ratio on local flow-speed ratios and flow angles in propeller-shank region (0.1D upstream from inlet). NACA 1-70-100 cowling.

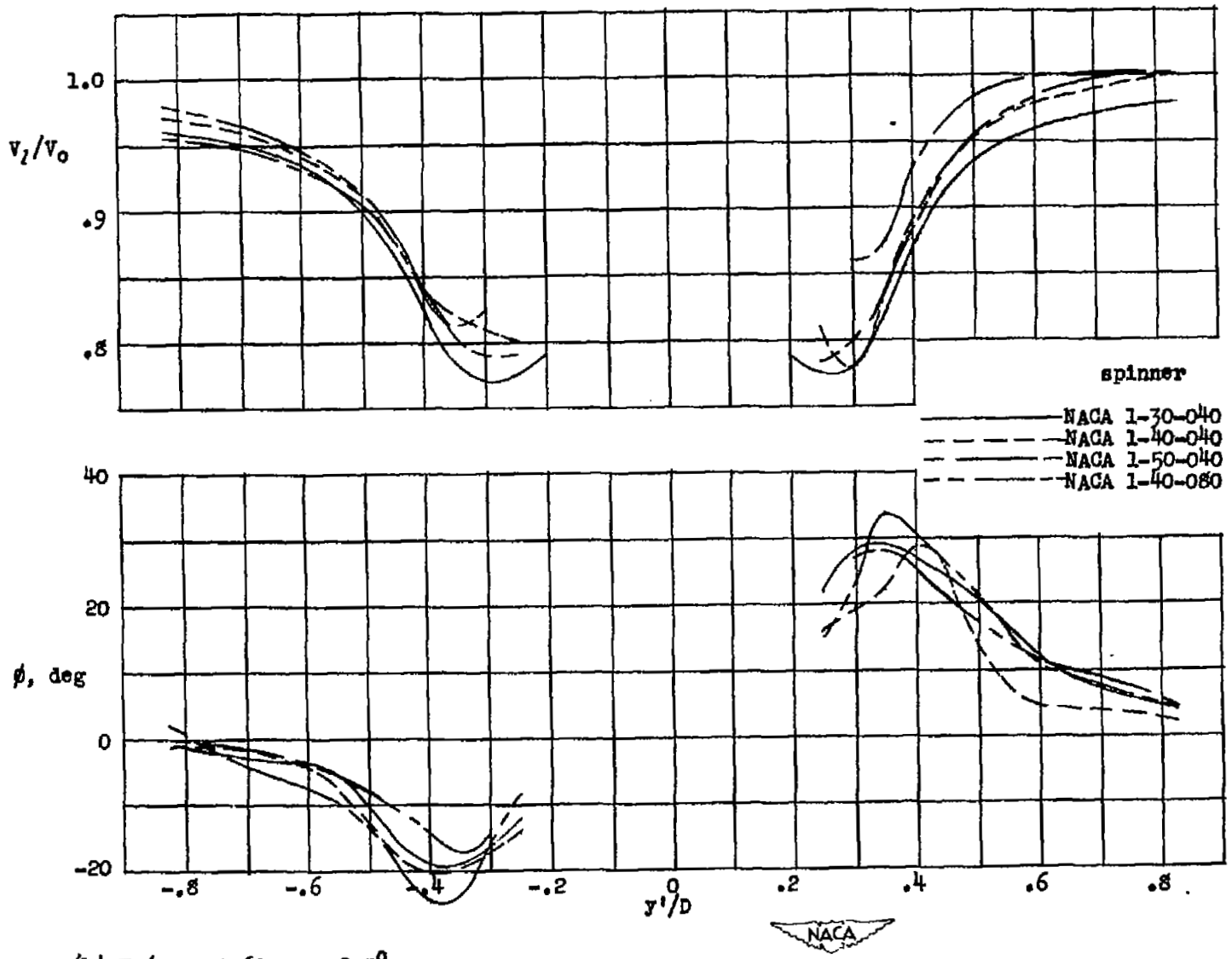

(b) $V_1/V_o = 0.60$; $\alpha = 2.5^\circ$.

Figure 20.-Continued.

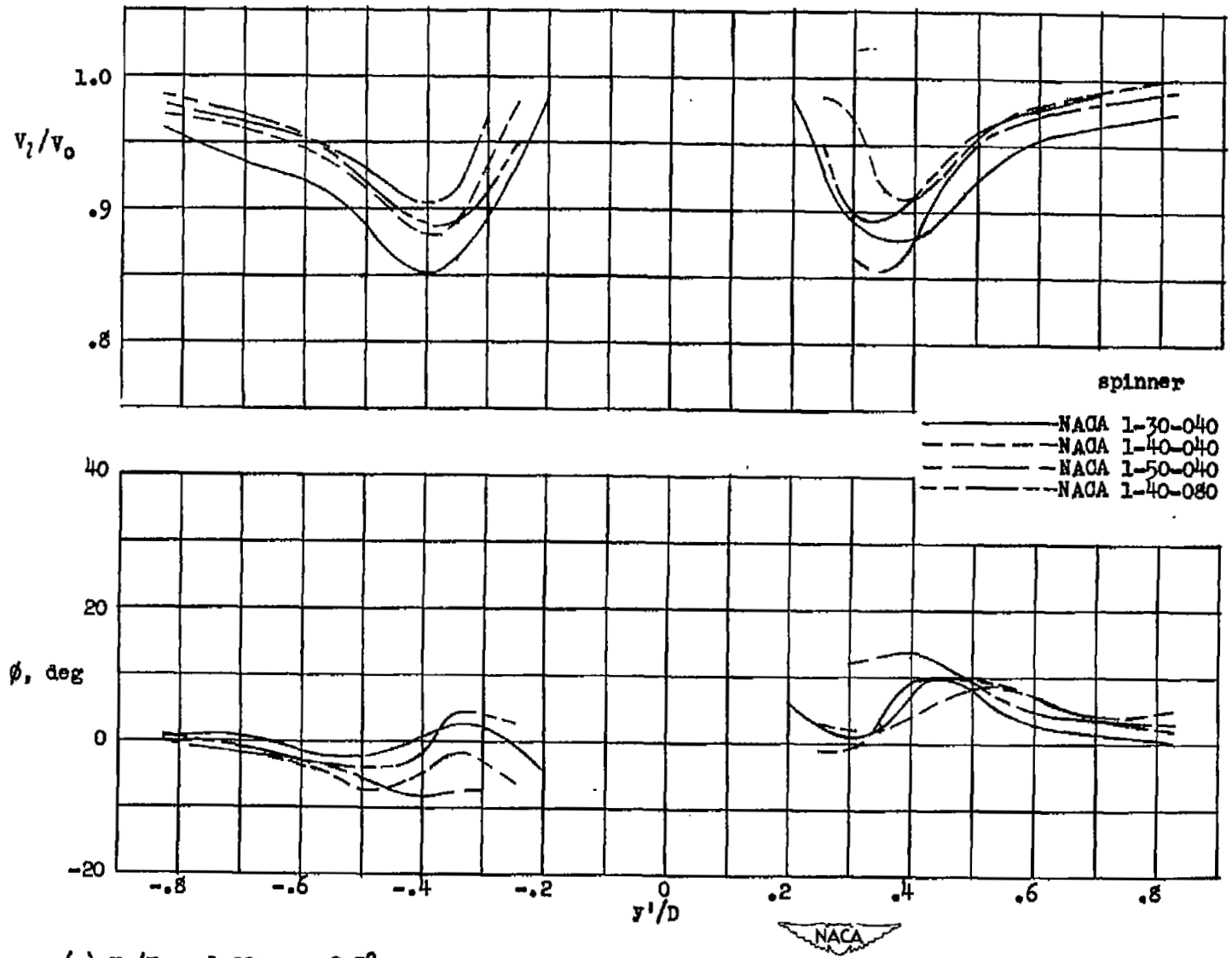

(c) $V_1/V_o = 1.00$; $\alpha = 2.5^\circ$.

Figure 20.-Continued.

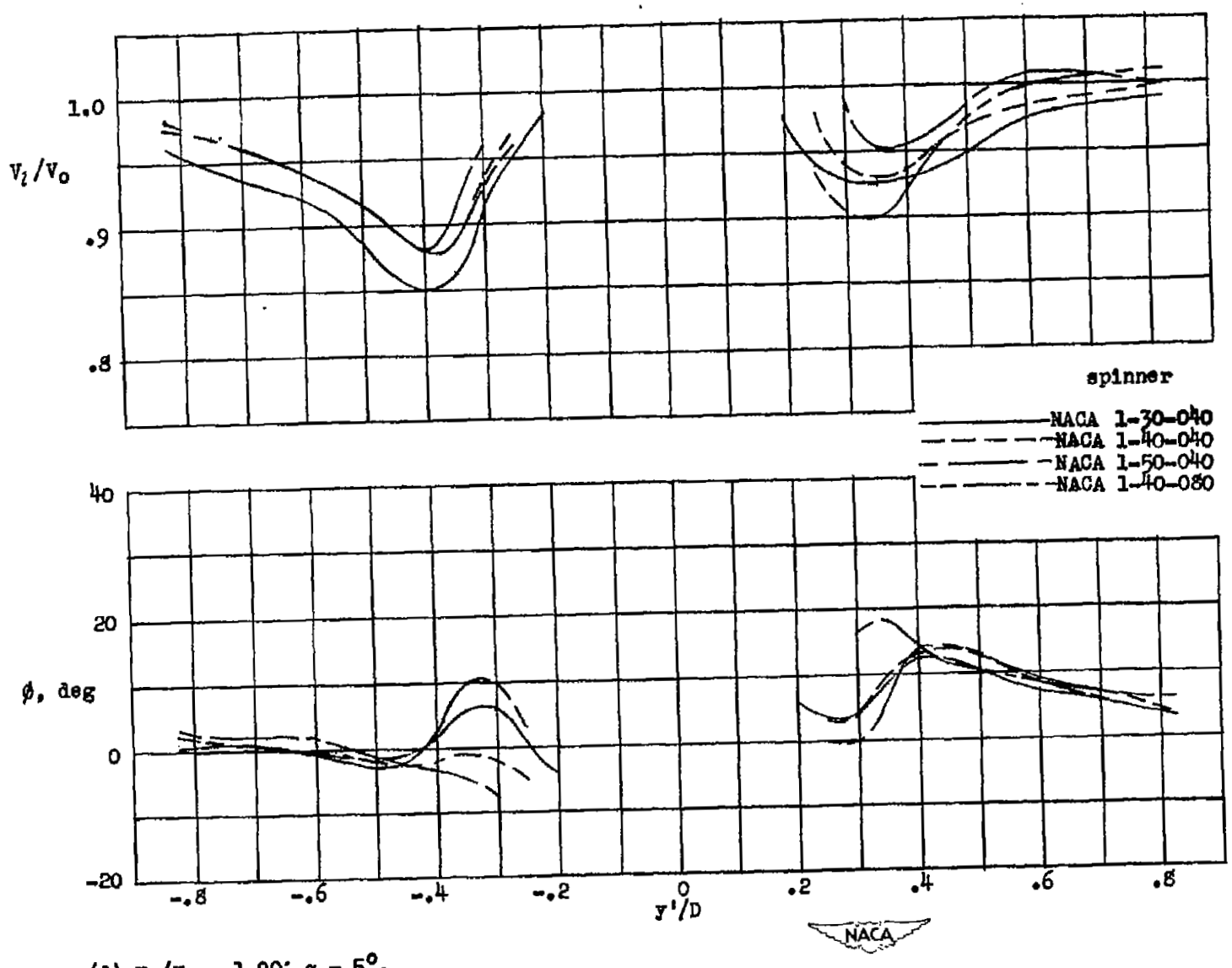

(d) $V_l/V_o = 1.00$; $\alpha = 5°$.

Figure 20.-Continued.

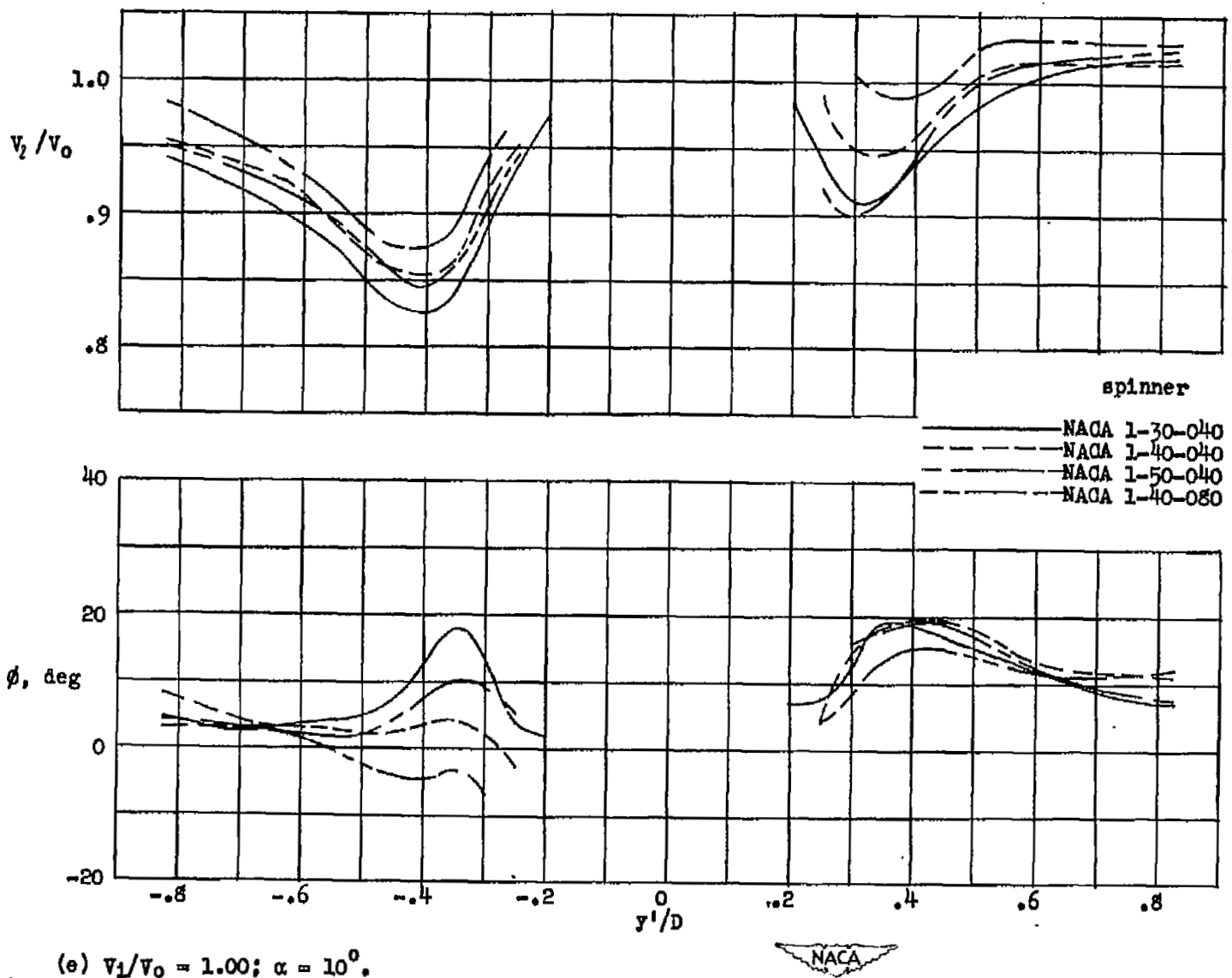

(e) $V_1/V_o = 1.00$; $\alpha = 10^o$.

Figure 20.-Concluded.

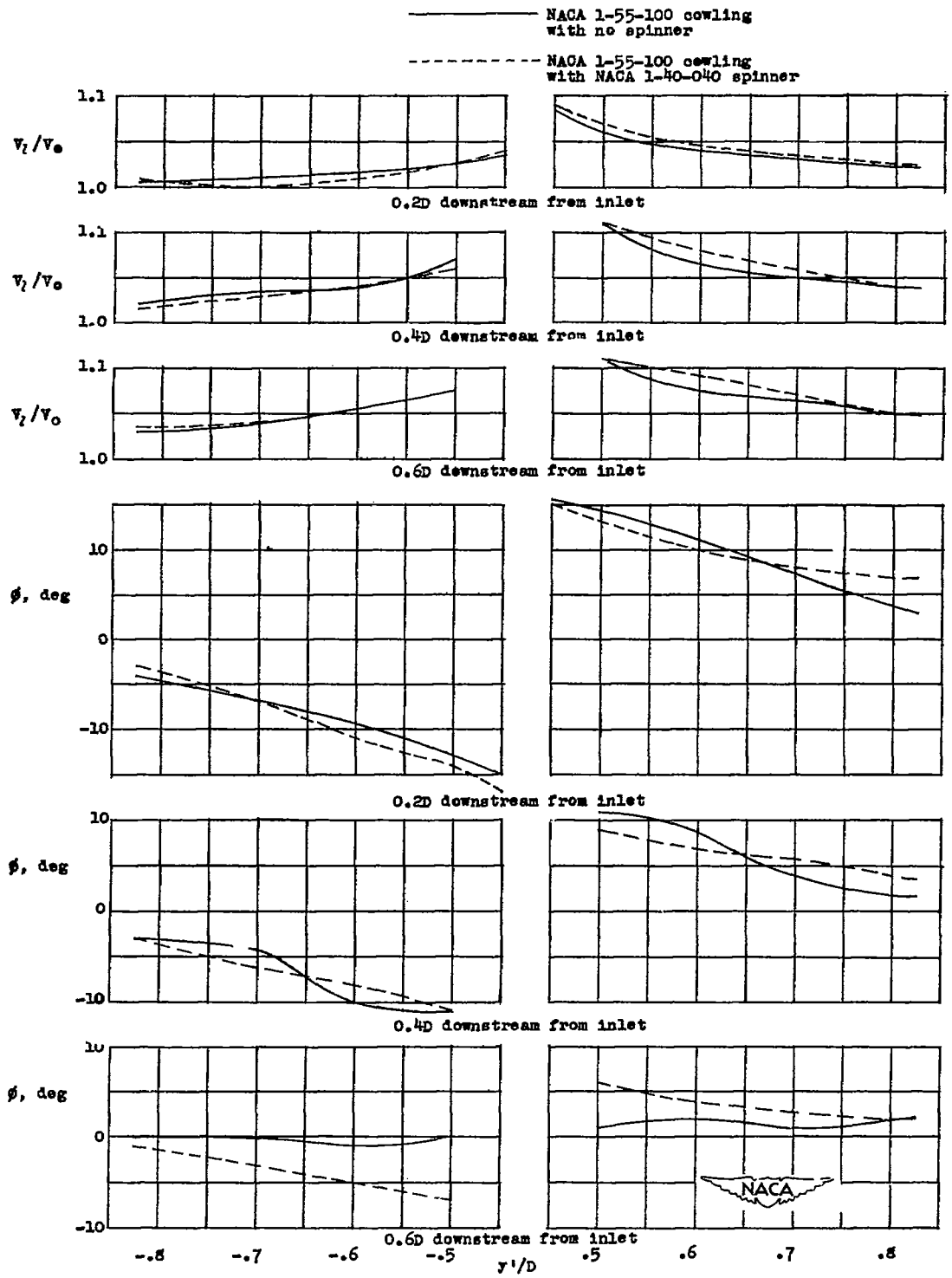

(a) $V_1/V_o = 0.53$; $\alpha \approx 2.5°$.

Figure 21.-Local flow-speed ratios and flow angles downstream from the inlet station for the NACA 1-55-100 cowling with no spinner and for the NACA 1-55-100 cowling with the NACA 1-40-040 spinner.

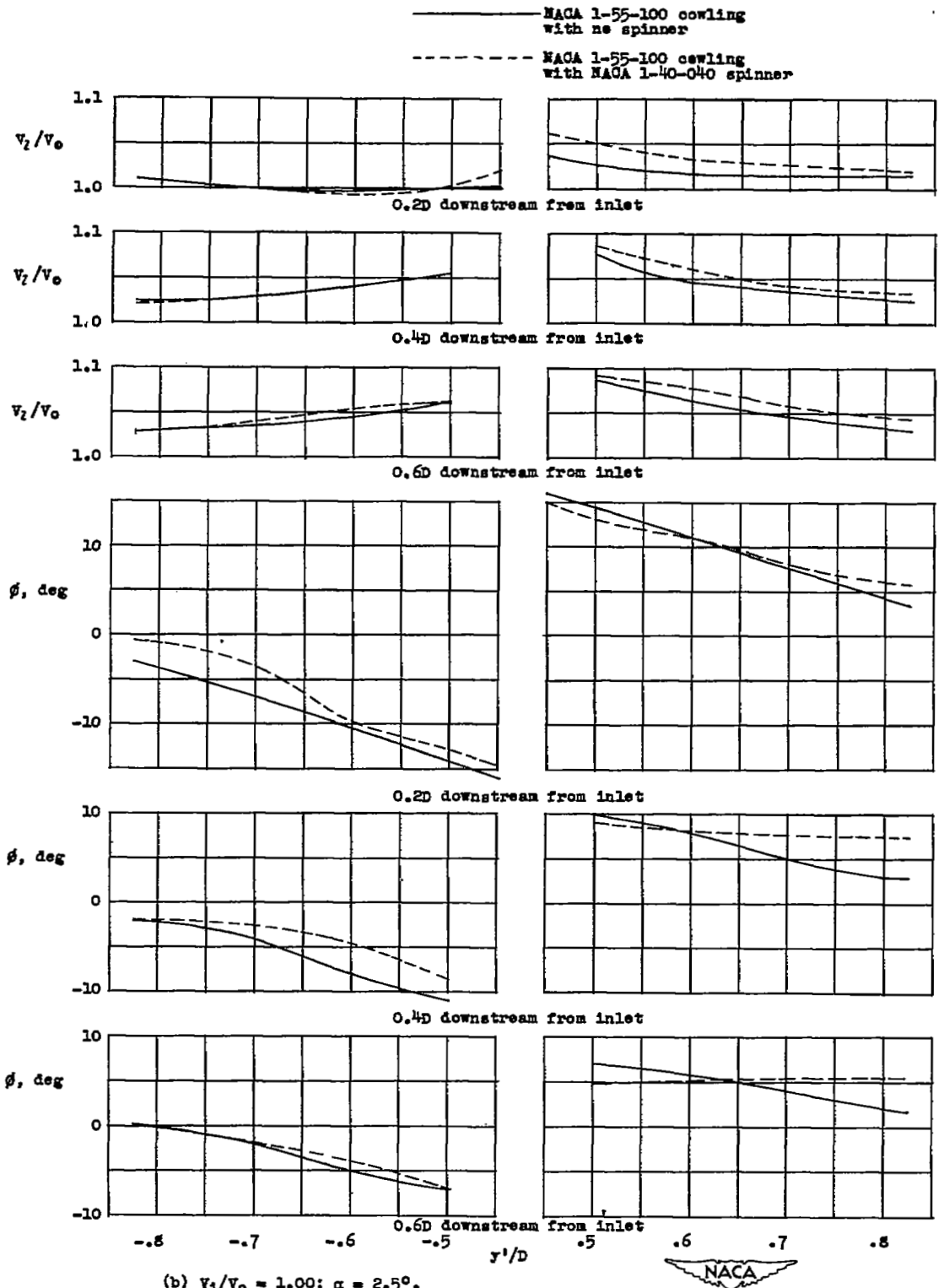

(b) $V_1/V_o = 1.00$; $\alpha = 2.5°$.

Figure 21.–Concluded.

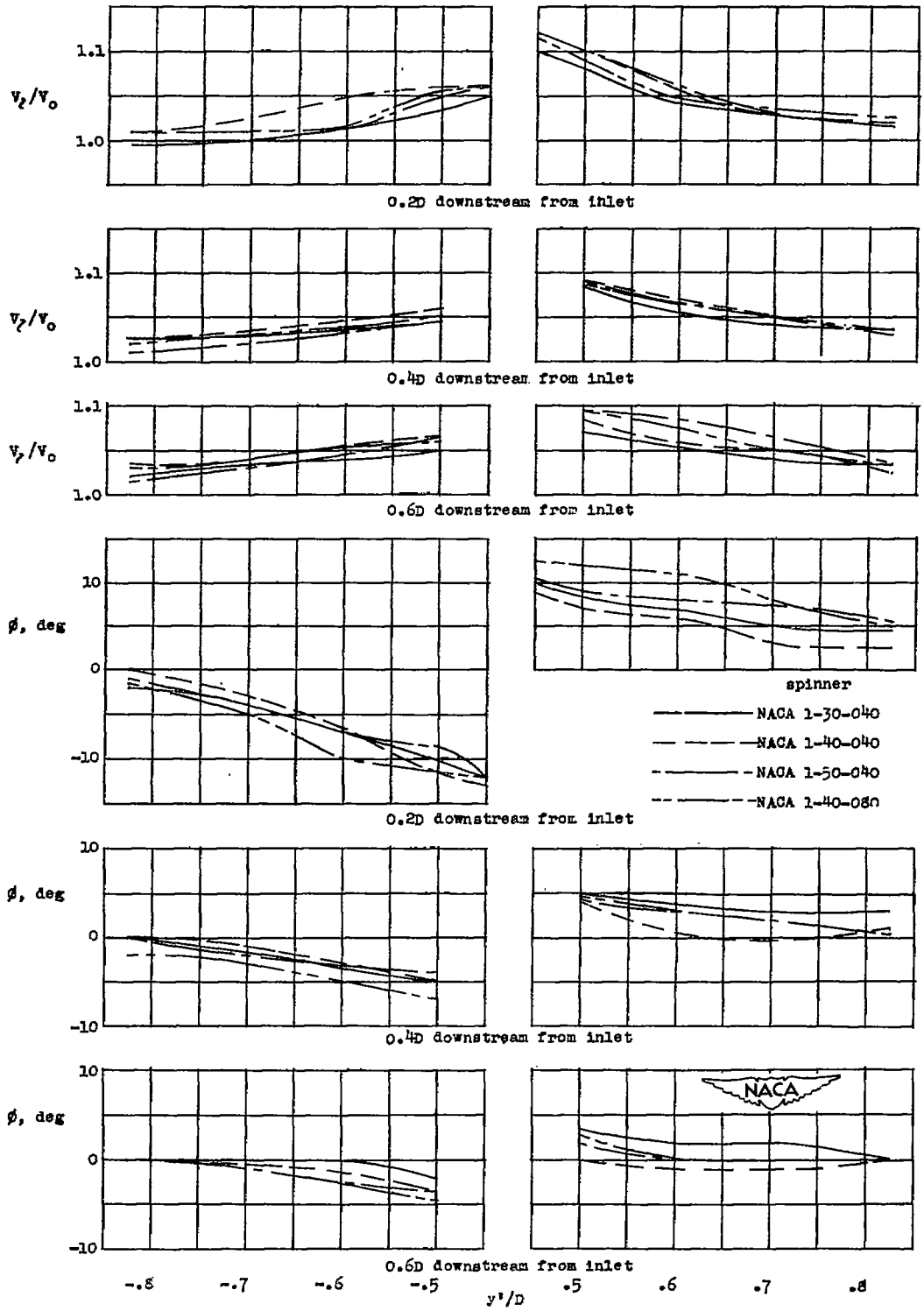

(a) $V_1/V_o = 0.60$; $\alpha = 2.5^\circ$.

Figure 22.-Effect of changes of spinner proportions on local flow-speed ratios and flow angles downstream from the inlet. NACA 1-70-100 cowling.

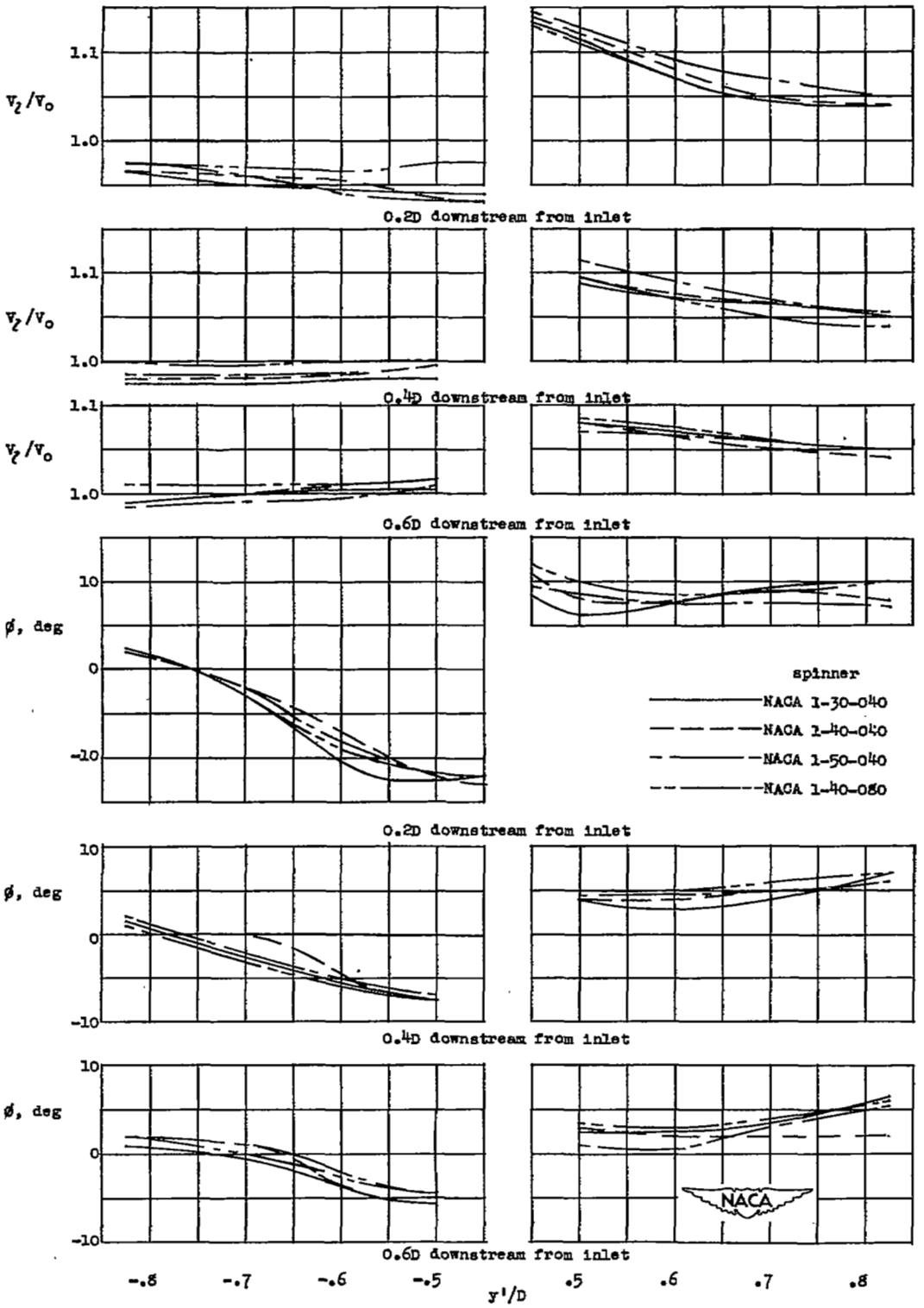

(b) $V_j/V_o = 1.00$; $\alpha = 10^o$.

Figure 22.–Concluded.

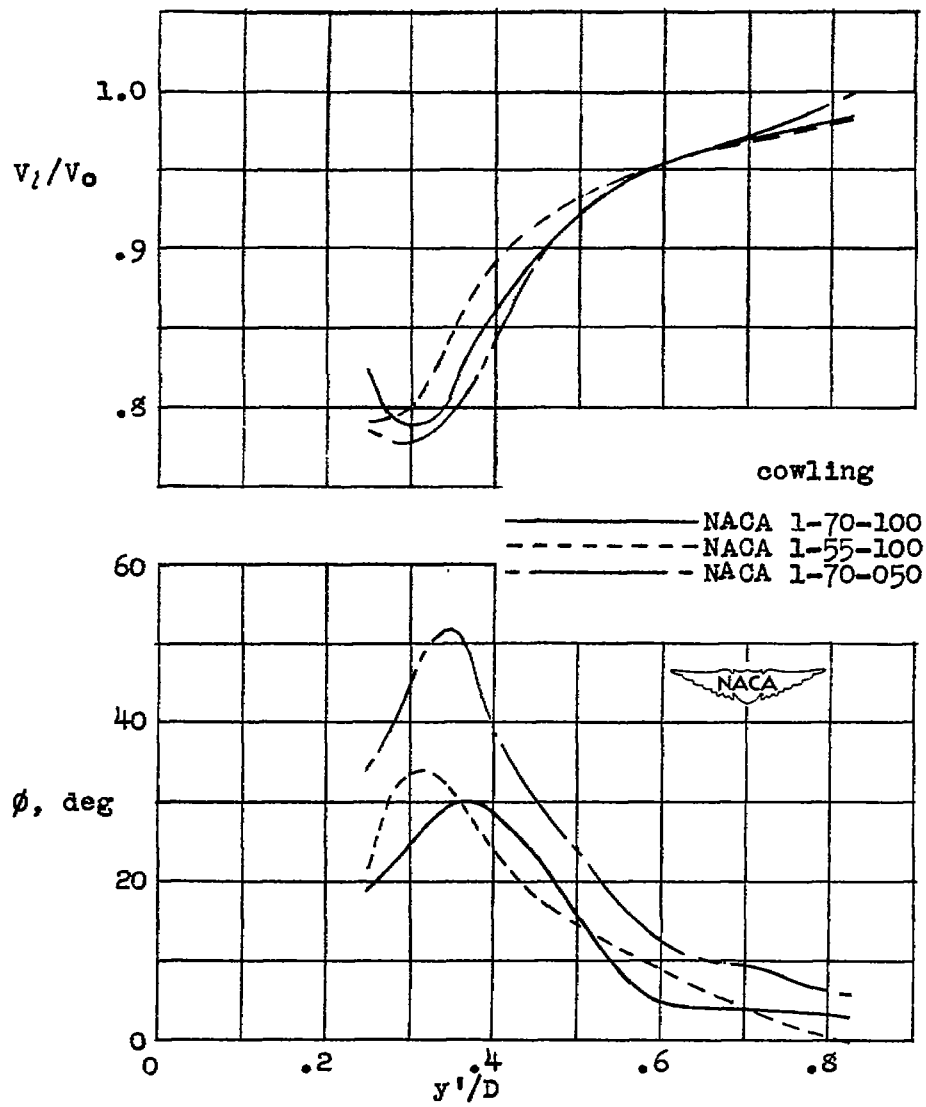

(a) $V_i/V_o = 0.60$; $\alpha = 0°$.

Figure 23.-Effect of changes in cowling-inlet-diameter ratio and cowling-length ratio on local flow-speed ratios and flow angles in propeller-shank region (0.1D upstream from inlet). NACA 1-40-040 spinners.

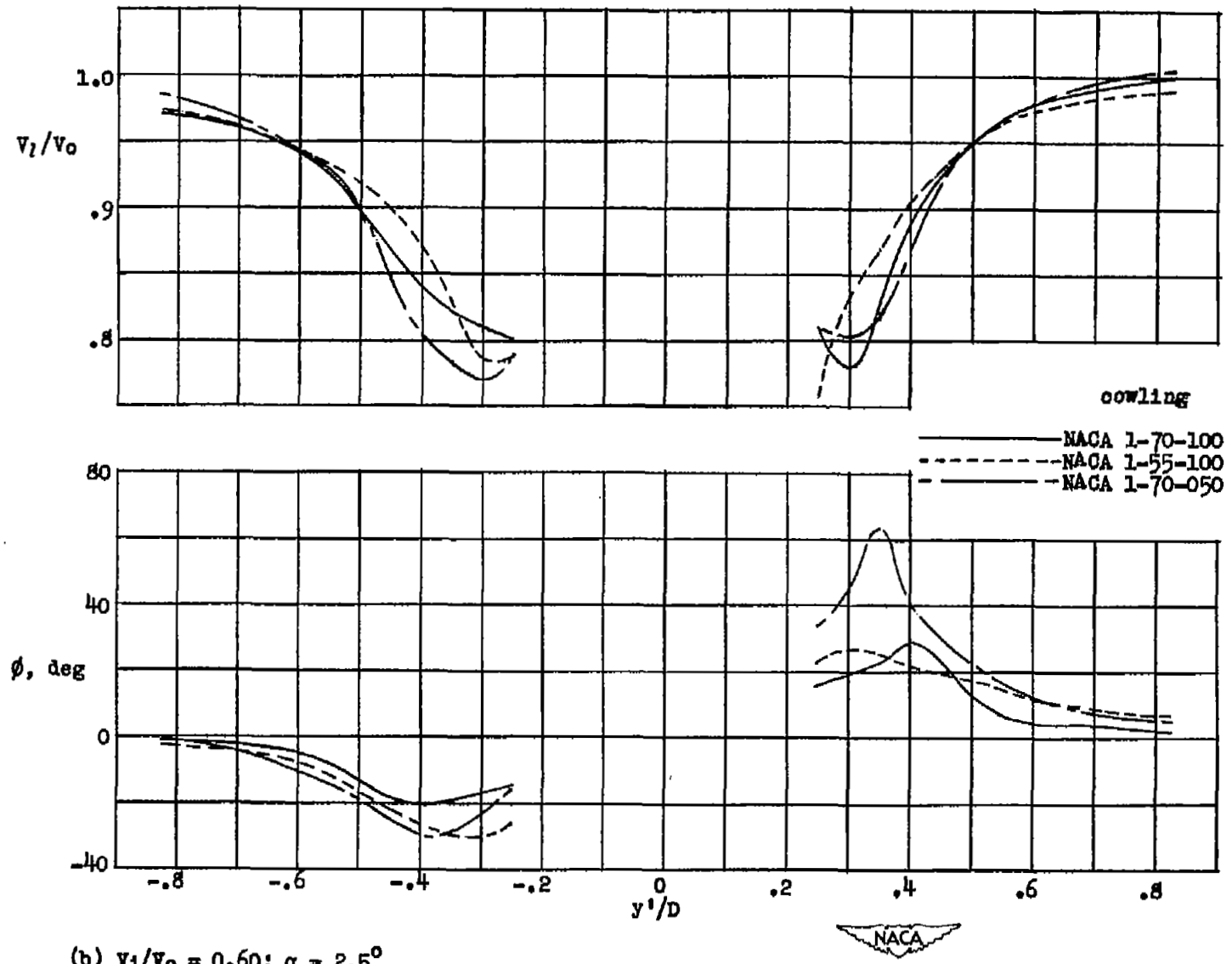

(b) $V_1/V_o = 0.60$; $\alpha = 2.5^\circ$.

Figure 23.-Continued.

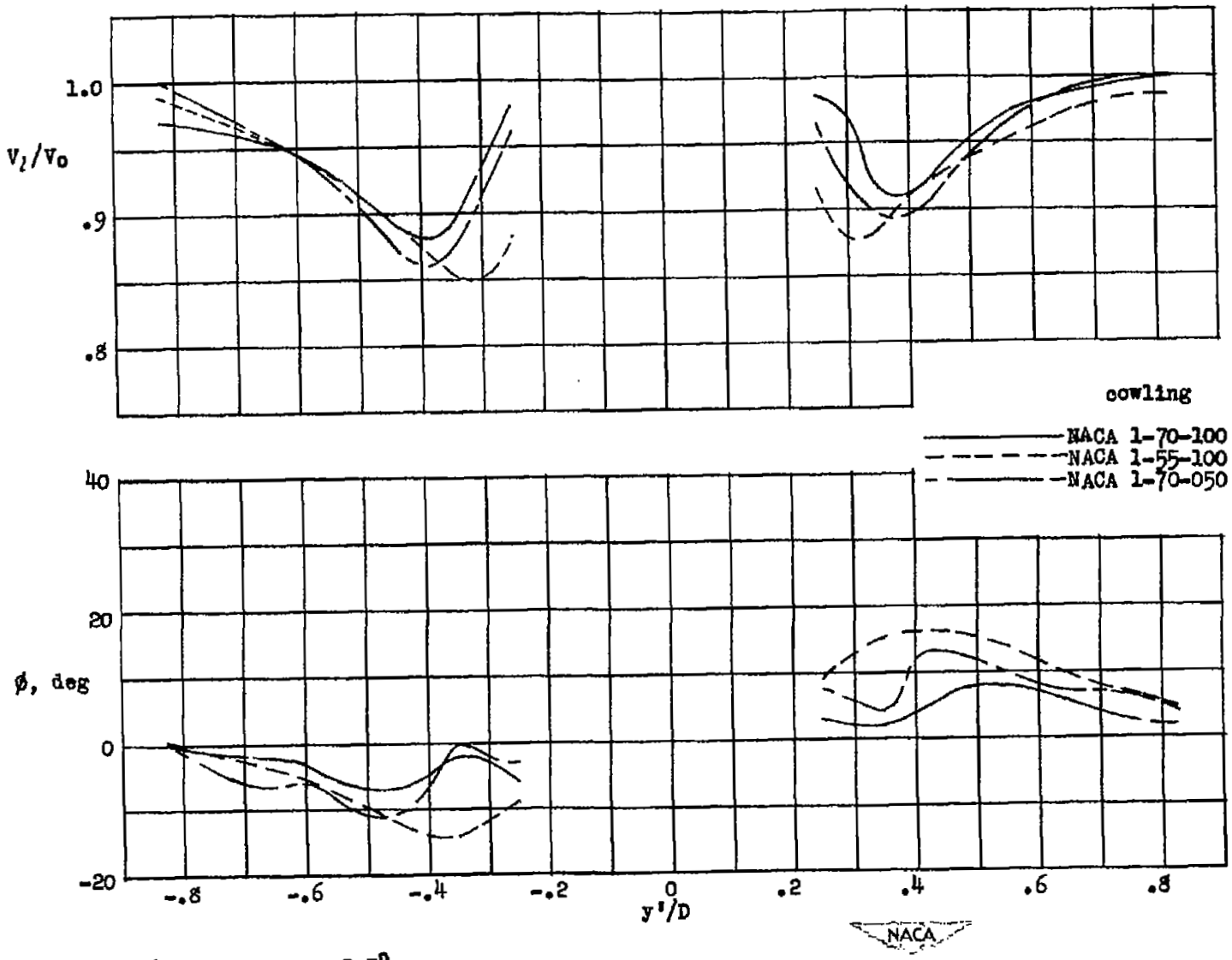

(c) $V_l/V_o = 1.00$; $\alpha = 2.5^\circ$.

Figure 23.-Continued.

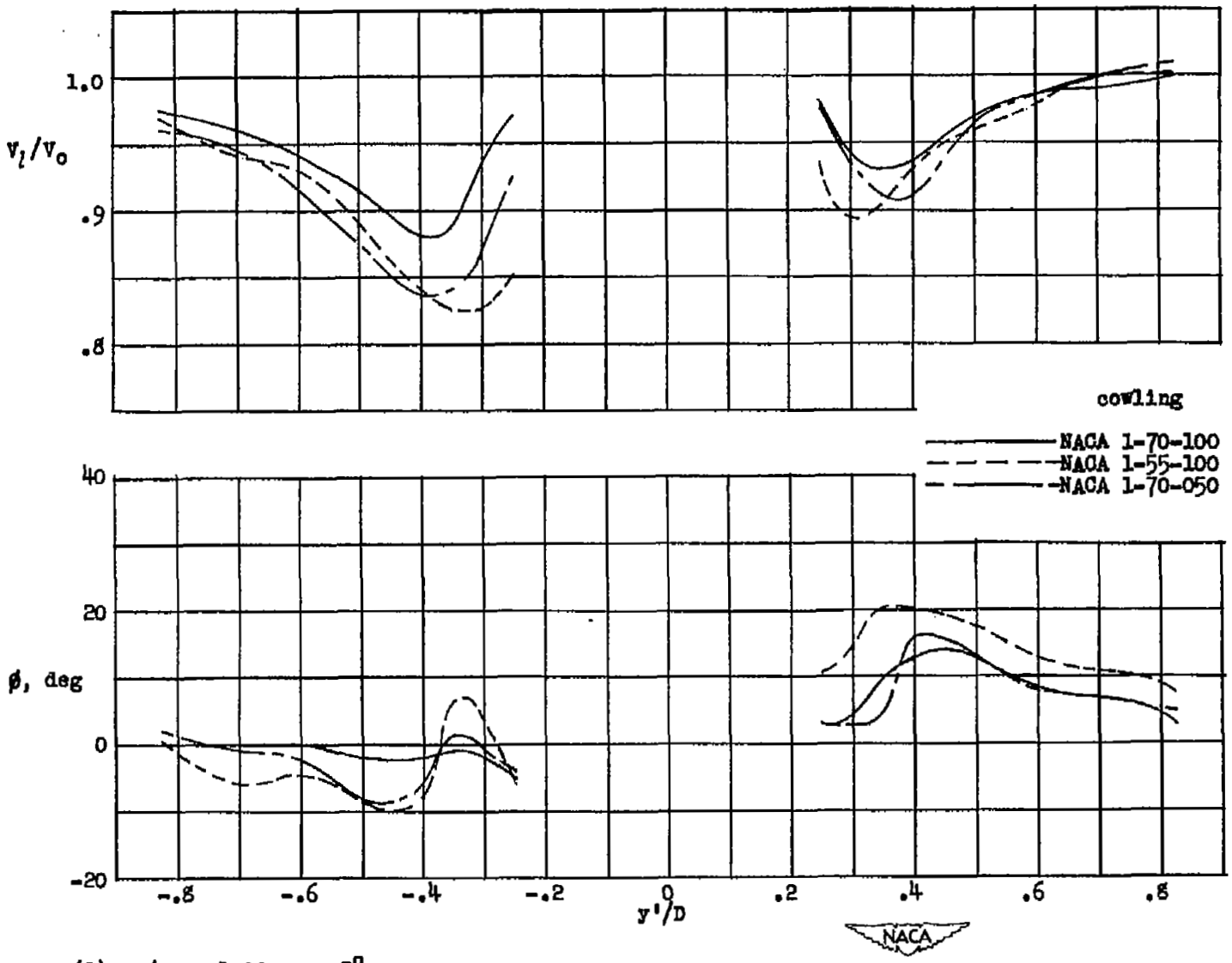

(d) $V_1/V_o = 1.00$; $\alpha = 5^o$.

Figure 23.-Continued.

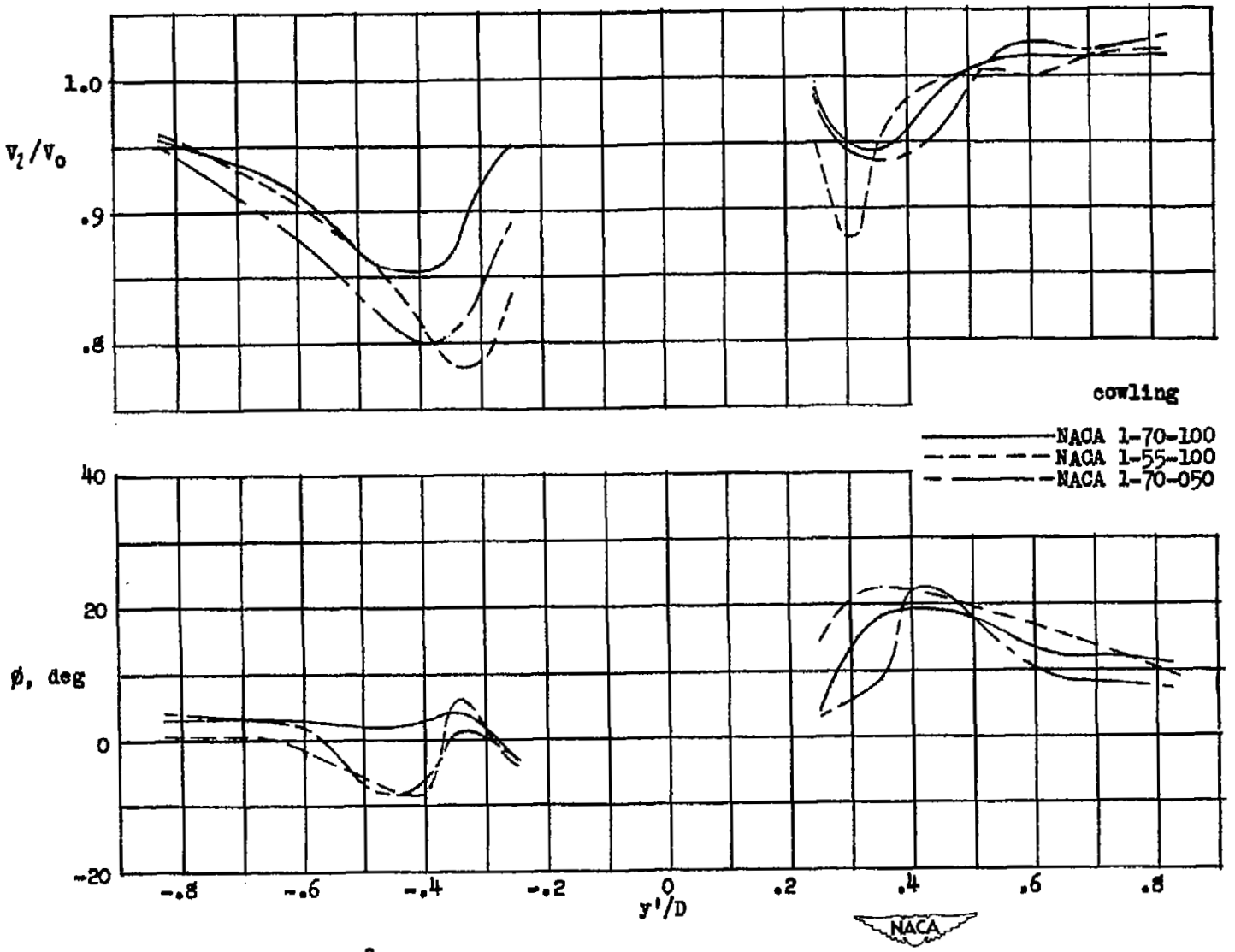

(a) $V_1/V_o = 1.00$; $\alpha = 10^\circ$.

Figure 23.-Concluded.

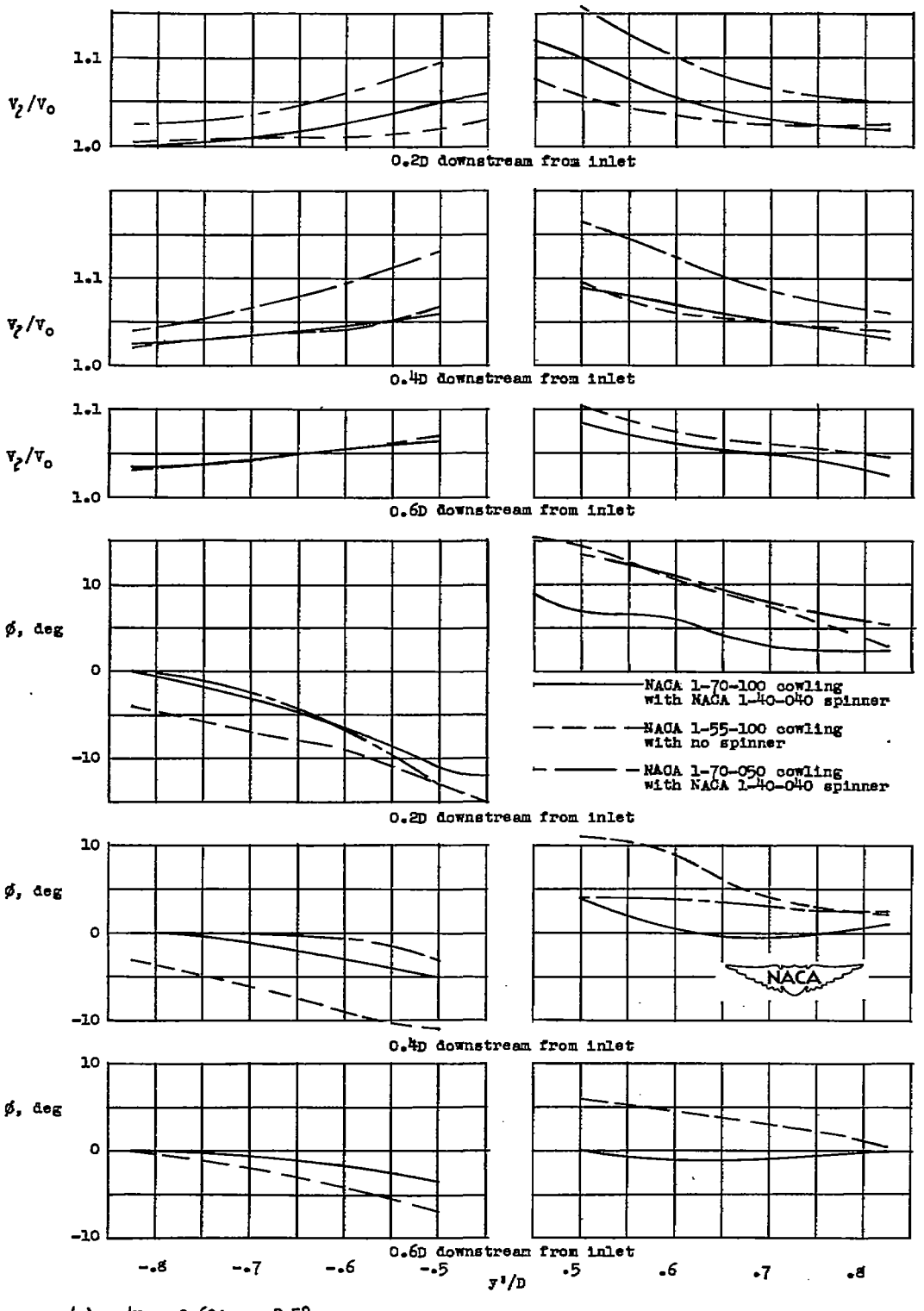

(a) $V_1/V_o = 0.60$; $\alpha = 2.5^o$.

Figure 24.-Effect of changes of cowling proportions on local flow-speed ratios and flow angles downstream from the inlet.

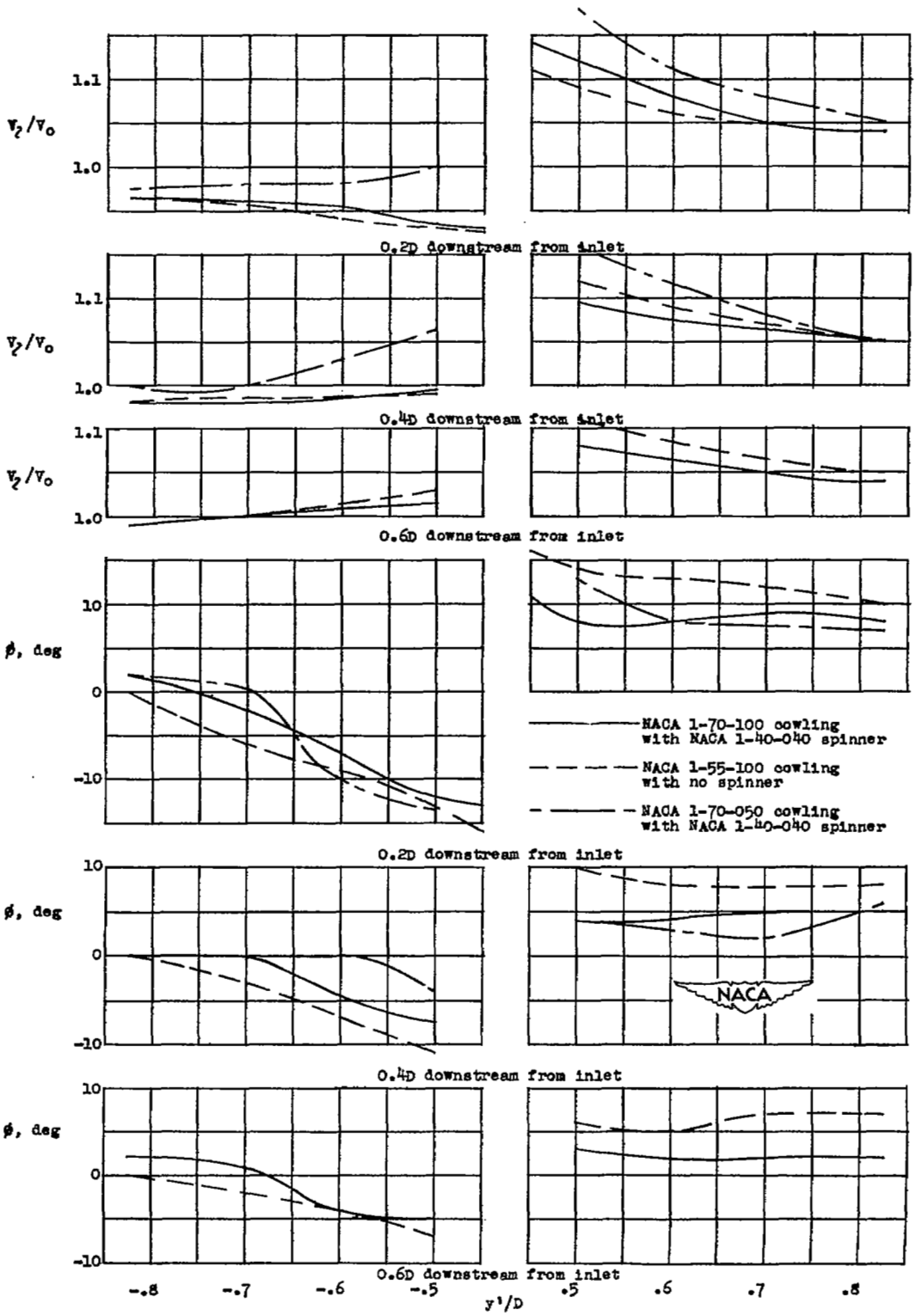

(b) $V_1/V_o = 1.00$; $\alpha = 10^o$.

Figure 24.-Concluded.

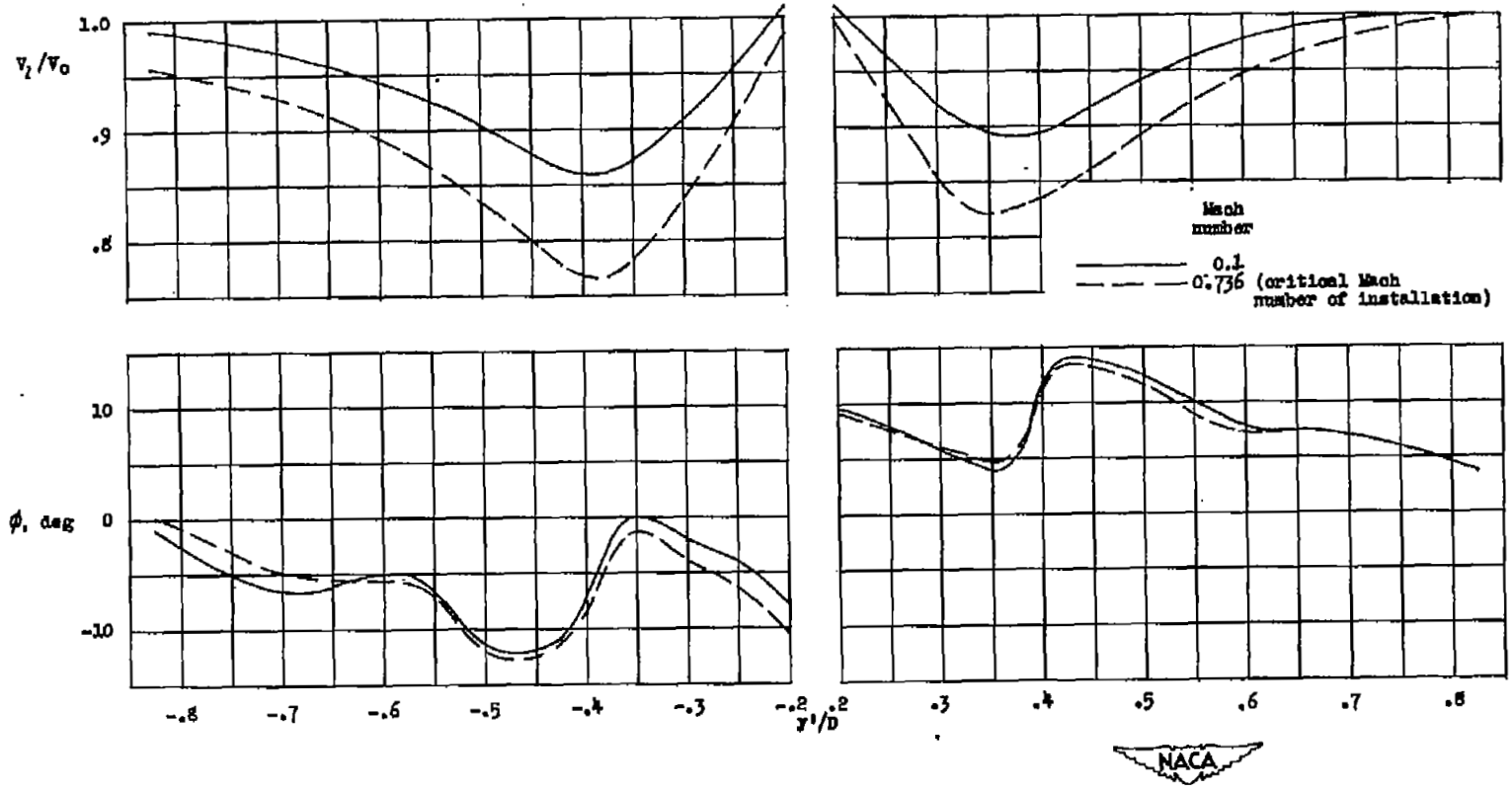

Figure 25.-Effect of compressibility on the speeds and directions of flow in the propeller shank region (0.1D upstream from inlet) of the NACA 1-70-050 cowling with the NACA 1-40-040 spinner as indicated by the Prandtl-Glauert method. $V_l/V_o = 1.00$; $\alpha = 2.5°$.

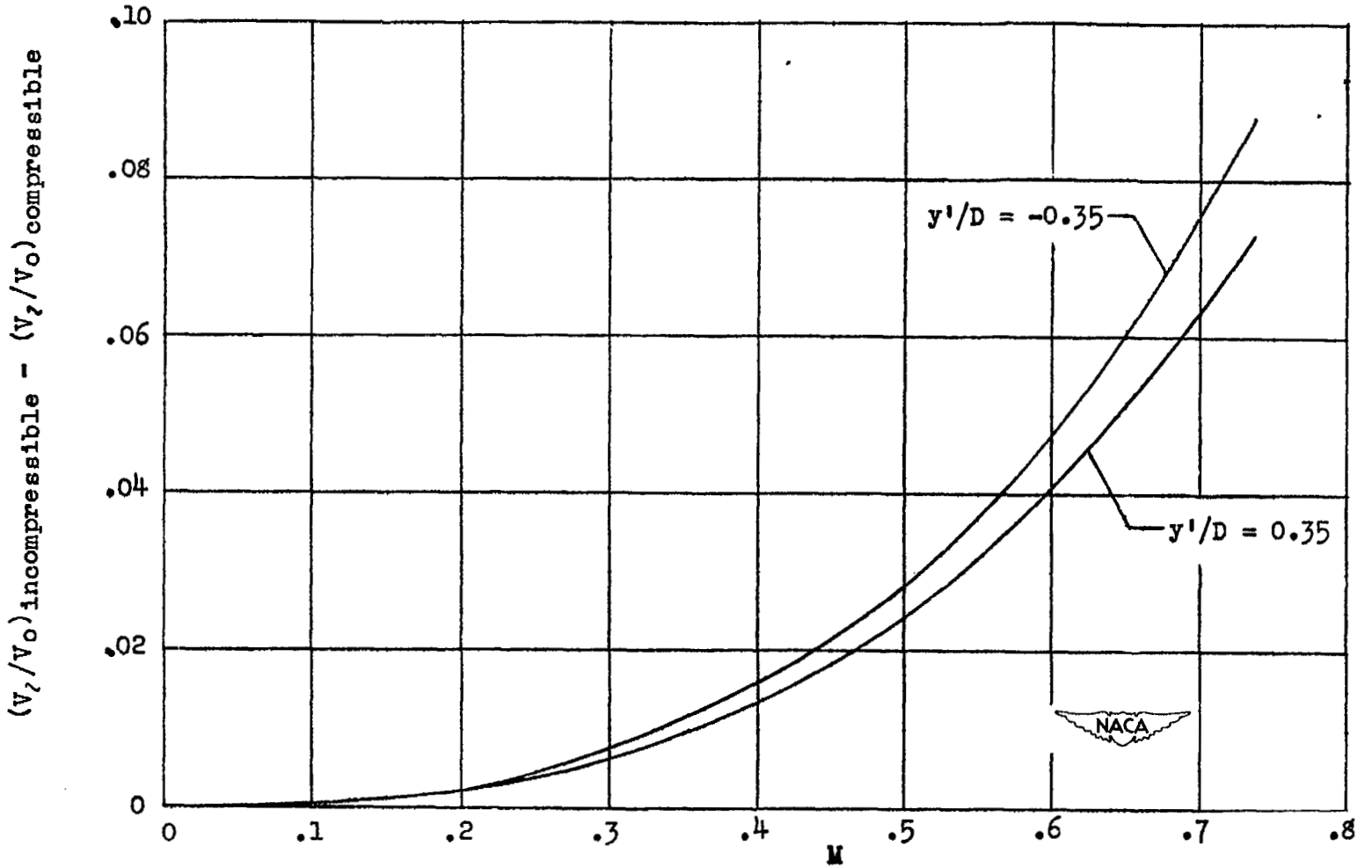

Figure 26.-Maximum difference between measured flow-speed ratio (essentially incompressible) and calculated compressible flow-speed ratio as a function of Mach number for the conditions specified in figure 25.